ZIRCONIA BASED /NAFION COMPOSITE MEMBRANES FOR FUEL CELL APPLICATIONS

by

Rudzani Sigwadi

Submitted in accordance with the requirements for
the degree of

Magister Technologiae

In the subject

Engineering: Chemical

At the

University of South Africa

Supervisor: Dr Touhami Mokrani

Co-supervisor: Dr Nosipho Moloto

: Professor M. Maaza

June 2013

Declaration

I declare that Zirconia Based/ Nafion Composite Membranes For Fuel Cell Applications is my own work and that all sources that I have used or quoted have been indicated and acknowledged by means of complete references.

……

……

……

SIGNATURE **DATE**

(Ms)

ABSTRACT

The nanoparticles of zirconium oxide, sulfated and phosphated zirconia were used to modify a Nafion membrane in order to improve its water retention, thermal stability, proton conductivity and methanol permeability so that it can be used at higher temperatures in fuel cell. These modified Nafion nanocomposite membrane with inorganic nanoparticles have been designed to run at operating temperatures between 120 ^{o}C and 140 ^{o}C because higher temperature operation reduces the impact of carbon monoxide poisoning, allows attainment of high power density and reduces cathode flooding as water is produced as vapor. The inorganic nanoparticles were incorporated within the Nafion matrix by recast, ion exchange and impregnation methods. The membrane properties were determined by ion exchange capacity (IEC), water uptake, methanol permeability and proton conductivity. The characterization of the inorganic nanoparticles within the nanocomposite membranes was determined by X-Ray diffraction (XRD), Brunau-Emmett-Teller (BET) surface area and Fourier transform infrared spectroscopy (FTIR) for structural properties. Thermal gravimetric analysis (TGA) and Differential scanning calorimetry (DSC) were used to determine the thermal properties, and the morphological properties were probed by Transmission electron microscopy (TEM) and Scanning electron microscopy (SEM).

Pristine ZrO_2, sulfated and phosphated ZrO_2 nanoparticles were synthesized successfully. The particle sizes ranged from 30 nm to 10 nm respectively. The resulted particles were incorporated to a Nafion membrane with good dispersity. The conductivity of the nanocomposite membrane were around 0.1037 S/cm at 25 ^{o}C with

a higher water uptake of 42 %. These results were confirmed by the highest IEC value of 1.42 meg.g^{-1} of Nafion/ S-ZrO_2 nanocomposites membrane. These high IEC value may due to the incorporation of superacid S-ZrO_2 nanoparticles which increased the membrane acid property for providing new strong acid site.

Acknowledgements

The author acknowledges the assistance and co-operation of Wits Chemistry Laboratory to allow me to do some testwork and makes me able to present this work today. I would like to thank NRF for financial support. I would like to thank my supervisor Dr. Touhami Mokrani for his supervision support and guidance during my research period. I would like to thank the Chemical Engineering administrative staff for their continuously support.

I would like to thank my advisor Dr Nosipho Moloto from Wits University for her assistance, support and guidance during my master's research. I would like to thank Dr Sipho Mavundla for his support and encouragement which makes me to be independent.

I would like to thank Dr James Wesley-Smith from CSIR and his colleague for TEM and SEM results and also Dr Shakes Nonjola from CSIR for the Methanol permeability and Proton conductivity.

I would also like to thank all of my friends and colleagues for being helpful at all the time. I would like to thank my parents, my family for their support and guidance throughout my life.

List of Abbreviations

AFC: Alkaline fuel cell

AFM: Atomic force microscopy

AC: Alternating current

BET: Brunauer Emmett Teller

CHP: Combined heat and power

DMF: Dimethylformamide

DMFC: Direct methanol fuel cell

DS: Degree of sulfonation

Ea: Activation energy (in eV)

FTIR: Fourier transform infrared

IEC: Ion exchange capacity

MCFC: Molten carbonate fuel cell

MeOH: Methanol

PAFC: Phosphoric acid fuel cell

PEM: Proton exchange membrane

PEMFC: Proton exchange membrane fuel cell

PVDF: Polyvinylidene fluoride

PBI: Polybenzimidazole

P- ZrO_2: Phosphated zirconia

PAEK: poly (aryl ether ketone)

PAES: poly (arylene ether sulfone)

PTFE: polytetrafluoroethylene

PVA: poly (vinyl alcohol)

RH: Relative humidity (%)

SPEEK: sulfonated poly (ether ether ketone)

S: Surface area (in cm^2)

SEM: Scanning Electron Microscopy

SOFC: Solid oxide fuel cell

S- ZrO_2: Sulfonated zirconia

TGA: Thermal Gravimetric Analysis

TEM: Transmission Electron Microscopy

XRD: X-ray diffraction

Keywords

Aging

Characterization

Fuel cells

Inorganic

Ion exchange

Membranes

Nafion

Nanoparticles

Nanocomposite

Proton conductivity

Phosphated zirconia

Sulfated zirconia

Thermal properties

Water uptake

Zirconium oxide

Table of Contents

List of Figures

List of Tables

CHAPTER ONE

1. INTRODUCTION

1.1. Background of study

Throughout the world, the need of hour is power generation with environmental protection [1]. Most of the global energy demand is currently produced from fossil fuels. These fossil fuels are not only limited, but also contribute towards environmental pollution and global warming. The main crises we are going to face around the world are shortages of the global energy supply. These energy shortages force us to look at renewable energy as an alternative energy source. Among renewable energies fuel cells are one of the best candidates because of their ability to produce clean energy and their compactness [2]. A fuel cell has a quick start-up, low sensitivity to orientation and favorable power to weight ratio [2]. It is a promising clean energy source for vehicles such as cars, buses and trucks.

A fuel cell can be defined as an electrochemical device that generates electricity by a chemical reaction. It is different from conventional electrochemical cell batteries in that it consumes reactant from an external source and can quickly charge by refueling [3]. Some fuel cells use hydrogen as their fuel and oxygen from the air as their oxidant. Others use hydrocarbons and alcohols. Fuel cells can be divided into different categories in relation to the nature of their catalysts - electrolytes, membranes, proton

conductive capabilities, fuel type, and operating temperatures. There are five main types of fuel cells namely: Proton exchange membrane fuel cells (PEMFCs), Solid oxide fuel cells (SOFCs), phosphoric acid fuel cells (PAFCs), alkaline fuel cells (AFCs) and molten carbonate fuel cells (MCFCs) [3]. Among these types of fuel cells, PEMFCs are the most preferred because they offer a high-power density, low weight and volume compared with other fuel cells. The proton exchange membrane, as the major key component of the fuel cell, must be designed in the way that it conducts only the protons while blocking the electrons, able to operate at a high temperature; has a resistance for fuel crossover, has adequate mechanical properties and excellent chemical stability, especially against oxygen and strong acid [4, 5]. PEMFC has an important role in future distributed electricity generation but do not display the required reliability and lifespan for long-term high temperature applications because of shortcomings in the membrane material. The development of proton exchange membrane fuel cells has been the subject of much attention during the last decades mainly due to the environmental impact [6]. Although, there are a number of protonic membranes, most of the advanced proton exchange membrane fuel cells do not possess the required combination of high ionic conductivity, mechanical strength, dehydration resistance, chemical stability and fuel permeability along with a reasonably low cost [7].

Nafion (perfluorosulfonic acid polymer) is the material mostly used in proton exchange membrane fuel cells because under high humidity it has high ionic conductivity, high chemical and thermal stability [8-10]. The main drawbacks of

Nafion are poor film forming capability with high solubility in water, high methanol permeability and high production cost [9]. However, progress is still required to reduce the manufacturing cost, increase operating temperature (>80 ^{o}C) and enable operation at low relative humidity [11, 12]. Much effort has gone into modifications of Nafion membranes based on low cost inorganic nanoparticles such as zirconium oxide (ZrO_2), silica oxide (SiO_2) and titanium dioxide (TiO_2) [13]. Among those metal oxides, ZrO_2 nanoparticles is the one that possesses both the characteristics of weak acid and weak base properties [14, 15], as well as having an oxidizing and reducing surface properties [16]. This research work will focus on the development of nanocomposite proton exchange membranes with chemical and mechanical stability at higher temperature, which can result into better fuel cell performance, and to improve the water retention characteristics of Nafion membranes by the addition of inorganic nanoparticles. Due to the increasing concern regarding the storage and transportation of hydrogen and it is necessary to search for an alternate fuel. Methanol is chosen as an alternate fuel, as it possesses a very simple chemical structure that can be reform into hydrogen in the presence of a suitable catalyst [8]. It has been observed that zirconium oxide can improve its water retention capability by adding inorganic solid acid to form sulfated zirconia nanoparticles [17- 19]. From previous research, compared with a Nafion membrane, the composite membrane exhibited higher cell performance, higher thermo-stability and fuel cell internal resistance at high temperatures and low relative humidity [20].

A sulfated zirconia/Nafion nanocomposite membrane should be designed to run at operating temperatures between 120 ^{o}C and 140 ^{o}C because higher temperature operation reduces the impact of carbon monoxide poisoning, allows attainment of high power density and reduces cathode flooding as water is produced as vapor.

1.2. Problem statement and Motivation

Throughout the world, there is a realization that a fuel cell membrane has the potential to generate an electric current capable of powering electronic devices. This potential has been turned into a challenge in the research to develop proton exchange membrane fuel cells which use fuels such as hydrogen, methanol or gasoline. But each of these fuels seems to have its limitations when it comes to application. Hydrogen is very expensive and gaseous, therefore it is difficult to use directly as a fuel due to the problems of storage, safety and infrastructure. Because gasoline is cheap and liquid, there are no problems of portability and infrastructure, but there are some problems in energy efficiency. Because methanol is cheap and liquid, the development of proton exchange membrane fuel cells is focused on finding suitable alternatives membranes that might allow the direct uses of methanol as in the direct methanol fuel cells (DMFCs) and able to work at temperature above 100^{o}C with lower humidification levels [21]. For this reason, the activity has been focused on the components development for inorganic Nafion nanocomposite membranes that are able to work at high temperature and lower humidity. This aim could be achieved by using zirconium oxide, sulfated zirconia and phosphate zirconia nanoparticles to improve membrane properties.

1.3. Objective

The objective of this research is to modify the Nafion membrane by incorporating Zirconium nanoparticles in order to improve properties such as water retention, methanol permeability and proton conductivity at higher temperature.

1.4. Scope of the research

In order to meet the objective the scope of work needs to be focused. The following procedures will be followed in order to achieve the stated objective.

(i) Preparation of zirconium oxide, phosphated zirconia and sulfated zirconia nanoparticles.

(ii) Preparation of Nafion/ zirconium oxide, Nafion/ phosphated zirconia and Nafion/ sulfated zirconia nanoparticles.

(iii) Compare the proton conductivity and methanol permeability of modified Nafion nanocomposite membranes with an additive-free Nafion membrane.

(iv) Explore the conductivity of those modified Nafion membranes which differs in addition of zirconia nanoparticles content.

(v) Examine the effect of inorganic materials added into Nafion membranes for water retention improvement and Ion exchange capacity (IEC).

(vi) Identify the specific method of membrane preparation which required improving proton conductivity

(vii) Establish the degradation rate of a modified Nafion membrane at higher temperatures.

1.5. Thesis Overview

The thesis included the synthesis and characterization of zirconia based/ Nafion nanocomposite membranes for fuel cell applications. Its main focus is the preparation of nanocomposite membranes and their properties. This thesis consists of six chapters. Chapter 1 gives the introduction of the fuel cell and the objective of the research. Chapter 2 summarizes the history, the types of fuel cell and its applications. It also Focus on the Nafion membrane and its modification and other types of alternative membranes. Chapter 3 introduces the methods used, chemical used and characterizations techniques used in nanopowder and nanocomposite membrane preparations. Chapter 4 consists of the powder preparations with the experimental procedure and discussions of the results. Chapter 5 consists of the membrane preparations with the experimental procedure and discussions of the results. Chapter 6 gives a general summary and conclusions of all the results.

1.6. References

[1] B. Smitha, S. Sridhar, A. A. Khan, *Journal of Membrane Science* **259** (2005) 10-26.

[2] X. Zhang, S. Liu, J. Yin, *Journal of Membrane Science* **258** (2005) 78-84.

[3] R. O'Hayre, S. Cha, W. Colella, F. B. Prinz, *Fuel Cell Fundamentals*, John Wiley& Sons, Inc, (2005) ISBN 0-471-74148-5.

[4] O. Savadogo, Journal *of Power Sources* **127** (2004) 135-161.

[5] Y. Gao, G. P. Robertson, M. D. Guiver, X. Jian ,S. D. Mikhailenko, K. Wang, S. Kaliaguine, *Journal of Membrane Science* **227** (2003) 39-50.

[6] J. R. Yu, B. L. Yi, D. M. Xing, F. Q. Liu, Z. G. Shao, Y. Z. Fu, *Physical Chemistry Chemical Physics* **5** (2003) 611-615.

[7] D. Sangeetha, *European Polymer Journal* **41** (2005) 2644-2652.

[8] P. P. Kundu, V. Sharma, *Critical Reviews in Solid State & Material Sciences* **32** (2007) 51-66.

[9] B. Smitha, S. Sridhar, A. A. Khan, *Journal of Membrane Science* **225** (2003) 63-76.

[10] S. Chen, L. Krishnan, S. Srinivasan, J. Benziger, A. B. Bocarsly, *Journal of Membrane Science* **243** (2004) 327-333.

[11] A. Sacc`a, I. Gatto, A. Carbone, R. Pedicini, E. Passalacqua, *Journal of Power Sources* **163** (2006) 47-51.

[12] C. Wang, E. Chalkova, C. Lute, M. Fedkin, S. Komarneni, M. Chung, S. Lvov, *Electrochemical Society Transactions* **16** (2008) 1451-1459.

[13] S. Ren, G. Sun, C. Li, S. Song, Q. Xin, X. Yang, *Journal of Power Sources* **157** (2006) 724-726.

[14] B. Q. Xu, T. Yamaguchi, K. Tanabe, *Chemistry Letters* **10** (1988) 1663-1666.

[15] M. S. Wong, D. M. Antonelli, J. Y. Ying, *Nanostructured Material* **9** (1997) 165-168.

[16] K. Tanabe, *Material Chemistry and Physics* **13** (1985) 347-364.

[17] A. D. Epifanio, M. A. Navarra, F. C. Weise, B. Mecheri, J. Farrington, S. Licoccia, S. Greenbaum, *Chemical Material* **22** (2010) 813-821.

[18] M. A. Navarra, C. Abbati, B. Scrosati, *Journal of Power Sources* **183** (2008) 109-113.

[19] M. A. Navarra, F. Croce, B. Scrosati, *New Journal of Materials Chemistry* **17** (2007) 3210-3215.

[20] Y. Zhai, H. Zhang, J. Hua, B. Yi, *Journal of Membrane Science* **280** (2006) 148-155.

[21] S. Hikita, K. Yamane, Y. Nakajima, *Society of Automotive Engineers of Japan Review* **22** (2001) 151-156.

CHAPTER TWO

2. LITERATURE REVIEW

2.1. Introduction

Fuel cell will be an alternative energy source as the world energy consumption is increasing day by day [1]. It is a safer way to power our vehicles and heat or cool our homes without combustion or air pollution. The research in fuel cell technology started long time ago and their improvement is made day by day. NASA Gemini program used Proton Exchange Membrane Fuel Cells (PEMFCs) in the 1960s for spacecraft [2]. For the next generation the researches believed that the fuel cell powered vehicle will eventually replace the gasoline and diesel internal combustion engines. This literature review will include history, the types of fuel cells, types of membranes but more focused on the Nafion modified membrane for fuel cell application.

2.2. Fuel cells

A fuel cell is an electrochemical device that combines hydrogen and oxygen to produce electricity, with water and heat as its by-product. The basic fuel cell consists of two electrodes, the positive electrode which is called the cathode and the negative electrode called the anode [3, 4]. The hydrogen gas enters a fuel cell at the anode

where it reacts with a catalyst and is converted into protons and electrons. The proton then passes through the electrolyte, while the electron travels through a circuit, creating a current. The oxygen gas in the form of air enters a fuel cell at cathode where it reacts with hydrogen ions and electrons to form water and heat. The membrane as a major key of fuel cell allows only protons to pass through. Electrons flow through an external circuit to generate electricity.

2.2.1 History

The fuel cell using hydrogen-oxygen was first invented in 1839 by William R. Grove, working from the knowledge that winning an electric current through water would produce hydrogen and oxygen, showed that combining hydrogen and oxygen could produce water and an electric current [2,5]. Ludwig Mond and Charles Langer in 1889 attempted to build the first practical fuel cell device which use air and industrial coal gas, Bacon in 1932 tried to modified it, it was recorded as the first alkaline fuel cell (AFC) [2,3].

Boris Shelishch and the GAZ automobile manufacturer ran a truck with hydrogen as fuel in 1941. Between 1955 and 1958 several groups of chemical engineers and scientists at General Electric (GE) worked on a suitable design of a fuel cell to generate electricity for the spacecraft of the near future. The first Proton Exchange Membrane (PEM) unit was a result of this research, credited to Willard Thomas Grubb. Over time, Leonard Niedrach refined the PEM-type fuel cell by using platinum

on the sulfonated polystyrene membranes (which were later replaced by Nafion ionomer in 1966) which served as catalyst for the necessary hydrogen oxidation and oxygen reduction reactions. This became known as the 'Grub-Niedrach' fuel cell. The Grub-Niedrach fuel cell was further developed in cooperation with NASA, and it became the first commercially used fuel cell in the Gemini space program [2].

Harry Karl Ihrig demonstrated the first fuel cell-powered vehicle and first commercial use of a fuel cell by combining 1,008 cells into a stack during 1959. Back in the 1960s, the Austrian-born Dr. Karl Kordesch, one of Union Carbide's researchers, was associated with constructing the Electro van's power-plant. An eminent battery specialist with many patents to his name, he continued to refine the alkaline fuel cell. In 1967 he attached one to a moped, which he used to travel around town [2].

During the 1970s and 1980s many auto companies started to convert engines to burn hydrogen. They had been reassured by a second well-trusted official agency of the safety of hydrogen. The Los Alamos National Laboratory, under Walter Stewart, had concluded that “hydrogen storage and refueling of a vehicle can be accomplished over an extended period of time without any major difficulty”. The laboratory had modified a 1979 Buick, and scores of people had refilled the car over three-year period at a self-serve liquid hydrogen pump [2].

2.2.2 Fuel Cell Construction

The fuel cells are constructed by three segments which are sandwiched together: namely the anode, electrolyte and the cathode as shown in Figure 2.1. Two chemical reactions occur at the interfaces of these three segments to produces electricity which can be used to power electrical devices. The electrolyte is designed to allow only the ions to pass through while blocking the electrons. The free electrons travel through a wire creating the electric current.

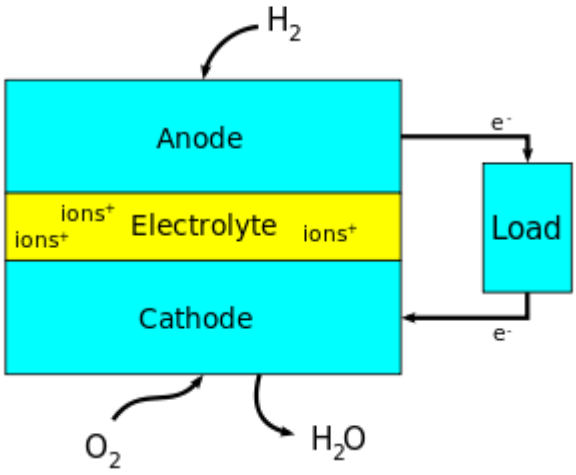

Figure 2. 1: Schematic representation of a fuel cell.

2.2.3. Types of Fuel Cells

Fuel cells have been classified based on the type of electrolyte they used and are of five main types.

2.2.3.1. Alkaline Fuel Cells (AFCs)

Alkaline fuel cells (AFCs) were one of the first fuel cell technologies developed, and they were the first type widely used in the U.S. space program to produce electrical energy and water on-board spacecrafts [4]. AFCs generally use a solution of potassium hydroxide (KOH) in water as their electrolyte. They operate at 100-250 °C with efficiency of 60% [4, 6]. They are, however, the cheapest type of fuel cell to manufacture so it is possible that they could be used in small stationary power generation units. AFCs are extremely sensitive to carbon monoxide and other impurities that would poison the catalyst. The designs of AFCs are similar to that of a PEM cell but with an aqueous solution or stabilized matrix of potassium hydroxide as the electrolyte. The electrochemistry is somewhat different in that hydroxyl ions (OH^-) migrate from the cathode to the anode where they react with hydrogen to produce water and electrons as shown in Figure 2.2 and equation 2.1 [7]. These electrons are used to power an external circuit then return to the cathode where they react with oxygen and water to produce more hydroxyl ions as shown in equation 2.2 [8].

The reactions in AFCs can be expressed by the following equations:

Anode Reaction: $H_2 + 2OH^- \rightarrow 2H_2O + 2e^-$ (2.1)

Cathode Reaction: $\frac{1}{2}O_2 + H_2O + 2e^- \rightarrow 2OH^-$ (2.2)

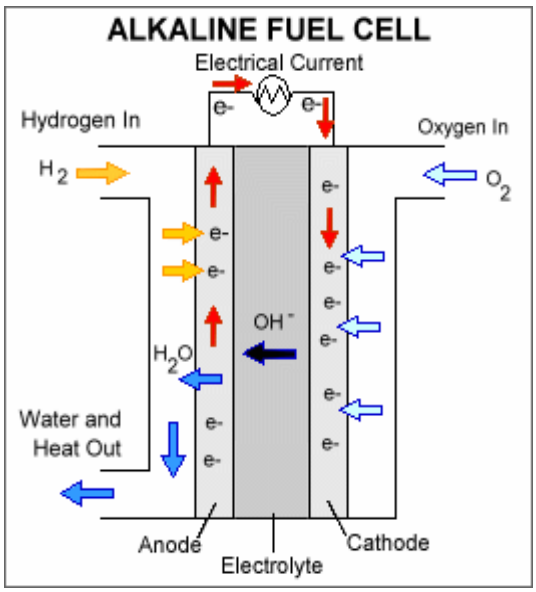

Figure 2. 2: Schematic representation of alkaline fuel cell [8].

2.2.3.2. Phosphoric Acid Fuel Cells (PAFCs)

The phosphoric acid fuel cells are currently the most commercially advanced fuel cell technology. PAFCs use liquid phosphoric acid as an electrolyte with a platinum catalyst [4]. PAFCs work slightly at higher temperatures than PEM or alkaline fuel cells around 150-200 ^{o}C making them more tolerant to reforming impurities [6]. PAFCs have been used for stationary power generation, but also used to power buses. There are currently a number of working units installed around the world providing power to hospitals, schools and small power stations. The anode and cathode reactions are the same as those in the PEM fuel cell with the cathode reaction occurring at a faster rate due to the higher operating temperature [7, 8]. A schematic diagram of a representative Phosphoric Acid Fuel Cell is shown in Figure 2.3 and their reaction in equation 2.3 and 2.4.

The reactions in PAFCs can be expressed by the following equations:

Anode Reactions: $H_2 \rightarrow 2H^+ + 2e^-$ (2.3)

Cathode Reaction: $\frac{1}{2}O_2 + 2H^+ + 2e^- \rightarrow H_2O$ (2.4)

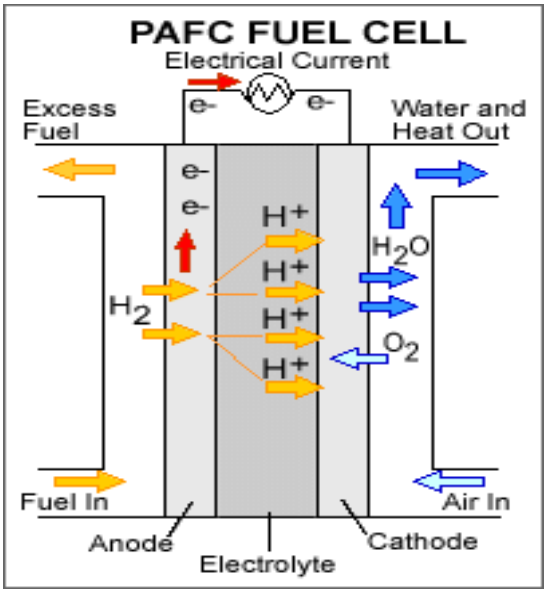

Figure 2. 3: Schematic representation of phosphoric acid fuel cell [8].

2.2.3.3. Molten Carbonate Fuel Cells (MCFCs)

Molten carbonate fuel cells (MCFCs) are currently being developed for natural gas and coal-based power plant for electrical utility, industrial and military applications [7]. These cells use molten carbonate salts mixture as the electrolyte. When heated to a temperature of around 650 °C these salts melt and generate carbonate ions which flow from the cathode to the anode where they combine with hydrogen to give water, carbon dioxide and electrons; as shown in Figure 2.4 and reaction 2.5 [4, 6]. These

electrons are routed through an external circuit back to the cathode, generating power on the way as illustrated in equation 2.6 [8].

The reactions in MCFCs can be expressed by the following equations:

Anode Reaction: $CO_3^{2-} + H_2 \rightarrow H_2O + CO_2 + 2e^-$ (2.5)

Cathode Reaction: $CO_2 + \frac{1}{2}O_2 + 2e^- \rightarrow CO_3^{2-}$ (2.6)

At high temperature the cells provides fuel flexibility. They can use hydrogen, simple hydrocarbons and simple alcohols, to generate hydrogen within the fuel cell structure. At the elevated temperatures there is only sulfur released. These fuel cells can work at up to 65% efficiency and this could potentially rise to 85% if the waste heat is utilized [9].

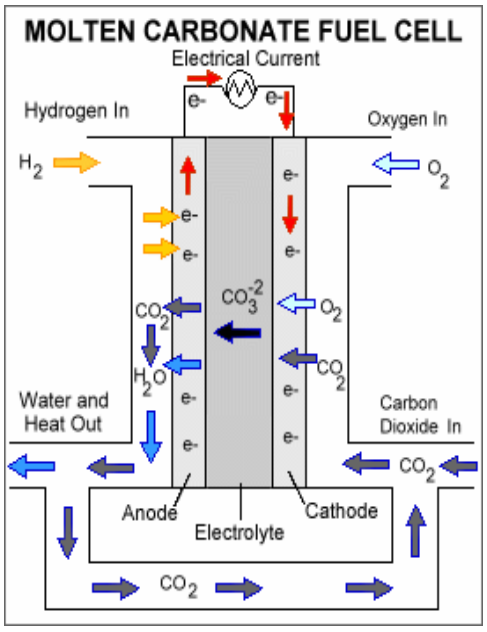

Figure 2. 4: Schematic representation of molten carbonate fuel cell [8].

2.2.3.4. Solid Oxide Fuel Cells (SOFCs)

Solid oxide fuel cells (SOFCs) use a hard, non-porous ceramic compound as electrolyte and operating at high temperature around 1000 °C [4, 6]. The high temperature means that this cell are resistant to poisoning by carbon monoxide as this is readily oxidized to carbon dioxide. SOFCs are sulfur-resistant fuel cell type. Energy is generated by the migration of oxygen anions from the cathode to the anode to oxidize the fuel gas, which is typically a mixture of hydrogen and carbon monoxide as shown in equation 2.7 and 2.8 [7]. The electrons generated at the anode move via an external circuit back to the cathode where they reduce the incoming oxygen, thereby completing the cycle as shown in Figure 2.5 and their overall reaction in equation 2.9 [9].

The reactions in SOFCs can be expressed by the following equations:

Anode Reactions: $H_2 + O^{2-} \rightarrow H_2O + 2e^-$ (2.7)

$CO + O^{2-} \rightarrow CO_2 + 2e^-$ (2.8)

Cathode Reaction: $\frac{1}{2}O_2 + 2e^- \rightarrow O^{2-}$ (2.9)

SOFCs have the efficiencies of 50-60% that are expected to be used for generating electricity and heat in industry and potentially for providing auxiliary power in vehicles [8].

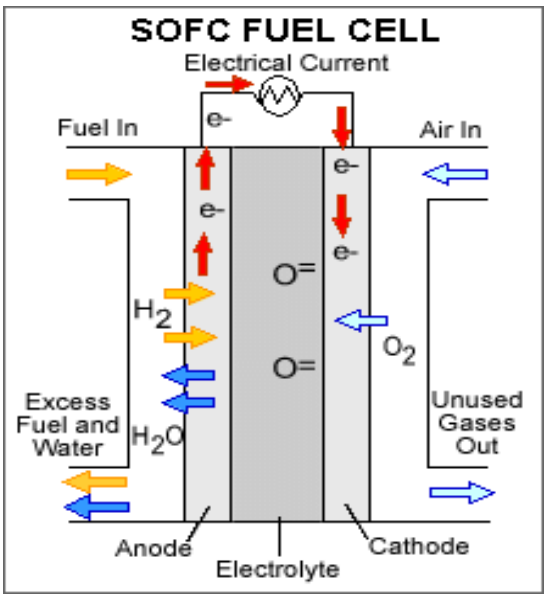

Figure 2. 5: Schematic representation of solid oxide fuel cell [8].

2.2.3.5. Solid polymer fuel cells (SPFC)

2.2.3.5.1. Direct methanol fuel cells (DMFCs)

DMFCs also use solid polymer as an electrolyte but differ from PEMFCs because they use liquid methanol fuel rather than hydrogen. DMFCs operate at slightly higher temperatures than PEMs 50-120 ^{o}C and achieve around 40% efficiency [3, 6]. DMFCs are directed toward small mobile power applications such as laptops and cell phones, using replaceable methanol cartridges at power ranges of 1-50 W [7]. It does not have many of the fuel storage problems typical of some fuel cells because methanol has a higher energy density than hydrogen. Methanol is also easier to transport and supply to the public using our current infrastructure because it is a liquid [8]. The liquid methanol (CH_3OH) is oxidized in the presence of water at the anode generating CO_2,

hydrogen ions and the electrons that travel through the external circuit as the electric output of the fuel cell. The hydrogen ions travel through the electrolyte and react with oxygen from the air and the electrons from the external circuit to form water at the anode completing the circuit. A schematic diagram of a representative DMFCs is shown in Figure 2.6 and their reaction in equation 2.10 and 2.11.

The reactions in DMFCs can be expressed by the following equations:

Anode Reaction: $CH_3OH + H_2O \rightarrow CO_2 + 6H^+ + 6e^-$ (2.10)

Cathode Reaction: $\frac{3}{2} O_2 + 6 H^+ + 6e^- \rightarrow 3 H_2O$ (2.11)

Major drawbacks of the DMFCs are poor performance of the anode where more efficient methanol electro-oxidation catalysts are needed [3].

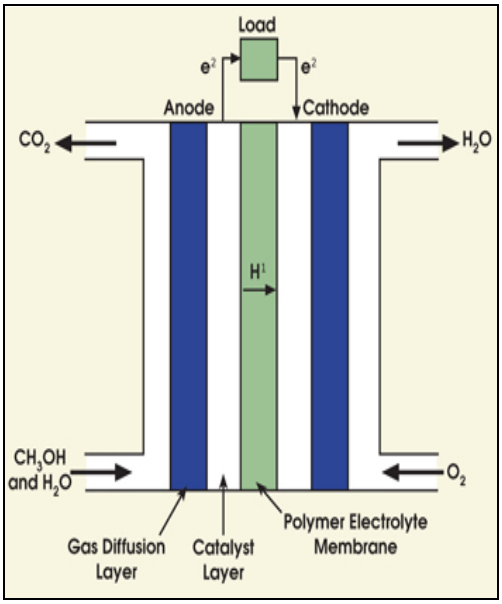

Figure 2. 6: Schematic representation of direct methanol fuel cells [3].

2.2.3.5.2. Proton exchange membrane fuel cells (PEMFCs)

The proton exchange membrane fuel cells (PEMFCs) are an energy conversion device by electrochemically convert energy of fuels such as hydrogen and methanol to electricity. It has attracted much attention as clean energy generation technologies with high power density, high efficiency, and low greenhouse gas emissions for various applications such as portable electronic devices, transportation and residential power generation [6]. PEMFCs have solid polymer as an electrolyte [10]. Improvements in the performance can be identified by evaluating the polarization curve. PEMFCs have quick starts, with full power available in a minutes or less, low weight and volume with good power to weight ratio at low temperature operation that makes them suitable used in automobiles [11]. PEMFCs usually operate at low temperatures 60-100 ^{o}C, which makes them also suitable for portable applications [4]. PEMFCs offer efficient operation up to 50% electrical efficiency for the fuel cell itself and over 85% total efficiency when waste heat is captured for small-scale space and water heating. Their performances are influence by many parameters such as operating temperature, pressure and relative humidity. The protons permeate through the polymer electrolyte membrane to the cathode as shown in Figure 2.7 and equation 2.12. The electrons travel along an external load circuit to the cathode, thus creating the current output of the fuel cell. Meanwhile, a stream of oxygen is delivered to the cathode as shown in Figure 2.7. At the cathode side oxygen molecules react with the protons permeating through the polymer electrolyte membrane and the electrons arriving through the external circuit to form water molecules as shown in equation 2.13 [4, 6, 7, 8].

The reactions in PEMFCs can be expressed by the following equations:

Anode Reactions: $H_2 \rightarrow 2H^+ + 2e^-$ (2.12)

Cathode Reaction: $\frac{1}{2}O_2 + 2H^+ + 2e^- \rightarrow H_2O$ (2.13)

The prime requirement of fuel cell membranes are high proton conductivity, low methanol/ water permeability, good mechanical properties and thermal stability [12,13,14]. PEMFCs face several challenges because of platinum catalysts are expensive and also subject to CO poisoning from hydrocarbon fuels, so catalyst improvements, non-precious metal catalysts and other alternatives are under investigation. Membranes more resistant to chemical impurities are also being developed. The attractiveness of this PEMFCs system has increased significantly with improvements in many areas.

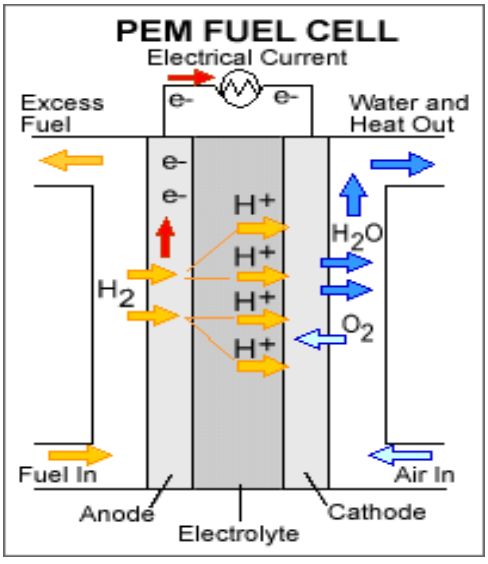

Figure 2. 7: Schematic representation of polymer electrolyte membrane fuel cell [8].

2.3. Low Temperature Fuel Cells

The low temperature fuel cells that are mostly used in automotive and portable electronic applications are the proton exchange membrane fuel cells (PEMFCs) and the direct methanol fuel cells (DMFCs). The DMFCs directly consumes liquid fuel (methanol) while the PEMFCs are fuelled with hydrogen [15]. This cell consists of six major parts: end plates, current collectors, graphite flow channel blocks, gaskets, gas diffusion layers and a membrane electrode assembly (MEA) [16]. Figure 2.8 shows the component of low temperature fuel cell. Performance has been a major problem for the DMFCs at low temperature as it typically produces only one third of the PEMFC's power density [17, 18]. Because the PEMFC uses a solid polymer electrolyte, it results in excellent resistance to gas crossover and a simpler design that requires less maintenance [6], and eliminates the corrosion and safety concerns associated with liquid electrolyte fuel cells. As the DMFC fuel anode reactions proceed so much slowly than with hydrogen [9], the majority of the work has involved developing materials, such as new anode and cathode electro catalysts and new proton conducting polymers, to promote the efficiency of the membrane electrode assemblies (MEAs) used in the DMFCs stack and interest in producing low temperature DMFCs systems has increased recently.

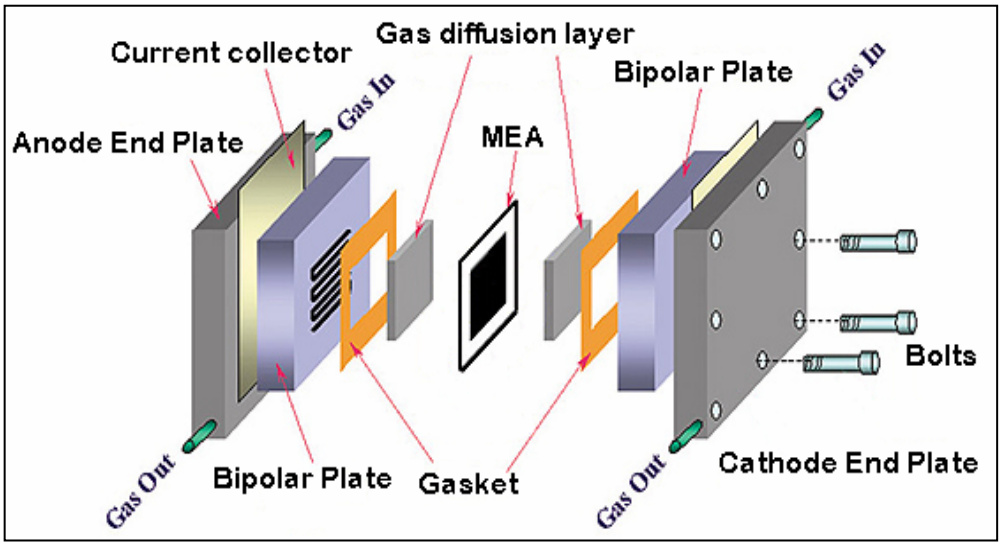

Figure 2. 8: Low Temperature fuel cell component [18].

2.3.1. Principle of the H_2-PEMFC

A H_2-PEMFC works by taking hydrogen into the fuel cell and allowing the molecules to travel through the bipolar plates as shown in Figure 2.9. At the anode of a H_2-PEMFC, hydrogen is consumed; electrons are released to the anode and transported via external circuit as shown in equation 2.14. The producing hydrogen ions (protons) are transported to the cathode side through a polymer electrolyte membrane. Oxygen in the air combines with electrons and protons to produce water at the cathode as shown in equation 2.15 and their overall reaction in equation 2.16.

Oxidation half reaction: Anode $2\ H_2 \longrightarrow 4H^+ + 4e^-$ (2.14)

Reduction half reaction: cathode $O_2 + 4H^+ + 4e^- \longrightarrow 2\ H_2O$ (2.15)

Overall reaction $2\ H_2 + O_2 \longrightarrow 2\ H_2O$ (2.16)

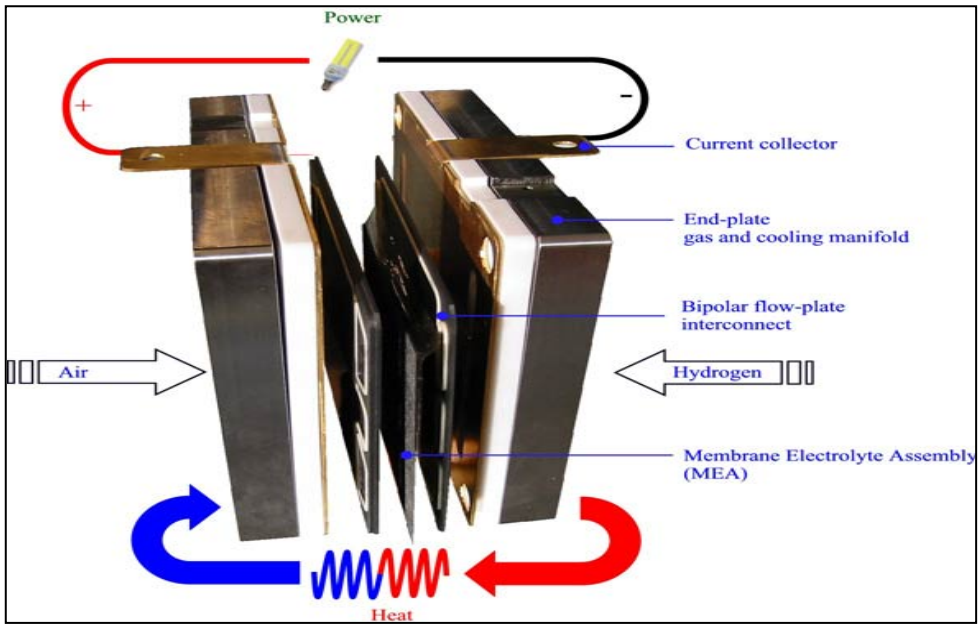

Figure 2. 9: Principles of Proton exchange membrane fuel cells (H_2-PEMFC).

2.3.2. *Principle of DMFCs*

The direct methanol fuel cell (DMFC) is a proton exchange membrane fuel cell that is fed with an aqueous solution of methanol. The two catalytic electrodes where the methanol oxidation (anode) and the oxygen reduction (cathode) occur are separated by a membrane which conducts protons from anode to cathode, while other compounds diffusion is blocked. The combination of electrodes and membranes is called membrane electrode assembly (MEA) and it is sandwiched between separators. A

methanol and water mixture is fed to the anode catalyst where the catalyst particles present in the anode help to oxidized methanol molecule into hydrogen atoms and carbon dioxide (CO_2) (See Figure 10). Each electrode is made of a gas diffusion layer and a catalytic layer (See Figure 10). It diffuses through the diffusion layer to the catalytic layer where it is electrochemically oxidized into mainly carbon dioxide. Electrons are collected by graphite bipolar plates which are the two poles of the cell.

The reaction of DMFC:

Oxidation half reaction: Anode $CH_3OH + H_2O \longrightarrow CO_2 + 6H^+ + 6e^-$ (2.17)

Reduction half reaction: cathode $^3/_2\ O_2 + 6H^+ + 6e^- \longrightarrow 3\ H_2O$ (2.18)

Overall reaction $CH_3OH + {}^3/_2\ O_2 \longrightarrow CO_2 + 2\ H_2O$ (2.19)

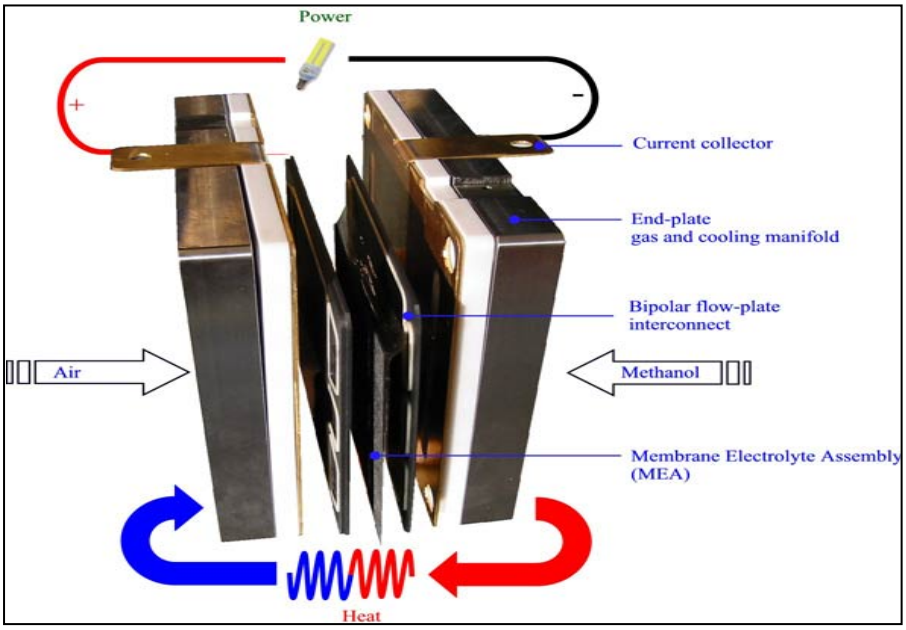

Figure 2. 10: Principles of Direct Methanol Fuel Cell (DMFC).

2.4. Proton Conductivity Mechanisms

The proton is unique in that it is the only ion which possesses no electronic shell. It therefore strongly interacts with the electron density of its environment. In the case of metals, the proton interacts with the electron density of the conduction band, and is considered to be a hydrogen atom with a protonic or hydridic character. Metals are also unique in that they allow the proton to have a high coordination number, typically four or six at a tetrahedral or octahedral site. In non-metallic compounds, the proton interacts strongly with the electron density of only one or two nearest neighbors. Proton transfer phenomena follow two principal mechanisms namely the vehicle mechanism and the structural diffusion (Grotthuss mechanism) where the proton remains shielded by electron density along its entire diffusion path, so that in effect the momentary existence of a free proton is not seen [19]. In this mechanism the proton diffuses through the medium together with a "vehicle" (for example, with H_2O as H_3O^+). The counter diffusion of unprotonated vehicles (H_2O) allows the net transport of protons [20]. In the other principal mechanism, the vehicles show pronounced local dynamics but reside on their sites. The protons are transferred from one vehicle to the other by hydrogen bonds (proton hopping). The Nafion proton transport and conductivity are strongly correlated to the water content. The water content in Nafion is specified by the quantity, which indicates number of water molecules per sulfonate group [21]. At high hydration level, structure diffusion dominates at the centre of hydrophilic domains and it results in a high diffusion coefficient of protons that approaches bulk water. At intermediate and lower hydration levels, the increased acid

concentration favours the vehicle mechanism. The presence of sulfonate groups will also retard the diffusion of H_3O^+ ions by electrostatic interactions.

2.5. Proton Conductivity Measurements

High proton conductivity is an important requirement for polymer membranes used as an electrolyte in fuel cell applications. A great challenge in fuel cell technology is to develop polymer membranes with high proton conductivity especially at dry conditions. Proton conductivity of fuel cell membrane is generally measured using an alternating current (a.c.) impedance spectroscopy technique. Accurate measurements of the specific conductivity of proton exchange membranes pose a significant experimental challenge. Many groups have studied the conductivity of Nafion membranes; predominantly using a.c. impedance although dc techniques have also been adopted.

2.6. Applications of Fuel Cells

Fuel cell has a low emission level, high efficiency and low maintenance requirement. It can use in stationary and portable power generation as well as transportation.

2.6.1. Stationary Power Generation

Fuel cells are considered for stationary power generation (1 - 500 kW) mainly due to the high conversion efficiencies, especially for Combined Heat and Power (CHP)

applications. Their efficiencies range from systems for residential use with a power of 1 to 10 kW to combined heat and power (CHP) plants of 250 kW. For instance, General Electric's Power Systems division and Plug Power have joined together to market, install and service residential natural gas fuelled PEMFC systems with capacities up to 35 kW [22]. The PEMFC offers rapid startup, which may be of paramount importance for auxiliary power supply systems. It allows on-site power generation, where the energy is actually required. The advantage in stationary systems is that there are not so strong weight and space constraints, which facilitates fuel cell system integration issues. Because of this, and the fact that cost targets for stationary fuel cell power plants are higher than for the other applications stationary power is currently viewed as the market where PEMFC systems will become competitive and commercial in the near future [23]. It is usually used as a backup power in buildings such as hotels, hospitals, industrial facilities or stand-by generators, factories, banks and shopping centres. It can be used to produce electricity and hot water in rural areas. A 7 kW module is already under trial operation at a home in the US. In the high power range, the joint venture between Alstom and Ballard introduced 250 kW PEMFC power systems operating on natural gas for premium power and back-up applications [24]. The plants are fuelled primarily with natural gas, and operation of complete, self-contained, stationary plants has been demonstrated using PEMFC, AFC, PAFC, MCFC, SOFC technology [25]. Using fuel cell as power generation will provide each housing development or apartment complex with its own power. This will remove the environmental pollution. Hospitals and airports have used fuel cell as backup power supplies in the time of a power failure.

2.6.2. Portable Applications

Portable fuel cells has extend the duration of grid independent operation with the production of less noise and higher quality of energy production [26]. It appears to be the most promising candidate for battery replacement for portable applications such as cellular phones, laptop, computers and video cameras, so that they can be functions in days or weeks without the need to plug a device into an electrical grid or use batteries, also safer and more environmentally friendly compared to batteries when it comes to recycling [25, 27]. It is very useful in areas where there's no electricity, it can be used to power telecommunications satellites and also provide power to computer chips. The Analytic Power Corporation reported on portable hydrogen fuelled PEMFC units, ranging from 50 to 500 W, for applications such as powering microclimate cooling systems [28]. It can safely produce power for biological applications, such as hearing aids and pacemakers [29]. These systems can be life savers in natural emergencies such as hurricanes, earthquakes, fires and ice storms. Portable fuel cells can provide reliable, high quality power in non-emergency situations as well, such as remote construction sites or even as a cost-effective solution for lighted trade show displays. In emergency response, military, law enforcement, transportation safety, and surveillance markets, fuel cells bring the benefits of longer run time and smaller, lighter, quieter systems.

2.6.3. Automotive Applications

PEM fuel cells have still remained the technology of choice for transportation systems. For automotive applications, primarily passenger cars and busses are the main issue and also the most challenging sector for mobile industries. The interest in fuel cells for vehicle propulsion is based on the demand for non-polluted environments and on the call for efficient energy use, resulting in less carbon dioxide emissions [30-32]. The car manufacturers like Toyota and Ford have chosen the methanol fuel cell as its storage and tank refilling is easy [33], while others such as Opel and General Motors have preferred to use pure hydrogen as there is enough storage space on the rooftop of the bus [31]. Since 1994, Daimler-Benz working in collaboration with Ballard built a series of PEMFC powered cars which fuelled with hydrogen. Daimler-Benz around 1997 introduced a methanol fuelled car with a 640 km range and also Ballard in that same year provided 205 kW PEMFC units for a small fleet of hydrogen-fuelled buses for demonstrations in Chicago, Illinois, and Vancouver, British Columbia [34].

2.7. Membranes

Membrane has become a separation technology over the past years and has been a competitive for conventional techniques. Their separation process is based on the presence of semi permeable membranes. Separation in synthetic membranes has put the terminology separation in a wider context. A range of separation of the chemicals/ mass transfer type have developed around the use of membranes including distillation,

extraction, absorption, adsorption, and stripping, as well as separations of the physical type such as filtration. This work will focus only on the Fuel cell membrane which classified according to their performance.

2.7. 1. Non-Perfluorinated Ionomers Membranes

The polymer electrolyte membranes based on aromatic hydrocarbon polymers are lower in cost, use in higher temperature and can be easily processed. But most of them have either lower proton conductivity or insufficient stability. These non-Perfluorinated membranes have high conductivity at higher sulfonation levels. Their drawback is they become water soluble, suffer from exclusive swelling and they have insufficient mechanical strength and also their sulfonation process is also difficult.

2.7.1.1. Poly (arylene ether ketone)s (PAEKs) / sulfonated poly(arylene ether ketone)s (SPAEKs)

Poly (arylene ether ketones)s **(**PAEKs**)** is an engineering plastic with high-performance [35, 36] having phenyl ring between ether and carbonyl linkages. These membranes are commercial high temperature membrane, having higher proton conductivity, good chemical resistance, good mechanical properties, good abrasion resistance, high fatigue endurance, excellent hydrolysis resistance, radiation resistance, thermal stability, resistance against burning and lower cost [37]. It can be used as alternatives to Nafion membrane as they have higher proton conductivity in their

sulfonation form [38-44] and also in their hydrated forms. Their shortcoming is that they have high water uptakes at higher temperature which resulted on the decreased of mechanical strength and proton conductivity and poor stability with relatively short life-time.

2.7.1.2. Polybenzimidazole (PBI)

Polybenzimidazole (PBI) membranes are a promising polymer electrolyte for both hydrogen and methanol fuel cells operating at high temperatures. PBI membrane is synthesised from aromatic bis-*o*-diamines and dicarboxylates (acids, esters, amides), either in molten state or in solution as shown in Figure 2.11 [45]. It is an amorphous thermoplastic polymer with a glass transition temperature (Tg) of 425-436 °C [46], having an excellent thermal and chemical stability, good mechanical properties [47], exhibits a good proton conductivity at low relative humidity and can produced cheaply [48]. This membrane has greater dimensional stability with a reduced methanol and hydrogen crossover when compared with Nafion membrane [49, 50]. PBI membrane can be modified by doping with several acids like sulphuric acid or phosphoric acid in order to improve its conductivity [47]. The conductivity is 2.2 x 10^{-2} S/cm at 190 ^{o}C for a PBI membrane with H_3PO_4 doping level of 5.01 [51].

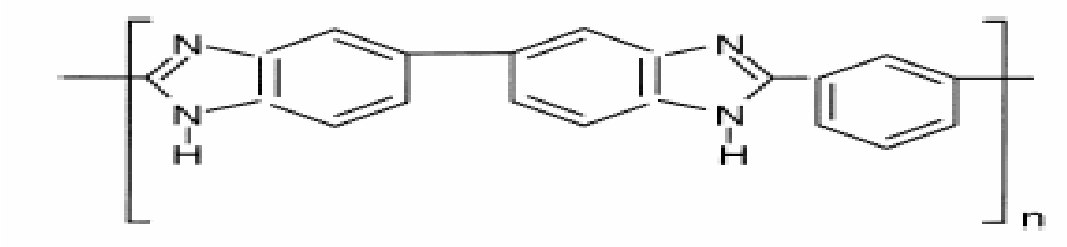

Figure 2.11: Chemical structure of PBI membrane.

2.7.1.3. Poly (ether etherketone)s (PEEK)s /sulfonated poly(ether ether ketone)s (SPEEK)s membranes

PEEK/SPEEK membrane is a high performance thermostable engineering polymer with an aromatic, non-fluorinated backbone. It's a semi-crystalline polymer for fuel cell application [52-55], their material are available and cheap [56] they have a good mechanical properties, chemical resistance, high thermal stability, toughness and high conductivity [57-60]. They have some disadvantages as low proton conductivity and their conductivity decreased with water content [61]. When they are sulfonated, they have shown good mechanical properties, proton conductivity and relatively low methanol permeability [62].Their proton conductivity is greatly dependent on the degree of sulfonation [63].The structure of sulfonated PEEK (SPEEK) is given in Figure 2.12. At low levels of sulfonation the aromatic polymers have lower water contents and reduced conductivity as the sulfonated groups of SPEEK were dispersed through the backbone of the polymers and not easily phase separated [64]. At high sulfonation, SPEEK membrane can swell under the humidified conditions of fuel cell environment and lose their mechanical strength and it can dissolve in water at high temperature [65, 66]. In order to reduce swelling the Sulfonated PEEK can be

chemically cross linked [67-69]. SPEEK-based PEM could have a lifetime of more than 3000 hours [70], which indicates that SPEEK may be durable enough under fuel cell operation conditions.

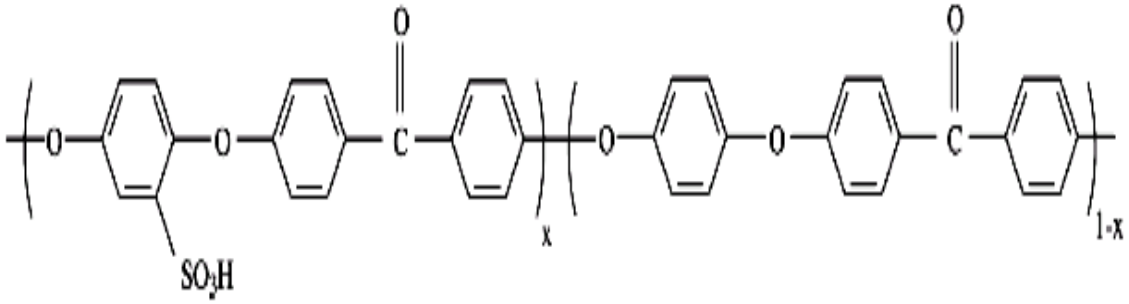

Figure 2. 12: Chemical structure of SPEEK membrane [71].

2.7.1.4.Poly(oxa-p-phenylene-3,3-phtalido-p-phenylene-oxa-p-phenilene-oxy-phenylene) (PEEK-WC)

Poly(oxa-*p*-phenylene-3,3-phtalido-*p*-phenylene-oxa-*p*-phenileneoxphenylene)(PEEK-WC) has a good chemical and mechanical stability, high proton conductivity, lower methanol permeability, high thermal and mechanical resistance. It is more amorphous and soluble in several organic solvents and also in some chlorohydrocarbons [72] and a lower cost when compared to that of the Nafion membrane. The use of chlorosulfonic acid as a powerful sulfonating agent led to formation of a polymer with a high degree of substitution without appreciable degradation [73]. It can also be modified with inorganic materials to obtain more efficient membranes for special applications [74].These membrane in its sulfonation state can be suitable used in fuel cell applications [75-78] because of its higher proton conductivity of $2.5x10^{-2}$ S/cm at 115 °C [79]. The higher degree of sulfonation can cause mechanical membrane failure

during operation [77]. The structural formula of SPEEK-WC is illustrated in Figure 2.13 below.

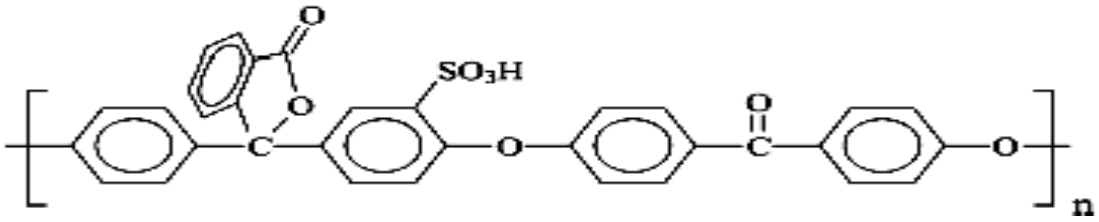

Figure 2. 13: **Structural formula of the SPEEK-WC membrane [79].**

2.7.1.5. Poly (arylene ether sulfone)(PAES) /Sulfonated poly (arylene ether sulfone) (SPAES) membranes

Poly (arylene ether sulfone)s (PAES) are engineering thermoplastics that have an excellent thermal and mechanical properties, as well as resistance to oxidation, radiation stability and the acid catalyzed hydrolysis [80-83]. These polymers can be used in the high temperature molding because of its good hydrolytic and thermo oxidative stability [84-88]. They are transparent, stiff (high modulus), tough thermoplastic materials with relatively high glass transition temperatures ranging from 180 - 250 ^{o}C. Their disadvantages is they are lower in proton conductivity, they depended on the water content of the membrane and their sulfonic acid groups are much lower than of Nafion.They can be sulfonated by sulfonic acid [89-93] to increases their proton conductivity and water absorption. It can function under high temperatures up to 160 °C under low humidity in its sulfonation state. The structural formula of PAES/SPAES membrane is illustrated in Figure 2.14.

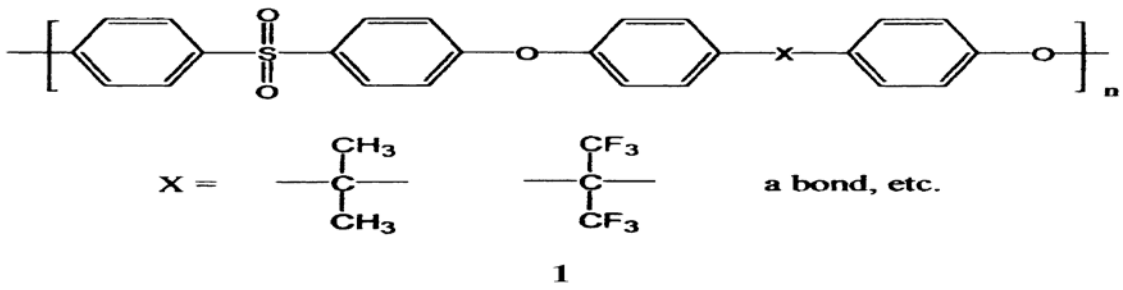

Figure 2. 14: Chemical structure of PAES/SPAES membrane.

2.7.1.6. Poly (4-phenoxybenzoyl-1, 4-phenylene) (PPBP)

The poly (4-phenoxybenzoyl-1, 4-phenylene) (PPBP) membrane are promising for high-performance polymers because of their excellent thermal and mechanical properties [94]. Their advantages are thy have higher performance in a direct hydrogen fuel cell, lower in cost, having excellence chemical and oxidative resistance, mechanical strength, high thermal stability and very high glass transition temperature, also have higher water uptake that makes them suitable function at higher temperature above 100 °C. PPBP membrane in its sulfonation form has high proton conductivities and high thermal stability when compared with that of Nafion membrane [95, 96]. Although SPPBP has excellent electrochemical potential as a PEM, its mechanical strength and flexibility are insufficient under humidified conditions. The micro-phase separation is important for hydrocarbon based polymer electrolyte membranes in order to achieve high conductivity comparable to Nafion at low relative humidity (RH) condition [97, 98].

2.7.1.7. Sulfonated poly (phthalazinone ether ketone) (SPPEK),

Sulfonated poly(phthalazinone ether ketone) (SPPEK) has chemical and oxidative resistance, mechanical strength, thermal stability, glass transition temperature (about 263 °C) and high proton conductivity [99-101] with a lower methanol permeation rate compared to Nafion membrane [102]. PPEK can be sulfonated by post-sulfonation and direct polymerization of pre-sulfonated monomers [99,100,103]. The SPPEK membrane prepared from direct polymerization of pre-sulfonated monomer has better performance in terms of thermal stability, water affinity and proton conductivity than that of post-sulfonation as the post-sulfonation technique may not only deteriorate the mechanical and thermal stabilities of resulting membrane material (because of the cleavage of ether bond), but also fail to control the degree and location of sulfonation [99].

2.7.1.8. Poly (vinyl acetate) (PVAc)

Poly (vinyl acetate) (PVAc) membrane is the most important water-soluble vinyl polymers. Its solubility in water depends on the degree of hydrolysis and the polymer chain length. It is prepared by partial or complete hydrolysis of PVAc [104]. PVAc membrane has a highly hydrophilic character, good film-forming properties and outstanding physical and chemical stability and is an excellent membrane material for the preparation of hydrophilic membranes. It is a useful material for the fabrication of reverse osmosis (RO) membranes, based on its hydrophilic nature and its reactivity toward cross-linking reagents [105, 106]. It is also widely used in medical, cosmetic,

packaging applications and as alcohol dehydrating agent. Its drawbacks are chemical constitution and water solubility which resulted on degradation and elimination of the membrane. PVAc membrane should be modified before use in order to produce long-term stability and higher proton conductivity of 10^{-2} S/cm. The modified membrane with the doped-impurity ions has reduced methanol crossover through the membrane than Nafion [107]. Therefore, PVAc based composite membranes can serve as a potential alternative polymer electrolyte membrane for DMFC applications.

2.7. 2. Partially fluorinated polymer

2.7.2.1. Poly (tetrafluoroethylene-co-hexafluoropropylene) (FEP)

FEP membrane has higher radiation resistance, excellent thermal, chemical, electrical (low dielectric constant), low surface energy properties and low cost [108-110]. Their disadvantages are for adhesion and wettability when bonding to other materials [111]. They can be modified using various methods such as wet chemical etching, electrochemical reduction, grafting, application and removal of metals, ion and electron beam techniques, and plasma modification [112]. FEP based radiation-grafted membranes its durability could be extended to several thousand hours when compared to that of Nafion membrane [113,114]. The structural formula of FEP membrane is illustrated in Figure 2.15.

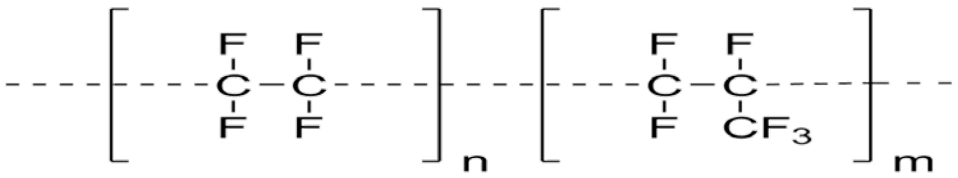

Figure 2. 15: Chemical structure of FEP membrane.

2.7.2.2. Poly (ethylene-alt- tetrafluoroethylene) (ETFE)

Poly (ethylene-*alt*-tetrafluoroethylene) (ETFE) has an excellent thermal stability, superior resistance to common solvents, heat resistance, mechanical stability, high resistance to radiation and fatigue [115]. ETFE membrane can be modified by grafted with other membrane followed by sulfonation and hydrolysis [116] in order to improve its selectivity and chemical stability. The modified membrane has a higher chemical stability than the traditional styrene/DVB-grafted membrane and six times lower methanol permeability compared to the Nafion 112 membrane [117].

2.7.2.3. Polytetrafluoroethylene (PTFE)

Polytetrafluoroethylene (PTFE) has excellent properties, such as an outstanding chemical resistance, thermal stability and hydrophobicity [118, 119]. Their property of chemical inertness makes it an ideal material for application in membrane filtration, especially in strong acid or highly corrosive liquid separation. The strong hydrophobic property of PTFE makes it widely applicable in gas separation, membrane distillation, osmotic distillation, supported liquid membranes and membrane contactors [120-123]. It can be modified by several method e.g dispersing zeolite in the PTFE matrix [124],

by preparing a pore-filling type PEM using porous PTFE substrates with an acrylic acid-vinylsulfonic acid cross linked gel [125], and also by cross linking of PTFE films by electron-beam irradiation and used them as substrates for grafting of two alkyl vinyl ether monomers, propyl vinyl ether (*n*PVE) and isopropyl vinyl ether (*i*PVE), followed by sulfonation reactions [126].

2.7. 3. Perfluorinated Ionomers Membranes

Perfluorinated ionomer membranes are well-established low temperature materials, which have a Teflon-like backbone structure with sulfonated side chains attached with ether groups. Within this family of polymers, Nafion membrane is the most advanced commercially available material.

2.7.3.1. Dow membrane

Dow membrane has a shorter side chain than Nafion membrane as shown in Figure 2.16 [127,128] but with similar structural and morphological properties. The Dow Chemical Company developed perfluorinated polymer membrane with low equivalent weight, typically in the range of 800-850 which make them applied in fuel cells as shown in Table 2.1 [129]. The performance of Dow membranes is superior to that of Nafion membrane with short life-time [130] and more expensive than Nafion membrane [131]. They have high proton conductivity and high chemical inertness but with high methanol permeation and water balance problems [132] and lack of safety

during manufacturing and use, requirements of supporting equipment and temperature-related limitations [133,134]. For fuel cells, this reduced resistance translates directly to performance and efficiency, since a membrane with this characteristic result in significantly enhanced proton transport rates with a lower e.m.f. driving force [135].

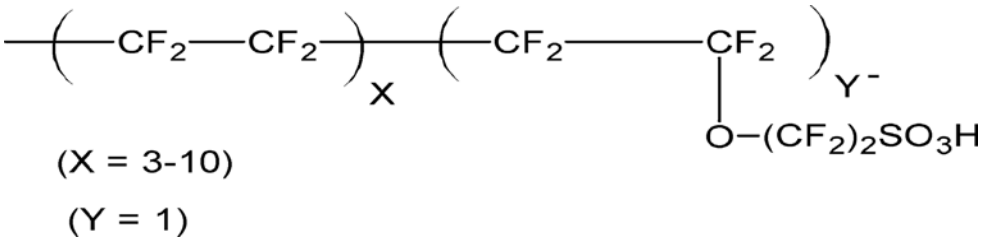

Figure 2. 16: Chemical structure of Dow ionomer membrane [132].

2.7.3.2. Aciplex-S

Aciplex-S is a sulfonated membrane with its performance similar to that of Nafion membrane [136]. Asahi Chemical Industry manufactured a series of Aciplex-S membranes, which have equivalent repeat unit molecular weights of 1000±1200 and dry state thicknesses of 25±100 mm as shown in Table 2.1 [137]. Aciplex-S membranes can be made thinner while still providing the same acid activity and thus a higher cation exchange capacity, and therefore a better conductivity [138]. It has good thermal, chemical, and mechanical properties due to their perfluorinated polymer backbones. Aciplex-S like other perfluorinated membranes is expensive. It has a complication and the longevity when manufacturing with the strongly toxic released [139]. The structural formula of Aciplex-S membrane is illustrated in Figure 2.17.

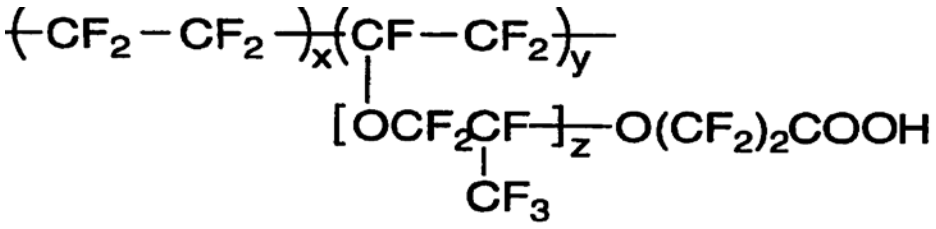

Figure 2. 17: Chemical structure of Aciplex perfluorinated membrane.

2.7.3.3. Flemion

Flemion membranes have a bi-layer structure that is comprised of sulfonic acid functional groups on the anode side and carboxylic acid functional groups on the cathode side [140]. Asashi Glass manufactured a series of Flemion membranes, which have equivalent repeat unit molecular weights of 1000 as shown in Table 2.1. This membrane can be made thinner while still providing the same acid activity and thus a higher cation exchange capacity, and therefore a better conductivity [137,141]. It has chemical stability, good mechanical properties and high ionic conductivity. Their main drawbacks are high in price, limited working temperature due to loss of water and reduced mechanical strength of the membrane above 100 ^{o}C, high methanol permeability and production process which release the strongly toxic to the environment [142, 143].

2.7.3.4. Nafion Membranes

Nafion membrane is the most widely used membranes in H_2-PEMFCs and direct methanol fuel cells (DMFCs) with the high proton conductivity around 0.2 S/cm at 80

°C and 100% relative humidity, good thermal and chemical stability [15,144,145,146]. It is the trade mark (produced by DuPont) of a perfluorinated material composed of carbon-fluorine backbone chains and perfluoro side chains with sulfonic acid ion-exchange groups which gives it high chemical resistance as shown in Figure 2.18 [147]. This Nafion membrane functions as both separator and an electrolyte in the fuel cell. Nafion membranes are now produced at various thicknesses, but mostly at about 1100 equivalent weights (Table 2.1). The researcher of Nafion membranes in the past several decades has shown that the membrane performance and intrinsic properties are dependent not only on its chemical identity but also on the method of film synthesis, the thermal history of the polymer (drying, exposure to high temperature, and membrane pretreatment) and the chemical history of the membrane (exposure to various cations, solvents, etc.) [148].

The development of Nafion began in the early 1960s when the DuPont Company's plastics exploration research group was expanding to fluorine technology that had previously resulted in the development of Teflon fluorocarbon resins and Viton fluoroelastomers. The group was studying new monomers for copolymerization with tetrafluoroethylene (TFE). They also developed a general method to synthesize perfluorinated vinyl ethers from perfluorinated acid fluorides, which resulted in vinyl ether-monomers, the starting point for Nafion as well as other novel commercial polymers. One of the acid fluorides studied, based on the reaction product of TFE and sulphur trioxide (SO_3^-), led to an unusual TFE copolymer containing branches with

pendant sulfonic acid groups (SO_3H) [149]. The structure of Nafion perfluorinated membrane is given in Figure 2.18.

Table 2. 1: Properties of perfluorinated membranes

Membrane Type	Typical Thickness (microns)	Equivalent Weight
Nafionseries (DuPont)		
Nafion120	260	1200
Nafion117	175	1100
Nafion 115	125	1100
Nafion112	50	1100
Nafion 111	25	1100
Nafion1135	87	1100
Nafion 1035	87	960
Nafion 105	125	960
Flemion series (Asashi Glass)		
Flemion T	120	1000
Flemion S	80	1000
Flemion R	50	1000
Aciplex-S (AsashiChemicals)		
Aciplex-S	25~100	1000~1200
Dow (Dow Chemicals)		
Dow	25	800

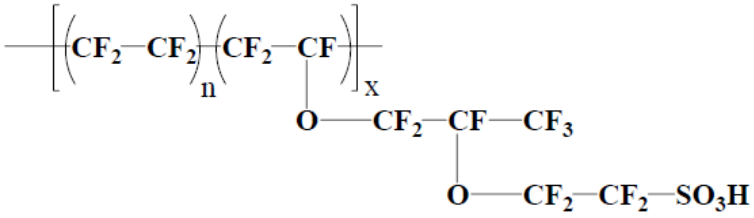

Figure 2. 18: Chemical structure of Nafion perfluorinated membrane.

a) Limitations of Nafion membranes

The performance of the PEM improves with increasing temperature until 90 ^{o}C, which reflects a decrease in the internal resistance of the cell. This decrease is due largely to the decrease in ohmic resistance of the electrolyte [150]. Nafion membranes do not perform well in DMFCs because of its high methanol crossover through the membrane from anode to cathode, high in production cost and also having a complicated and time-consuming manufacturing process [151]. Methanol crossover has two bad effects to the cells. Firstly, the chemical energy of methanol is lost when it crosses through the membrane, thus severely lowering the efficiency of fuel utilization [152]. Secondly, it is oxidized by the cathodic electro-catalyst, which depolarizes the electrode and subsequently increases the amount of air or oxygen. Since none of the energy from this oxidation is extracted as electricity, it all ends up as waste heat that increases the cooling load on the cell [153]. Nafion membrane performs very well in a saturated environment; its proton conductivity has a strong dependence on water content but if it is not properly hydrated, proton conduction becomes slow [154]. At higher temperatures, the PEM will dehydrate and lose proton conductivity, and may result in irreversible mechanical damage. However, higher working temperatures are

favourable for the kinetics of Pt catalyst and may improve its tolerance to contaminants [150]. Nafion membranes has osmotic swelling problem and is also potentially dissolved in methanol solution when increasing methanol concentration and temperature [147].The efforts to increase membrane working temperature and decrease the relative humidity are currently conducted on the laboratory scale, one of which is to incorporate nanoparticles.

2.7.4. Modification of Nafion Membranes

The modification efforts of Nafion membrane have recently been focused on minimizing the methanol crossover, which is particularly serious in the DMFC system. Many strategies have been developed to improve the water retention capability to enhance the proton conductivity of Nafion-based membranes at above 100 °C by the inclusion of hydrophilic ceramic/ inorganic fillers inside Nafion membrane.

One of the most commonly adopted methods is to introduce inorganic nanoparticles into the Nafion membrane, including silicon oxide (SiO_2), titanium dioxide (TiO_2) and zirconium oxide (ZrO_2) [155-165].The working temperature of Nafion membranes is limited at around 80-90 ^{o}C with high relative humidity, which constrains the tolerance of Pt catalysts to contaminants. Furthermore, poor proton conductivity at low hydration levels complicates the design of water management systems. Materials based on e.g. zirconium oxide, sulfated zirconia oxide, phosphated zirconia oxide, titanium dioxide and silicon oxide have been used to modify Nafion membrane.

2.7.4.1. Zirconium oxide nanoparticles membranes

The inorganic nanoparticles such as silica (SiO_2), titanium dioxide (TiO_2) and zirconium oxide (ZrO_2) etc. have been used for the modification of Nafion membranes. Incorporation of inorganic nanoparticles in the composite Nafion membranes improved the high temperature performance. It is found that the surface states of the inorganic nanoparticles play key role in holding water within the membrane, by the establishment of specific Lewis acid–base interactions. It is expected that the extent of water retention may depend on the degree of acidity of the ceramic powder and, thus, that further improvement may be obtained by using fillers with properly modified surface conditions [166]. Nafion/ZrO_2 nanocomposite membranes prepared by recast method showed a higher water uptake and conductivity than unmodified Nafion membranes at a higher temperature. All the nanocomposites exhibited better thermo mechanical properties than Nafion membrane. The degradation temperatures and *T*g improved for all nanocomposites. This shows that these membranes are tolerant to high temperature above 120 ^{o}C, which is a design goal of this work. Thus, both chemical and physical properties were modified by incorporating nanoparticles inorganic additives having higher acidity and water uptake properties. The membranes synthesized by recast methods were also very homogeneous. Since Nafion/ ZrO_2 nanocomposite membranes exhibited better water sorption and acidity.

2.7.4.2. Sulfated zirconia nanoparticles membranes

Sulfated zirconia (S-ZrO_2), a solid state super acid, is known to be a catalyst used for isomerization of *n*-butane at low temperatures and was widely studied in catalytic field [167, 168]. The sulfated zirconia nanoparticles provide extra proton sources in addition to their Nafion matrix [5, 169]. The advantages of these Nafion/ S-ZrO_2 nanocomposites membrane is to reduce swelling, better mechanical properties and reduction of methanol crossover. These nanocomposite membranes can be prepared through the following methods, recasting method, ion exchange method or swelling method. The sulfated zirconia in the form of nanoparticles was synthesized by precipitation method in order to obtain the smallest nanoparticles which are high in proton conductivity [170]. The modification of zirconium oxide by sulfuric acid, followed by a calcinations at about 600 ^{o}C, this making it attractive in terms of cost and resources [171]. Zirconia modified with sulfates exhibits superior catalytic activity. The presence of sulfates increases the stability of zirconia as well as the content of the tetragonal crystal phase, which is the one, believed to be catalytically active [172]. It had been reported that S-ZrO_2 exhibited a Hammett acid strength H_0 of -16.03, whereas for 100% sulfuric acid is only -11.99 and shows higher strength [173]. The properties of Nafion/ S-ZrO_2 nanocomposites membrane depend on the preparation method. Nafion/ S-ZrO_2 nanocomposites membrane prepared by three different methods and found that it had a high conductivity of >10^{-2} S/cm at 60-150 ^{o}C [170]. The high water affinity and the intrinsic acidity of the inorganic additive enhance the conductivity of the composite membrane and allow the cells using it to

operate at low relative humidity levels. In addition, the use of S-ZrO_2 based composite membranes also improves the high temperature response [174]. The high-temperature impedance response of the S-ZrO_2-doped Nafion-based cell was highly improved, showing a well-controlled charge-transfer resistance [166].

2.7.4.3. Phosphated zirconia membranes

Metal oxides nanoparticles have been obtained to have a strong acidity as well as a high catalytic activity. Zirconia activity is due to acidic, basic, oxidizing and reducing surface properties. It is known that zirconia assumes three polymorphic crystalline structures, monoclinic, tetragonal and cubic, depending on the calcinations temperatures. Incorporation of small amounts of phosphate anions, onto metal oxides has been found to remarkably increase the surface acidic properties and bulk crystalline of the oxides [175]. A proton conductivity of about 10^{-5} S/cm (at 150 ^{o}C under low humidity conditions) has been reported for layered hydrogen phosphated zirconium synthesized under hydrothermal conditions. A proton conductivity of 10^{-2} S/cm (at room temperature under humidified conditions) has been measured in phosphated zirconium glasses prepared through a sol-gel route.

2.7.4.4. Silicone Oxide

Nafion membrane was modified by incorporating of silica (SiO_2) through both solvent casting and in-situ synthesis methods. The results showed the methanol permeability was reduced with high silica content [176, 177]. There's a three-fold increase in the proton conductivity of a 4.3% SiO_2/ Nafion composite membrane (0.3 S/cm) when compared to that of Nafion membrane [178]. Nafion-silica membranes formed from in-situ synthesis techniques have also shown proton conductivity of 0.08 S/cm at 145 °C [179]. Though the fuel cell operation temperature exceeds 100 °C, performance decay was not observed for the modified Nafion membrane due to the inclination of membrane dehydration phenomenon as the hydrophilic inorganic particles (silica) retained more water content and influences the water transfer to the cathode [180]. The tensile strength of the silica modified membrane was 5.4×10^3 psi which is much higher than unmodified membrane whose tensile strength was 3.2×10^3 psi [181]. The modified Nafion membrane exhibited four times higher current density than that of unmodified Nafion at 130 °C under 3atm pressure [181]. Though the conductivities achieved for the composite range of $4.17 \times l0^{-7}$ cm^2 s^{-1} achieved for the 5 wt.% silica loaded membrane with the higher thermal stability influence its viable application [182]. At lower silica loadings, the hydrophilic silica particles may mainly exist around the hydrophilic ion cluster and the ion channels. Addition of silica particles increases tortuous nature of the methanol transport channels by changing the microstructure of Nafion. The cell voltage of 5 wt.% silica composite membrane was increased due to the lower methanol crossover [182].

2.7.4.5. Titanium oxide

Titanium dioxide (TiO_2) is a semiconductor material which has wide applications in optical and electronics materials because of its remarkable physical, chemical, optical characteristics, having powerful oxidation strength, high photo stability, and non-toxicity [183, 184]. TiO_2 is good hydrophilic filler to the polymer membranes, because it allows a suitable hydration of the membrane to be maintained, and the mechanical properties could be improved under fuel cell operating conditions [185,186]. The Nafion/TiO_2 composite membranes results show that the morphological properties of the filler play a major role in the performance of the composite membranes at a high operating temperature [187-191]. Nafion membrane incorporated with TiO_2 by sol-gel method showed an improved cell performance at 130 ^oC [192]. The incorporation of 3-5 wt% TiO_2 in Nafion membranes has shown superior performance in high temperature DMFCs, with a power density of 350 $mW.cm^{-2}$ at 145 ^oC with oxygen feed [183].The fuel cell performance increased with decreasing TiO_2 particle size, thus further suggesting that the filler morphology influences the electrochemical properties of the composite membrane [184]. But an increase in the TiO_2 content resulted in an increase in potential and current density [187].

2.8. References

[1] S. F. Au, *Innovative high temperature fuel cell systems*, DUP science, ISBN 90-407-2375-3 (2003).

[2] G. Wand, *Fuel cell history*, (2006) Part one.

[3] G. Hoogers, *Fuel cell technology handbook*, (2003) CRC press, ISBN 0-8493-0877-1.

[4] R. O'Hayre, S. Cha, W. Colella, F. B.Prinz, *Fuel cell fundamentals*, John Wiley & Sons, Inc, (2006) ISBN 0-471-74148-5.

[5] P. P. Kundu,V. Sharma, *Critical Reviews in Solid State and Materials Sciences* **32** (2007) 51-66.

[6] S. Basu, *Recent trends in fuel cell science and technology*, Anamaya, (2007) ISBN 0-387-355375.

[7] Alternative Energy eMagazine, http://www.fuelcells.org/.

[8] Fuel Cell Technologies Program,www.eere.energy.gov.

[9] J. Larminie, A. Dicks, *Fuel cell systems explained*, John Wiley& Sons, Ltd, (2003) ISBN 0-470-84857-X.

10] M. Tohidi, S. H. Mansouri, H. Amiri, *International Journal of Hydrogen Energy* **35** (2010) 9338-9348.

[11] V. Mishra, F. Yang, R. Pitchumani, *Journal of Power Sources* **141** (2005) 47-64.

[12] O. Savadogo, *Journal of Power Sources* **127** (2004) 135-161.

[13] L. Qingfeng, H. A. Hjuler, N. J. Bjerrum, *Journal of Applied Electrochemistry* **31** (2001) 773-779.

[14] M. X. Reinholdt, S. Kaliaguine, *Langmuir* **26** (2010) 11184-11195.

[15] W. Vielstich, H. Yokokawa, H. A. Gasteiger, *Handbook of Fuel cells Fundamentals Technology and Applications*, John Wiley & Sons, Inc, (2009) ISBN 978-0-72311-1.

[16] W. Lee, C. Ho, J. W. Van Zee, M. Murthy, *Journal of Power Sources* **84** (1999) 45-51.

[17] L. J. M. J. Blomen, M. N. Mugerwa, *Fuel cell systems*, Plenum press, (1993) ISBN 0-306-44158-6.

[18] M. P. Hogarth, T. R. Ralph, *Platinum Metals Review* **46** (2002) 146-164.

[19] A. A. Kornyshev, A. M. Kuznetsov, E. Spohr, J. Ulstrup, *Journal of Physical Chemistry* **107** *(*2003) 3351-3366.

[20] K. D. Kreuer, W. Weppner, A. Rabenau, *Solid State Ionics* **3/4** (1981) 353-358.

[21] D. P. Wilkinson, J. Zhang, R. Hui, J. Fergus, X. Li, *Proton exchange membrane fuel cells: Materials properties and performance*, CRC Press, (2010) ISBN 978-1-4398-0664-7.

[22] N. E. Vanderborgh, J. Guante, R. E. Dean, R. D. Sutton, *Fuel Cell Seminar* (1988) 52-56.

[23] H. A. Gasteiger, N. M. Markovic, P. N. Ross, *Journal of Physical Chemistry* **99** (1995) 16757-16767.

[24] H. -F. Oetien, V. M. Schmidt, U. Stumming, F. Tola, *Journal of Electrochemical Society* **143** (1996) 3838-3842.

[25] EG & G Technical Services, Inc, *Fuel Cell Handbook*, Science Applications International Corporation, DOE/NETL-2002/1179.

[26] J. G. Highfield, E. Unala, F. Geiger, V. Shklover, *ISIAnnual'Report / Annex V*(1995) 7-9.

[27] Fuel cell and hydrogen energy association,www.fchea.org.

[28] R. Kumar, S. Ahmed, M. Krumpelt, *Fuel Cell Seminar* (1996) 624-627

[29] R. M. Moore, S. Gottesfeld, P. Zelenay, *Electrochemical Society* **98** (1999) 365-379.

[30] R. Adzic, S. Brankovic, J. Wang, US Patent No: 6,670,301B2 (2003)

[31] B. Emonts, J. B. Hansen, S. L. Jorgensen, B. Hohlein, R. Peters, *Journal of Power Sources* **71** (1998) 288-293.

[32] J. Meusinger, B. Hohlein, R Menzer, E. Riensche, U. Summing, *2nd International Symposium on New Materials for Fuel Cell and Modern Battery Systems*, Ed. by O. Savadogo, P. R. Roberge, Montreal, Canada (1997) 522-535.

[33] R. Dillon, S. Srinivasan, A. S. Aricò, V. Antonucci, *Journal of Power Sources* **127** (2004) 112-126.

[34] K. Kordesch, G. Simader, *Fuel Cells and Their Applications*, VCH, (1996) ISBN 3-527-28579-2.

[35] L. H. Perng, *Journal of Polymer Science: Part A: Polymer Chemistry* **37** (1999) 4582-4590.

[36] X.Yue, H. Zhang, W. Chen, Y. Wang, S. Zhang, G. Wang, Z. Jiang, *Polymer* **48** (2007) 4715-4722.

[37] V. Percec, J. H. Wang, L.Yu, *Polymer Bulletin* **27**(1992) 503-510.

[38] M. L. Einsla, Y.S. Kim, M. Hawley, H–S. Lee, J. E. McGrath, B. Liu, M. D. Guiver, B. S. Pivovar, *Chemistry of Material* **20** (2008) 5636-5642.

[39] B. J. Liu, G. P. Robertson, D. S. Kim, M. D. Guiver, W. Hu, Z. H. Jiang, *Macromolecules* **40** (2007) 1934-1944.

[40] X. H. Ma, C. J. Zhang, G.Y. Xiao, D.Y.Yan, G. M. Sun, *Journal of Polymer Science: Part A: Polymer Chemistry* **46** (2008) 1758-1769.

[41] B. Lafitte, M. Puchner,P. Jannasch, *Macromolecular Rapid Communications* **26** (2005) 1464-1468.

[42] D. S. Kim, G. P. Robertson,M. D. Guiver, *Macromolecule* **41** (2008) 2126-2134.

[43] Y. Gao, G. P. Robertson, Y. S. Kim, K. Chen, A. S. Hay, *Macromolecules* **40** (2007) 4744-4746.

[44] J. H. Pang, H. B. Zhang, X. F. Li, Z. H. Jiang, *Macromolecules* **40** (2007) 9345-9442.

[45] D. J. Jones, J. Rozière, *Journal of Membrane Science* **185** (2001) 41-58.

[46] Q. Li, R. He, R.W. Berg, H.A. Hjuler, N.J. Bjerrum, *Solid State Ionics* **168** (2004) 177-185.

[47] S. R. Samms, S. Wasmus, R. F. Savinell, *Journal of Electrochemical Society* **143** (1996) 1225-1232.

[48] R. Bouchet, E. Siebert, *Solid State Ionics* **118** (1999) 287-299.

[49] B. S. Pivovar, Y. Wang, E. L. Cussler, *Journal of Membrane Science* **154** (1999) 155-162.

[50] P. Staiti, F. Lufrano, A. S. Aricò, E. Passalacqua, V. Antonucci, *Journal of Membrane Science* **188** (2001) 71-78.

[51] J. S. Wainright, J. T. Wang, D. Weng, R. F. Savinell, M. Litt, *Journal of Electrochemical Society* **142** (1995) L121-L123.

[52] O. Savadogo, *Journal of New Material Electrochemical System***1** (1998) 47-66.

[53] G. Inzelt, M. Pineri, J. W. Schultze, M. A. Vorotyntsev, *ElectrochimicaActa* **45** (2000) 2403-2421.

[54] G. Alberti, M. Casciola, L. Massinelli, B. Bauer, *Journal of Membrane Science* **185** (2001) 73-81.

[55] H. -H. Ulrich, G. Rafler, *Die Angewandte Makromolekulare Chemie* **263** (1998) 71-78.

[56]. K. D. Kreuer, *Solid State Ionics* **97**(1997) 1-15.

[57] A. E. Steck, C. Stone, in *Proc. 2nd International Symposium on New Materials for Fuel Cell and Modern Battery Systems,* Montreal *(*1997) 792-807.

[58] T. Kobayashi, M. Rikukawa, K. Sanui, N. Ogata, *Solid State Ionics* **106** (1998) 219-225.

[59] P. Xing, G. P. Robertson, M. D. Guiver, S. D. Mikhaelenko, K. Wang, S. Kaliaguine, *Journal of Membrane Science* **229** (2004) 95-106.

[60] M. H. D. Othman, S. L. Ho, A. Mustafa, A. F. Ismail, *The 3rd Regional Symposium on membrane Technology for Industry and Environmental Protection*, ITB-Bandung, Indonesia (2005).

[61] S. M. J. Zaidi, S. D. Mikhailenko, G. P. Robertson, S. Kaliaguine, *Journal of Membrane Science* **173** (2000) 17-34.

[62] M. J. Coplan, G. Gotz, US Patent no. 4,413,106 (1983).

[63] L. Li, J. Zhang, Y. Wang, *Journal of Membrane Science* **226** (2003) 159-167.

[64] C. Zhao, X. Li, Z. Wang, Z. Dou, S. Zhong, H. Na, *Journal of Membrane Science* **280** (2006) 643-650.

[65] C. Wu, S. Bo, M. Siddiq, G. Yang, T. Chen, *Macromolecules* **29** *(*1996) 2989-2993.

[66] S. D. Mikhailenko, S. M. J. Zaidi, S. Kaliaguine, *Catalysis Today* **67** (2001) 225-236.

[67] J. Kerres, W. Zhang, T. Haering, *Journal of New Materials for Electrochemical Systems* **7** (2004) 299-309.

[68] J. Kerres, A. Ullrich, T. Haring, M. Baldauf, U. Gebhardt, W. Preidel, *Journal of New Materials for Electrochemical Systems* **3** (2000) 229-239.

[69] J. Kerres, A. Ullrich, F. Meier, T. Haring, *Solid StateIonics* **125** (1999) 243-249.

[70] F. G. Wilhelm, I. G. M. Punt, N. F. A. van der Vegt, H. Strathmann, M. Wessling, *Journal of Membrane Science* **199** *(*2002) 167-176.

[71] M. Gil, X. Ji, X. Li, H. Nab, J. E. Hampsey, Y. Lu, *Journal of Membrane Science* **234** (2004) 75-81.

[72] H. Zhang, T. Chen, Y. Yuan, China Patent 85,108,751 (1985).

[73] F. Trotta, E. Drioli, G. Moraglio, E. B. Porna, *Journal of Applied Polymer Science* **70** (1998) 477-482.

[74] C. Yang, S. Srinivasan, A.B. Bocarsly, S. Tulyani, J. B. Benziger, *Journal of Membrane Science* **237** (2004) 145-161.

[75] A. Basile, L. Paturzo, A. Iulianelli, I. Gatto, E. Passalacqua, *Journal of Membrane Science* **281** (2006) 377-385.

[76] L. Paturzo, A. Basile, A. Iulianelli, J. C. Jansen, I. Gatto, E. Passalacqua, *Catalysis Today* **104** (2005) 213-218.

[77] A. Regina, E. Fontananova, E. Drioli, M. Casciola, M. Sganappa, F. Trotta, *Journal of Power Sources* **160** (2006) 139-147.

[78] D. J. Jones, J. Roziere, *Journal of Membrane Science* **185** (2001) 41-58.

[79] E. Drioli, A. Regina, M. Casciola, A. Oliveti, F. Trotta, T. Massari, *Journal of Membrane Science* **228** (2004) 139-148.

[80] L. M. Robeson, A. G. Farnham, J. E. McGrath, *Midland Macromolecular Institute Monographs* **4** (1978) 405-526.

[81] Y. S. Kim, M. A. Hickner, L. Dong, B. S. Pivovar, J. E. McGrath, *Journal of Membrane Science* **243** (2004) 317-326.

[82] Y.S. Kim, L. Dong, M. A. Hickner, B. S. Pivovar, J. E. McGrath, *Polymer* **44** (2003) 5729-5736.

[83] J. J. Dumais, A. L. Cholli, L. W. Jelinski, J. L. Hedrick, J. E. McGrath, *Macromolecules* **19** (1986) 1884-1889.

[84] S. Wang, J. E. McGrath, *Synthesis of Poly(Arylene Ether)s, in Synthetic Methods in Step-Growth Polymers* (Eds M. E. Rogers and T. E. Long), John Wiley & Sons, Inc, (2003) DOI: 10.1002/0471220523.

[85] J. B. Rose, *Polymer* **15** (1974) 456-465.

[86] P. M. Hergenorther, J. W. Connell, J. W. Labadie, J. L. Hedrick, *Advances in Polymer Science* **117** (1994) 67-110.

[87] P. J. Blackwell, W. H. Beever, US Patent No:5,049,446 (1991).

[88 Y. Gao, G. P. Robertson, M. D. Guiver, X. Jian, S. D. Mikhailenko, K. Wang, S. Kaliaguine, *Journal of Polymer Science Part A: Polymer Chemistry* **41** (2003) 2731-2742.

[89] J. Kerres, W. Cui, S. J. Reichle, *Polymer Science, Part A: Polymer Chemistry* **34** (1996) 2421-2438.

[90] F. Wang, M. Hickner, Y. S. Kim, T. A. Zawodzinski, J. E. McGrath, *Journal of Membrane Science* **197** (2002) 231-242.

[91] K. Miyatake, Y. Chikashige, M. Watanabe, *Macromolecules* **36** (2003) 9691-9693.

[92] L. E. Karlsson, P. Jannasch, *Journal of Membrane Science* **230** (2004) 61-70.

[93] S. Matsumura, A. R. Hlil, C. Lepiller, J. Gaudet, D. Guay, Z. Shi, S. Holdcroft, A. S. Hay, *Macromolecules* **41** (2008) 281-284.

[94] H. Ghassemi, G. Vdip, J. E. McGrath, *Polymer* **45** (2004) 5855-5862.

[95] J. -M. Bae, I. Honma, M. Murata, T. Yamamoto, M. Rikukawa, N. Ogata, *Solid State Ionics* **147** (2002) 189-194.

[96] T. Kobayashi, M. Rikukawa, K. Sanui, N. Ogata, *Solid State Ionics* **106** (1998) 219-225.

[97] H. S. Lee, A. S. Badami, A. Roy, J. E. McGrath, *Journal of Polymer Science Part A*, **45** (2007) 4879-4890.

[98] H. S. Lee, A. Roy, O. Lane, S. Dunn, J. E. McGrath, *Polymer* **49** (2008) 715-723.

[99] S. H. Tian, D. Shua, Y. L. Chen, M. Xiao, Y. Z. Meng, *Journal of Power Sources* **158** (2005) 88-93.

[100] Y. Gao, G. P. Robertson, M. D. Guiver, X. Jian, S. D. Mikhailenko, K. Wang, S. Kaliaguine, *Journal of Membrane Science* **227** (2003) 39-50.

[101] Y. Gao, G. P. Robertson, M. D. Guiver, X. Jian, S. D. Mikhailenko, S. Kaliaguine, *Solid State Ionics* **176** (2005) 409-415.

[102] S. P. Nunes, B. Ruffmann, E. Rikowski, S. Vetter, K. Richau, *Journal of Membrane Science* **203** (2002) 215-225.

[103] Y. H. Su, Y. L. Liu, Y. M. Sun, J. Y. Lai, M. D. Guiver, Y. Gao, *Journal of Power Sources* **155** (2005) 111-117.

[104] E. Chiellini, A. Corti, S. D'Antone, R. Solaro, *Progress in Polymer Science* **28** (2003) 963-1014.

[105] A. M. Hassanien, M. A. El-Hashash, M. A. Mekewi, D. B. Guirguis, A. M. Ramadan, *Hydrology Current Research* **4** (2013) 1-6.

[106] G. S. Mukherjee, N. Shukla, R. K. Singh, G. N. Mathur, *Journal of Scientific and Industrial Research* **63** (2004) 596-602.

[107] B. S, Pivovar, Y., Wang, E. L. Cussler, *Journal of Membrane Science* **154** (1999) 155-162.

[108] A. L. Logothetis, *Progress in Polymer Science* **14** (1989) 251-296.

[109] B. Ameduri, B. Boutevin, G. K. Kostov, *Progress in Polymer Science* **26** (2001)105-187.

[110] A. Taguet, B. Ameduri, B. Boutevin, *Advances in Polymer Science* **184** (2005) 127-211.

[111] C. R. Davis, F. D. Egitto, *Chemtech* **25** (1995) 44-50.

[112] L. M. Siperko, R. R. Thomas, *Journal of Adhesion Science and Technology* **3** (1989) 157-173.

[113] L. Gubler, S. A. Gu¨rsel, G. G. Scherer, *Fuel Cells* **5** (2005) 317-335.

[114] L. Gubler, H. Kuhn, T. J. Schmidt, G. G. Scherer, H. P. Brack, F. Simbeck, *Fuel Cells* **4** (2004) 196-207.

[115] D. P. Carlson, W. Schmiegel, in: W. Gerhartz (Ed.), *Ullmanns Encyclopedia of Industrial Chemistry* **A13** (1988) 393-427.

[116] J. Chen, M. Asano, T. Yamaki, M. Yoshida, *Journal of Membrane Science* **269** (2005) 194-204.

[117] M. Shen, S. Roy, J. W. Kuhlmann, K. Scott, K. Lovell, J. A. Horsfall, *Journal of Membrane Science* **251** (2005) 121-130.

[118] D. Newman, F. Morizio, S. Kidd, US Patent 6,274,043(2001).

[119] Z. Ding, R. Ma, A. G. Fane, *Desalination* **151** (2002) 217-227.

[120] C. S. Feng, R. Wang, B. L. Shi, *Journal of Membrane Science* **277** (2006) 55-64.

[121] M. Goessi, T. Tervoort, *Journal of Membrane Science* **42** (2007) 7983-7990.

[122] K. Kurumada, T. Kitamura, N. Fukumoto, M. Oshima, M. Tanigaki, S. Kanazawa, *Journal of Membrane Science* **149** (1998) 51-57.

[123] H. K. Lonsdale, *Journal of Membrane Science* **10** (1981) 81-181.

[124] Z. Połtarzewski, W. Wieczorek, J. Przyłuski, V. Antonucci, *Solid State Ionics* **119** (1999) 301-304.

[125] T. Yamaguchi, F. Miyata, S. Nakao, *Journal of Membrane Science* **214** (2003) 283-292.

[126] J. Chen, M. Asano, T. Yamaki, M.Yoshida, *Journal of Membrane Science* **256** (2005) 38-45.

[127] K. Prater, *Journal of Power Sources* **29** (1990) 239-250.

[128] P. Costamagna, S. Srinivasan, *Journal of Power Sources* **102** (2001) 242-252.

[129] F. Babir, T. Gomez, *International Journal of Hydrogen Energy* **21** (1996) 891-901.

[130] R. Souzy, B. Ameduri, *Progress Polymer Science* **30** (2005) 644-687.

[131] V. I. Basura, C. Chuy, P. D. Beattie, S. Holdcroft, *Journal of Electroanalytical Chemistry* **501**(2001) 77-88.

[132] S. Surampudi, S. R. Narayanan, E. Vamos, H. Frank, G. Halpert, A. LaConti, J. Kosek, G. K. Surya Prakash, G. A. Olah, *Journal of Power Sources* **47** (1994) 377-385.

[133] S. M. J. Zaidi, T. Matsuura (eds.), *Polymer Membranes for Fuel Cells* (2009) 7-25.

[134] J. Hoadley, R. Lawrence, *Proceeding Fuel Cell Seminar, Long Beach, CA, United States of America (1988)* 263-266.

[135] *G.* A. Eisman, *Journal of Power Sources **29*** (1990) 389-398.

[136] A. P. Sunda, A. Venkatnathan, *Soft Matter* **8** (2012) 10827-10836.

[137] M. H. D. Othman, A. F. Ismail, A. Mustafa, *Malaysian Polymer Journal* **5** (2010) 1-36.

[138] A. Weber, Z. Newman, J. Newman, *Journal of the Electrochemical Society* **150** (2003) A1008-A1015.

[139] J. A. Kerres, *Journal of Membrane Science* **185** (2001) 3-27.

[140] N. Yoshida, T., Ishisaki, A. Watakabe, M. Yoshitake, *Electrochimica Acta* **43** (1998) 3749-3754.

[141] J. T. Hinatsu, M. Mizuhata, H. Takenaka, *Journal of the Electrochemical Society* **141** (1994) 1493-1498.

[142] J. Ding, Q. Tang, S. Holdcroft, *Australian Journal of Chemistry* **55** (2002) 461-466.

[143] M. Baldauf, W. Preidel, *Journal of Power Sources* **84** (1999) 161-166.

[144] S. Ren, G. Sun, C. Li, S. Song, Q. Xin, X. Yang, *Journal of Power Sources* **157** (2006) 724-726.

[145] M. Hogarth, X. Glipa, *High temperature membranes for solid polymer fuel cells***,** Johnson Matthey Technology Centre, DTI Publication, URN 01/893, 1-72.

[146] K. Miyatake, H. Iyotani, K. Yamamoto, E. Tsuchida, *Macromolecules* **29** (1996) 6969-6971.

[147] L. C. Kleina, Y. Daikoa, M. Aparicio, F. Damay, *Polyme*r **46** (2005) 4504-4509.

[148] J. E. Hensley, J. D. Way, S. F. Dec, K. D. Abney, *Journal of Membrane Science* **298** (2007) 190-201.

[149] S. Banerjee, D. E. Curtin, *Journal of Fluorine Chemistry* **125** (2004) 1211-1216.

[150] C. Yang, P. Costamagna, S. Srinivasan, J. Benziger, A. B. Bocarsly, *Journal of Power Sources* **103** (2001) 1-9.

[151] K. M. Taft, M. R. Kurano, US Patent no 6,630,265 (2003).

[152] B. Libby, W. H. Smyrl, E. L. Cussler, *AIChE Journal* **49** (2003) 991-1001.

[153] J. O. Murphy, A. L. Cisar, US Patent no 6**,**387,230 (2002).

[154] T. A. Zawodzinski, J. Davey, J. Valerio, S. Gottesfeld, *Electrochimica Acta* **40** (1995) 297-302.

[155] K. T. Adjemian, R. Dominey, L. Krishnan, H. Ota, P .Majsztrik, T. Zhang, J. Mann, B. Kirby, L. Gatto, M. Velo-Simpson, J. Leahy, S. Srinivasant, J . B. Benziger, A. B. Bocarsly, *Chemistry of Materials* **18** (2006) 2238-2248.

[156] K. T. Adjemian, S. J. Lee, S. Srinivasan, J. Benziger, A. B. Bocarsly, *Journal of the Electrochemical Society* **149** (2002) A256-A261.

[157] K. T. Adjemian, S. Srinivasan, J. Benziger, A. B. Bocarsly, *Journal of Power Sources* **109** (2002) 356-364.

[158] G. Alberti, M. Casciola, D. Capitani, A. Donnadio , R. Narducci , M. Pica , M. Sganappa, *Electrochimica Acta*, **52** (2007) 8125-8132.

[159] P. Costamagna, C. Yang, A. B. Bocarsly, S. Srinivasan, *Electrochimica Acta* **47** (2002) 1023-1033.

[160] M. Casciola, D. Capitani, A. Comite, A. Donnadio, V. Frittella, M. Pica, M. Sganappa, A. Varzi, *Fuel Cells* **8** (2008) 217-224.

[161] T. Jian-Hua, G. Peng-Fei, *International Journal of Hydrogen Energy* **33** (2008) 5686-5690.

[162] P. L. Antonucci, A. S. Aroco, P. Creti, R. Ramunni, V. Antonucci, *Solid State Ionics* **25** (1999) 431-437.

[163] P. Dimitrova, K. A. Friedrich, B. Vogt, U. Stimming, *Journal of Electroanalytical Chemistry* **532** (2002) 75-83.

[164] Z. Shao, H. Xu, M. Li, I. Hsing, Solid *State Ionics* **177** (2006) 779-785.

[165] W. Xu, T. Lu, C. Liua, W. Xinga, *Electrochimica Acta* **50** (2005) 3280-3285.

[166] M. A. Navarra, F. Croce, B. Scrosati, *Journal of Materials Chemistry* **17** (2007) 3210-3215.

[167] G. Larsen, E.Lotero, R. D.Parra, L. M. Petkovic, H. S. Silva, S. Raghavan, *Applied Catalysis* **130** (1995) 213-266.

[168] B. H. Davis, A. R. Keogh, R. Srinivasan, *Catalysis Today* **20** (1994) 219-256.

[169] A. D'Epifanio, M. A. Navarra, F. C. Weise, B. Mecheri, J. Farrington, S. Licoccia, S. Greenbaum, *Chemistry of Material* **22** (2010) 813-821.

[170] S. Tominaka, N. Akiyama, F. Croce, T. Momma, B. Scrosati, T. Osaka, *Journal of Power Sources* **185** (2008) 656-663.

[171] S. Hara, M. Miyayama, *Solid State Ionics* **168** (2004) 111-116.

[172] A. Zarubica, B. Jovic, A. Nikolic, P. Putanov, G. Boskovic, *Journal of the Serbian Chemical Society* **12** (2009) 1429-1442.

[173] G. D. Yadav, J. J. Nair, Microporous and Mesoporous Materials **33** (1999) 1-48.

[174] M. A. Navarra, C. Abbati, B. Scrosati, *Journal of Power Sources* **183** (2008) 109-113.

[175] F. Abbattista, A. Delastro, G. Gozzelino, D. Mazza,M. Vallino, G. Busca, V. Lorenzelli, *Journal of the Chemical Society, Faraday Transactions* **86** (1990) 3653-3658.

[176] N. Miyake, J. S. Wainright, R. F. Savinell, *Journal of Electrochemical Society* **148** (2001) A905-A909.

[177] R-H. Song, S. Dheenadayalan, D-R. Shin, *Journal of Power Sources* **106** (2002) 167-172

[178] P. Dimitrova, K. A. Friedrich, B. Vogt, U. Stimming, *Jourmal of Electroanalytical Chemistry* **532** (2002) 75-83.

[179] D. H. Jung, S. Y. Cho, D. H. Peck, D. R. Shin, J. S. Kim, *Journal of Power Sources* **106** (2002) 173-177

[180] P. Antonucci, A. Arico, P. Creti, E. Ramunni, V. Antonucci, *Solid State Ionics* **125** (1999) 431- 437.

[181] N. Miyake, J. Wainright, R. Savinell, *Journal of Electrochemical Society* **148** (2001) A898-A904.

[182] R. Jiang, H. Kunz, J. Fenton, *Journal of Membrane Science* **272** (2006) 116-124.

[183] Z. L. Liu, B. Guo, J. C. Huang, L. Hong, M. Han, L. M. Gan, *Journal of Power Sources* **157** (2006) 207-211.

[184] E. Chalkova, M. B. Pague, M. V. Fedkin, D. J. Wesolowski, S. N. Lvov, *Journal of The Electrochemical Society* **152** (2005) A1035-A1040.

[185] E. Chalkova, M. B. Pague, M. V. Fedkin, D. J. Wesolowski, S. N. Lvov, *Journal of The Electrochemical Society* **152** (2005) A1742-A1747.

[186] B. R. Matos, E. I. Santiago, F. C. Fonseca, M. Linardi, V. Lavayen, R. G. Lacerda, L.O. Ladeira, A. S. Ferlauto, *Journal of The Electrochemical Society* **154** (2007) B1358-B1361.

[187] V. Baglio, A. S. Aric‘o, A. D. Blasi, V. Antonucci, P. L. Antonucci, S. Licoccia, E. Traversa, F. S. Fiory, *Electrochimica Acta* **50** (2005) 1241-1246.

[188] V. Baglio, A. D. Blasi, A. S. Aric‘o, V. Antonucci, P. L. Antonucci, C. J. Trakanprapai, V. Esposito, S. Licoccia, E. Traversa, *Journal of Electrochemical Society* **152** (2005) A1373-A1377.

[189] A. Sacc’a, A. Carbone, E. Passalacqua, A. D’Epifanio, S. Licoccia, E. Traversa, E. Sala, F. Traini, R. Ornelas, *Journal of Power Sources* **152** (2005) 16-21.

[190] C. Trakanprapai, V. Esposito, S. Licoccia, E. Traversa, *Journal of Material Research* **20** (2005) 128-134.

[191] S. Y. Chen, C. C. Han, C. H. Tsai, J. Huang, Y.W. Chen-Yang, *Journal of Power Sources* **171** (2007) 363-372.

[192] E. I. Santiago, R. A. Isidoro, M. A. Dresch, B. R. Matos, M. Linardi, F. C. Fonseca, *Electrochimica Acta* **54** (2009) 4111-4117.

CHAPTER THREE

3. CHEMICALS, CHARACTERAZATION TECHNIQUES AND METHODS

3.1. Chemicals

N, N-dimethylformade (Merck)

1-Propanol (Merck)

Sulfuric Acid (Merck)

Toluene (Merck)

Zirconium oxychloride hydrate (Merck)

Methanol (Merck)

Iso-propanol (Merck)

Nafion solution (Ion Power)

Nafion 117 (Aldrich)

Ammonia solution (Merck)

Ethanol (Merck)

Diammonium hydrogen phosphate (Merck)

N, N-Dimethylacetamide (Merck)

Sodium chloride (Merck)

Sodium hydroxide (Merck)

Phenolphthalein (Merck)

Silver Nitrate (Merck)

3.2. Characterization Techniques

The nanoparticles and membrane films synthesized in this thesis were characterized by using various techniques such as XRD, TGA, FTIR, BET, SEM and TEM which will be explain further in this section.

3.2.1. The X-ray powder diffraction (XRD) analysis

X-ray diffraction was used to identify the crystallinity, crystal size and elemental composition in the samples. A diffracto-meter with a Cu tube was used with a wavelength λ = 1.5 nm. The diffracto-meter operates in the (θ -2θ) geometry. The detector rotates at twice the rate of the sample and is at an angle of 2θ with respect to the incoming x-ray beam. The x-rays reflected from the different planes in the crystal undergo interference with each other as illustrated in Figure 3.1.

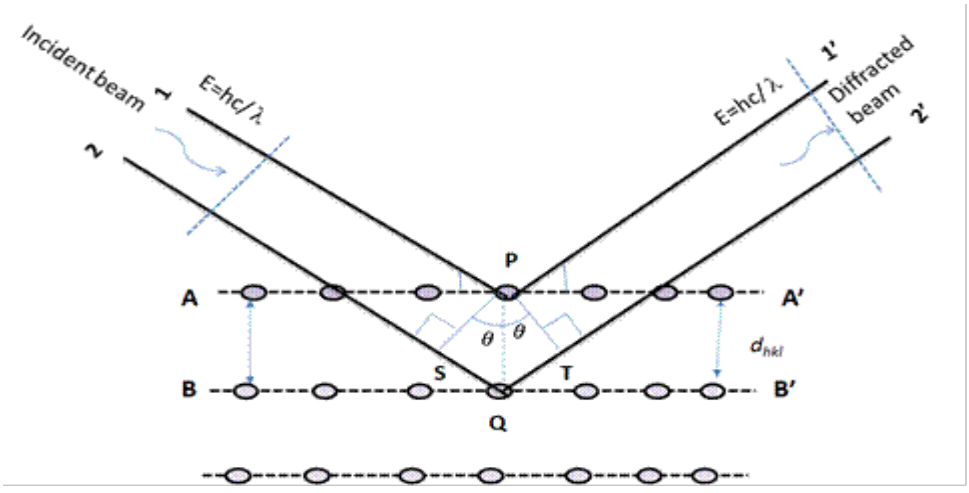

Table 3. 1: Interference of radiation between atomic planes in a crystal.

The basis for x-ray diffraction is described by the Bragg's law, equation 3.1, which describes the condition of constructive interference of x-rays, scattered from atomic planes of a crystal by this equation:

$$n\lambda = 2dSin\theta \tag{3.1}$$

where n is an integer, λ is the wavelength of the radiation, d is the spacing between atomic planes and θ the angle between the radiation and atomic planes, known as the Bragg angle [1]. This relation demonstrates that interference effects are observable only when radiation interacts with physical dimensions that are approximately the same size as the wavelength of the radiation. During the first order reflection constructive and destructive interference takes place. Constructive interference occurs if the rays that are scattered by all atoms in all the planes are in phase and reinforce one another to form a diffracted beam. While in destructive interference all the scattered beams are out of phase and cancel one another leading to no scattering. For the first order diffraction, n =1, the Bragg's law can be written as:

$$\lambda = 2dSin\theta \tag{3.2}$$

Figure 3.1 show the interference of radiation between atomic planes in a crystal. Two parallel planes of atoms A–A' and B–B' which have the same h, k, and l Miller indices separated by the interplanar spacing d_{hkl} are shown in Figure 3.1. If we assume that a parallel, monochromatic, and coherent (in-phase) beam of x-rays of wavelength λ is incident on these two planes at an angle θ. Two rays in this beam, labelled 1 and 2, are scattered by atoms P and Q. Constructive interference of the scattered rays 1′ and 2′

occurs also at an angle θ to the planes, if the path length difference between 1–P–1′ and 2–Q–2′ is equal to a whole number, n, of wavelengths. That is the condition for Bragg's law.

In this work, the XRD analysis was performed using a Philips X-ray automated diffracto-meter (Model: PW 1830 diffracto-meter, Phillips, Netherland) with filtered 0.154056 nm Cu Kα radiation. The analyzed materials were finely grounded, homogenized, and average bulk composition was determined. Samples are scanned in a continuous mode from 10° - 90° with a scanning rate of 0.026 (degree) / 1 (sec). The diffraction patterns, (versus *I*:*I*°) *d*-spacing (A), were compared, for identification purposes, with relevant ASTM and JCPDS standards. The diffraction measured in the above mentioned steep scan range were due to the following: the (111)t reflections of the metastable tetragonal phase and the $(111)^{-m}$ and $(111)_m$ reflections of the stable monoclinic phase.

3.2.2. Powder and membrane thermo-gravimetric analysis (TGA)

The thermal properties of the samples were studied by thermal gravimetric analysis (TGA) under nitrogen flow. TGA data was obtained with model STA (Simultaneous Thermal Analyzer) 1500 (supplied by Rheometric Scientific Ltd, UK), over nitrogen and at a heating rate of 10 °C/min from 50 ^{o}C to 1000 ^{o}C.

3.2.3. Fourier Transform Infrared Spectroscopy (FTIR)

Fourier transform infrared spectroscopy (FTIR) is a powerful tool used to determine the chemical structure of the sample. The sample information on FTIR is obtained by passing IR radiation through a sample and some of the FTIR radiation will be absorbed by the sample and some will be transmitted or reflected. The resulting spectrum will represents the molecular absorption and transmission, creating a molecular fingerprint of the sample. This makes FTIR spectroscopy useful for several types of analysis such as identifying unknown materials. The FTIR spectra were obtained using a Perkin-Elmer Paragon 1000 FTIR instrument over the range of 4000-500 cm^{-1} and a resolution of 4 cm^{-1}. A small amount of material was placed on the diamond coated detector and pressed onto the electrode to get FTIR measurements.

3.2.4. Brunau-Emmett-Teller (BET) surface area.

The BET analysis provides precise specific surface area evaluation of materials by nitrogen multilayer adsorption measured as function of relative pressure using a fully automated analyzer. The technique encompasses external area and pore area evaluation to determine the total specific area in m^2/g yielding important in studying the effects of surface porosity and particle size in many applications. The BET analysis was performed using Accelerated SA (ASAP) 2010 system. A dry sample was evacuated of all gas and cooled to 77 K, using liquid nitrogen. A layer of inert gas physically adheres to the sample surface, lowering pressure in the analysis chamber.

The surface area was calculated from the measured absorption isotherm of the experiment. Before analysis, all the samples were out-gassed at 200-300^{o}C under vacuum for 2 hours. Test materials were out gassed to the pressure of 3×10^{-5} mbar for 2 hours at 470 K, prior to adsorption measurements. The measurements were carried out on the synthesized powders. The particle size was calculated by the Equation (3.3).

$$S = \frac{6}{\rho D_{BET}} x10^{3} \qquad (3.3)$$

Where ρ is the theoretical density of the materials which equal to 6.27 g/cm^3 [2] and D_{BET} is the particle size in nm.

3.2.5. Scanning electron microscopy (SEM)

The SEM utilizes a focused beam of high-energy electrons that systematically scans across the surface of a specimen. The electron beam is generated within an electron gun, accelerated by a high voltage and formed into a fine probe by electromagnetic lenses. The electron-optical column, through which the beam passes, is held under high vacuum to allow a free path for the electrons to pass through as well as to prevent high voltage discharge. The first lens that influences the beam is the condenser lens, which causes the beam to converge and pass through a focal point just above a condenser aperture. The intensity of the electron beam when it strikes the specimen,

and hence the brightness of the image signal is primarily determined by the condenser lens, in conjunction with the chosen accelerating voltage. The beam diverges again below the condenser aperture and is brought into focus at the specimen through the demagnification of a final lens, the objective lens. This final lens demagnification determines the diameter of the spot size of the electron beam at the specimen, which in turn determines the specimen resolution.

The instrument used to obtain the surface and cross-section of the composite membranes and nanoparticles was Hitachi x650 (FEI, Mode:Quanta 200). Scanning electron microscopy (SEM) samples were prepared by placing some of the nanoparticle materials onto an aluminium stub using adhesive carbon tape. The samples were sputter-coated with gold to prevent charging effects inside the microscope. The composite membranes were cut into small pieces under liquid nitrogen and their cross-section was also sputtered with gold before analysing.

3.2.6. Transmission electron microscopy (TEM)

Transmission electron microscopy (TEM) is a microscopy technique whereby a beam of electrons is transmitted through an ultra-thin specimen, interacting with the specimen as it passes through. The Leo 912 TEM was used to estimate the particle size of the powder and observe the morphology of the nanopowder and membranes cross section. The powders were suspended in methanol in an ultrasonic bath, followed by dropping some suspension onto a copper grid. For membrane sectioning, a Reichert

Ultracut S (Leica) ultramicrotome was used. The sample was embedded in resin. Then, a cross section was cut off using the ultramicrotome with a glass knife fitted with a water boat. After sectioning, the copper grids were dipped in the boat to capture the samples.

3.3. METHODS

3.3.1. Conductivity Measurement

The ionic conductivities of nanocomposite membrane were measured in a two electrode cell using a.c. impedance spectroscopy at different temperatures and relative humidity (RH) [3-5]. Conductivity measurements can be performed using a four-point collinear probe method [6]. The ionic conductivity was determined using an Autolab PGSTAT302 at galvanostatic mode with ac current amplitude of 0.1 mA over frequencies ranging from 1MHz to 10Hz, under the 100% RH for 25-80 ^{o}C and 50 RH% for 85-90 ^{o}C [7]. Using a Bode plot, the frequency region over which the impedance had a constant value was checked, and the electrical resistance was then obtained from a Nyquist plot [8]. The ionic conductivity (k) was calculated according to the following equation [9]:

$$k = \frac{L}{RWd} \qquad (3.4)$$

where R is the obtained membrane resistance, L is the distance between potential-sensing electrodes (1 cm), and W and d are the width (2 cm) and thickness of the

membrane. For conductivity testing, the membrane was immersed in 1M sulfuric acid solution for 6 hours at room temperature. The membrane was then rinsed with deionized water several times to remove any excess H_2SO_4 and then immersed in deionized water for 6 hours at 60 ^oC. All the membranes were kept in deionized water at room temperature before conductivity testing measurement.

3.3.2. Water uptake (Wup %)

The water-uptake of the membrane was determined by immersing the membrane into water at room temperature for 24 hours. The membrane will be taken out, wiped with tissue paper and weighed immediately on the micro-balance. Water uptake will be calculated according to the following equation:

$$\mathrm{Wup}(\%) = \frac{(\mathrm{mwet} - \mathrm{mdry})}{\mathrm{mdry}} * 100 \qquad (3.5)$$

Where Wup is the percentage of water uptake, mwet is the weight of a swollen membrane immediately after immersing the membrane into water at room temperature for 24 hours and mdry is the weight of the same membrane after being dried.

3.3.3. Ion exchange capacity (IEC)

The IEC was defined as the ratio between the numbers of the surface ionogenic groups (inmmol) and the weight of the dry materials [10]. The titration technique was used to determine the IEC of the membranes. Firstly, the membrane was dried at 60 °C for 24 hours and measured the weight. The dried membranes in the proton form (H^+) were immersed in 60 ml of 1 M NaCl at 50-60 °C for 24 hours to exchange the H^+ ions with Na^+ ions. Then, the 60 ml of H^+ ions solution were titrated with a 0.01 M NaOH solution using phenolphthalein as the endpoint indicator [11].

3.4. References

[1] René Guinebretière**,** Polycrystalline Materials, X-ray Diffraction, Great Britain and the United States in by ISTE Ltd, 2007.

[2] J. S. Read, Principles of Ceramics Processing, John Wiley & Sons Inc., USA, 1995.

[3] M. J. Park, K. H. Downing, A. Jackson, E. D. Gomez, A. M. Minor, D. Cookson, A. Z. Weber, N. P. Balsara, *Nano Letters* **7** (2007) 3547-3552.

[4] D. Pletcher, A *First Course in Electrode Processes*, The Electrochemical Consultancy, (1991) ISBN: 09517307039.

[5] T. A. Zawodzinski, M. Neeman, L. O. Sillerud, S. Gottesfeld, *Journal of Physical Chemistry* **95** (1991) 6040-6044.

[6] P. Jannasch, *Current Opinion in Colloid and Interface Science* **8** (2003) 96-102.

[7] W. Zhengbang, T. Haolin, P. Mu, *Journal of Membrane Science* **369** (2011) 250-257.

[8] L. Wu, G. Zhou, X. Liu, Z. Zhang, C. Li, T. Xu, *Journal of Membrane Science* **371** (2011) 155-162.

[9] Y. Sone, P. Ekdunge, D. Simonsson, *Journal of Electrochemical Society* **143** (1996) 1254-1259.

[10] P. Dimitrova, K. A. Friedrich, U. Stimming, B. Vogt, *Solid State Ionics* **150** (2002) 115-122.

[11] S. R. Yoon, G, H. Hwang, W. I. Cho, I. H. Oh, S. A .Hong, H. Y. Ha, *Journal of power sources* **106** (2002) 215-223.

CHAPTER FOUR

4. POWDER PREPARATION AND CHARACTERIZATION

4.1. Introduction

A zirconium oxide (ZrO_2) nanoparticle is non-corrosive, catalytically active and stable under different conditions, excellent properties such as mechanical strength, chemical inertness, thermal stability and wear resistance which make them suitable used as catalysis [1]. Its good thermal matching with metals makes it suitable for protective coatings [2, 3]. It is also a promising constituent present in the transition metal based catalysts used in exhaust gas purifying devices [4]. ZrO_2 nanoparticles can exist in a number of polymorphs at atmospheric pressure which it is monoclinic, tetragonal, cubic and orthorhombic [5]. Depending on its crystalline structure it can be an insulator used as high resistance ceramic or an n-type semiconductor [6]. It is used in a wide range of reactions including alkylation, isomerization, biodiesel production, synthesis of 1, 5-benzodiazepine and diaryl sulfoxides, benzylation of toluene, etc. [7].

These ZrO_2 nanoparticles can be modified by sulphuric acid in order to improve its water retention [8-12] and being more stable than other solid super acids [13-14]. The presence of sulfates increases the stability of zirconia as well as the content of the tetragonal crystal phase, which is the one believed to be catalytically active [15]. It has been demonstrated that the proton conductivity of sulfated zirconia ($S\text{-}ZrO_2$) as well as

its surface and crystallographic properties, varies largely depending on the method of preparation, in particular on the thermal treatments [16-17]. Incorporation of small amounts of phosphate anions, onto zirconium oxides has been found to remarkably increase the surface acidic properties and bulk crystalline of the oxides and this phosphate zirconia (P-ZrO_2) was first investigated as a material for high performance liquid chromatography [18-19]. The impacts of sintering phase composition, crystal growth and extent and rate of phase transformation have been examined in relation to the texture stability of zirconia and phosphated zirconia samples [20]. The modified zirconia is recently attracting interest as fuel cell membrane additive because of it high acidity [21]. Hara et.al [16] found that surface of sulfate species existed as bidentate complexes strongly bonded with ZrO_2 powder calcinated at 620 ^oC. The ZrO_2 was aged; aim was to reduce the particle dimensions down to the nanometer domain. The tetragonal phase should play more dominating role in these small particles as the application of zirconia as catalyst support necessarily implies the presence of high specific surface area.

4.2. Experimental

4.2.1. Preparation of zirconium oxide (ZrO_2)

The ZrO_2 nanoparticles was prepared by precipitation method, zirconium oxychloride hydrate ($ZrOCl_2$.$8H_2O$) and ammonia (NH_3) were used as starting materials. All the chemicals were used as received without any further purification. Zirconium

hydroxide's precipitation ($Zr(OH)_4$) was obtained by adding an NH_4OH aqueous solution drop wise to the aqueous solution of 0.2M $ZrOCl_2.8H_2O$ at room temperature while vigorously stirring in 500ml glass beaker until the desired pH 10 was reached [16]. The precipitate was divided into two parts. The one part of the precipitate was washed with deionized water until the chlorine ions (Cl^-) were not detected by the silver nitrate ($AgNO_3$) test and filtered by filter paper to obtained wet powders Zr (OH) $_4$. The wet powder was dried in an oven at 100^{o}C overnight. Zirconia nanopowder (ZrO_2) was obtained through calcinations of the dried zirconium hydroxide at 600 ^{o}C for 6 hours. The remaining part of the precipitate formed as described above was aged in the mother liquor [22] for 48 hours at room temperature, after which it was filtered, then washed and calcinated according to the first one's procedure.

4.2.2. Preparation of Sulfated zirconia (S-ZrO_2)

Sulfated zirconia nanopowder was prepared by vigorously stirring the dried ZrO_2 nanopowder obtained from 4.2.1 in 0.5 M H_2SO_4 for 30 minutes at room temperature. The resulting solid was filtered and dried at 100 ^{o}C for 48 hours. The dried S-ZrO_2 nanopowder was then calcined at 600 ^{o}C for 2 hours and the resulting particles were crushed with a mortar and pestle [16].

4.2.3. Preparation of Phosphated zirconia (P-ZrO_2)

The P-ZrO_2 nanoparticle was prepared from ZrO_2 nanoparticles obtained from 4.2.1 in diammonium hydrogen phosphate solution. The P-ZrO_2 nanoparticle was obtained by impregnation of an aqueous solution diammonium hydrogen phosphate onto pure ZrO_2 nanoparticle, using minimal amount of the impregnating solution (25 ml/g) to give 6 wt% PO_4^{3-} [20]. A portion of the ZrO_2 nanopowder was dissolved in aqueous solutions of diammonium hydrogen phosphate solution with a magnetic stirrer at room temperature for 30 minutes. The P-ZrO_2 nanoparticle suspension obtained was filtered and dried at 100 ^oC for 48 hours, the dried P-ZrO_2 nanopowder was then calcined at 600 ^oC for 2 hours. The resulting particles were crushed with a mortar and pestle.

4.3. Results and discussion

4.3.1. The X-ray powder diffraction (XRD) analysis

Figure 4.1 show the diffraction pattern of the as-prepared ZrO_2, S-ZrO_2 and P-ZrO_2 powder samples. The crystallinity of the samples is evidenced by sharper diffraction peaks at respective diffraction angles which can be readily indexed for its tetragonal and monoclinic structure. The obtained structures are comparable to the (JCPDS Card No. -37-1484) [23-24] for the monoclinic and standard JCPDS data (Card No. 17-0923) [25] for the tetragonal structure. All the samples exhibit the monoclinic phase and the major peaks appeared at 24.4°, 28.2°, 31.5°, 34.5° and 62.3°. The tetragonal

phase peaks appeared at 30.2°, 50.2°, 59.3° and 60.2° [26]. The strongest diffraction peak of monoclinic structure which appeared at 28.2° is due to the (111) plane and the major peak for the tetragonal structure is seen at 30.5° corresponds to the (101) plane. If one looks at the intensity of the monoclinic and tetragonal peaks, it can be concluded that the powder samples contain more monoclinic structure than tetragonal.

The XRD patterns of the samples synthesized by aging method are shown in Figure 4.2. All the samples showed similar patterns at 30.2°, 50.2° and 60.2° 2theta which are characteristics of zirconium in a tetragonal phase [26]. The peaks at 30.2°, 50.2° and 60.2° correspond to the planes (h k l) at 101, 112 and 211 respectively. These XRD patterns show that these materials are amorphous as evident by peaks and humps. From these results it can be deduced that the slow aging of samples favoured the tetragonal structure growth.

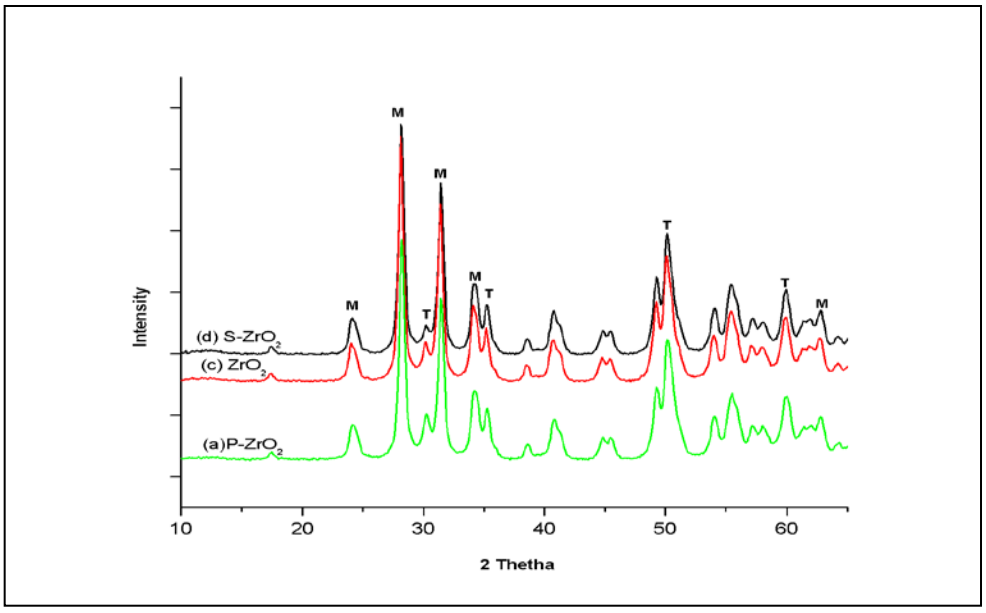

Figure 4. 1: XRD patterns of ZrO_2, S-ZrO_2 and P-ZrO_2 nanoparticles.

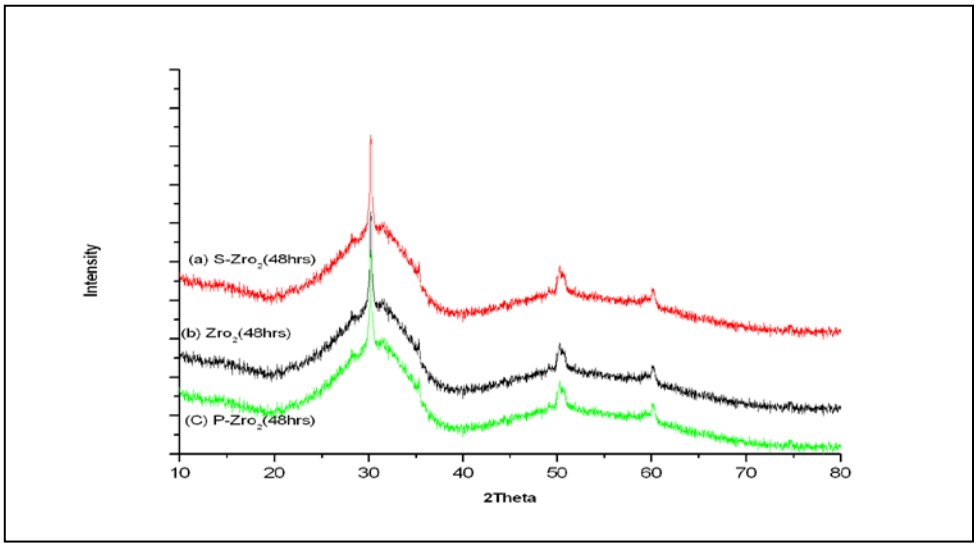

Figure 4. 2: XRD patterns of (b) ZrO_2, (a) S-ZrO_2 and (c) P-ZrO_2 nanoparticles at 48hours.

4.3.2. Powder thermo-gravimetric analysis (TGA)

The thermo-gravimetric analysis (TGA) curves obtained from nanopowders of the ZrO_2, S-ZrO_2 and P-ZrO_2 nanoparticles are shown in Figure 4.3. Figure 4.3 indicates that the thermal decomposition process occurs in two stages. The TGA curve (b) indicates that the thermal decomposition occurs initially between 20 °C and 200 °C, with mass loss of 0.4 % associated to dehydration. And the second stage of thermal decomposition is related to powder degradation and carbonaceous phase decomposition. The total weight loss of original material reaches about 1.2%. The TGA curve (c) indicates that ZrO_2 a little loss of its original weight on heating up to 900 °C.

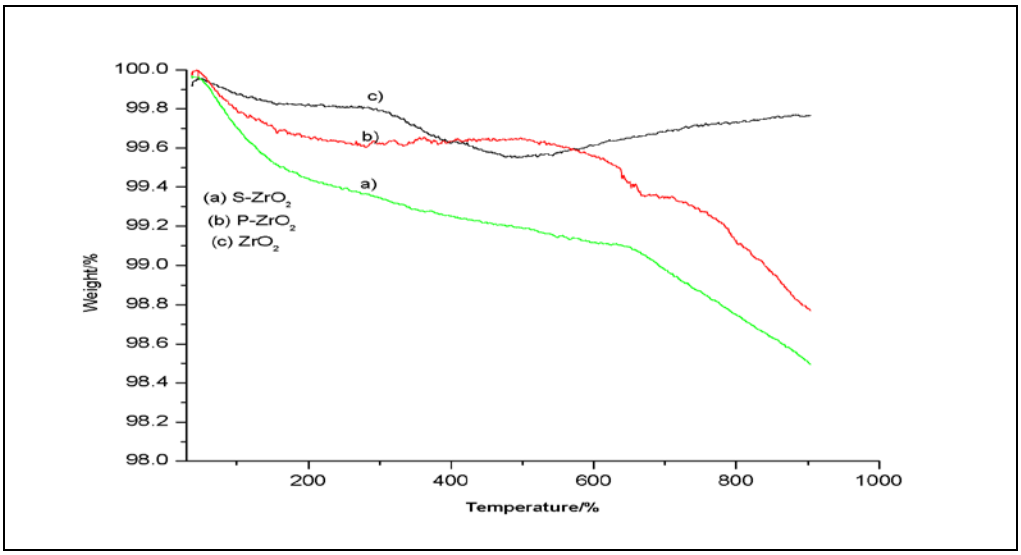

Figure 4. 3: Thermogravimetric analysis of (c) ZrO_2, (a) S-ZrO_2 and (b) P-ZrO_2 nanoparticles.

The ZrO_2, P-ZrO_2 and S-ZrO_2 nanopowder was evaluated by means of thermo-gravimetric analysis (TGA). Figure 4.4 (a) shows the TGA results of the sulfated zirconia nanoparticles aged at 48 hours. The TGA curve also shows two weight loss stages. The first weight loss is assigned to the water loss which is below 200 ^oC temperatures and the second weight loss between 200 and 400 ^oC was attributed to the loss of the sulfate groups [21, 27]. Both the S-ZrO_2 and S-ZrO_2 (48hrs) nanopowder showed a weight loss occurring in the region 25-400 ^oC, it is assumed to be due to the decomposition of the SO_4^{-2} groups bound to the ZrO_2 surface and released as sulfur oxides [22]. The TGA curve (a) indicates the sample weight loss as the function of temperature, the sample weight decreased by about 4.5% when heated up to 400 ^oC. The TGA curve (b) indicates the P-ZrO_2 nanoparticles samples aged. The samples showed the weight loss of about 1.4 % at temperatures lower than 200 ^oC due to the removal of adsorbed water. The second weight loss occurring at higher temperature is

attributed to the decomposition of phosphate ion bound to the surface of ZrO_2. The S-ZrO_2 (48 hrs) nanoparticles has a weight loss of about 4.0% at 200 ^oC and about 4.8% at the temperature ranging from 450 ◦C to 800 ^oC.

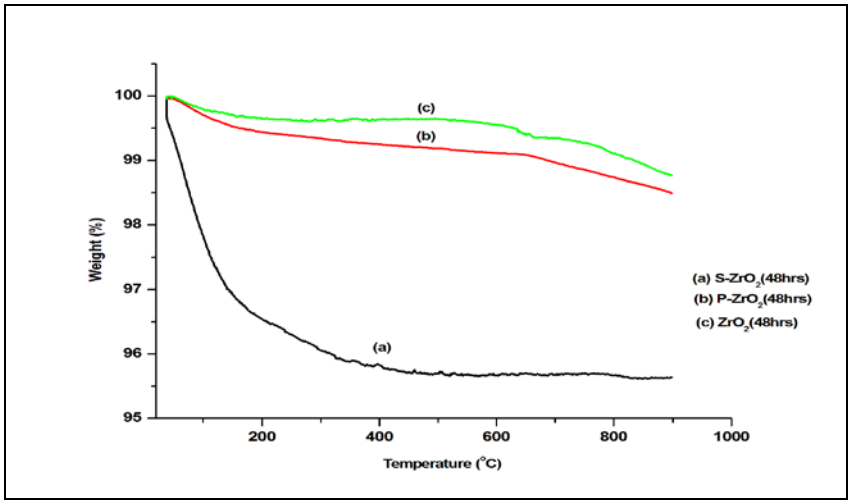

Figure 4. 4: Thermogravimetric analysis of (a) S-ZrO_2 (48 hrs), (b) P-ZrO_2 (48 hrs) and (c) ZrO_2 (48 hrs) nanoparticles.

4.3.3. Fourier Transform Infrared (FTIR) spectroscopy

The FTIR spectra of ZrO_2, S-ZrO_2 and P-ZrO_2 nanoparticles are shown in Figure 4.5. The broad band exhibited by all spectra at 3700 to 2700 cm^{-1} is due to the hygroscopic nature of ZrO_2 is which is due to the -OH group presence of water [28]. The broad peak from 800 to 1200 which is centred at 983 cm^{-1} is due to asymmetric frequencies of stretching vibration of S=O, S-O and P-O bonds which are an indication that we have sulfated and phosphated zirconium. The band around 1600cm^{-1} can be attributed to the two bend vibrations of –OH groups of the physisorbed moisture [29]. The region between 2800cm^{-1} and 3060cm^{-1} indicate the presence of hydroxyl group,

mainly from water [30].

The FTIR spectra of ZrO_2, S-ZrO_2 and P-ZrO_2 nanoparticles aged at 48 hours are given in Figure 4.6. In Figure 4.6 the results indicated that all the nanoparticles have a broad peak at 3600 to 3000cm^{-1} region, which is due to -OH bonds presence of water. The broad band at 1620cm^{-1} is assigned to the bending mode of coordinated molecular water associated with the sulfate group [31-33]. A broad peak in region of 800 to 1350cm^{-1} with four clear peaks at 1202cm^{-1}, 1123cm-1,1043cm^{-1} and 983cm^{-1} was assigned to asymmetric and symmetric stretching frequencies of S=O and S-O bonds [34].

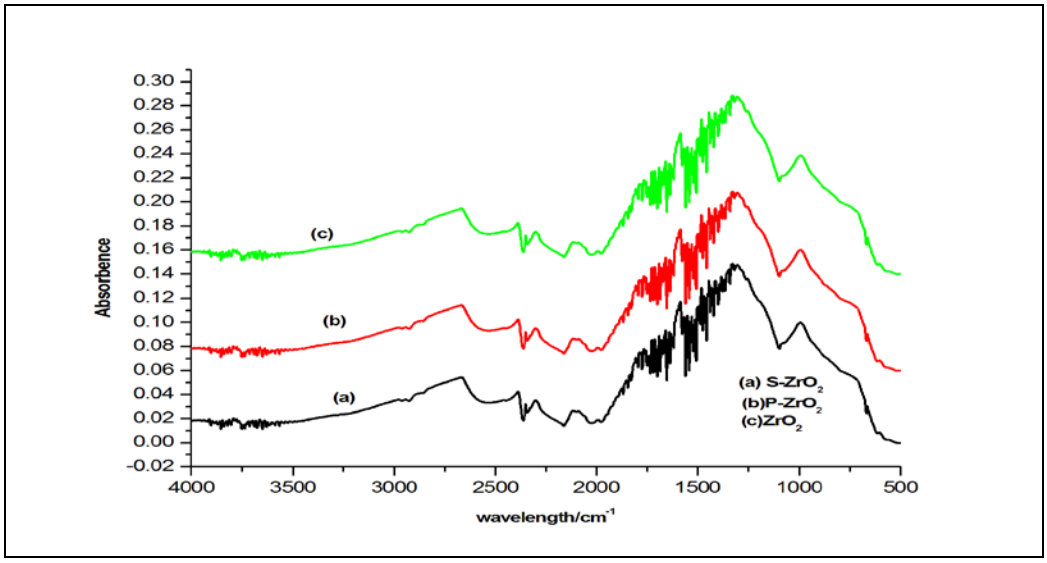

Figure 4. 5: Fourier Transform Infrared analysis of (a) ZrO_2, (b) S-ZrO_2 and (c) P-ZrO_2 nanoparticles.

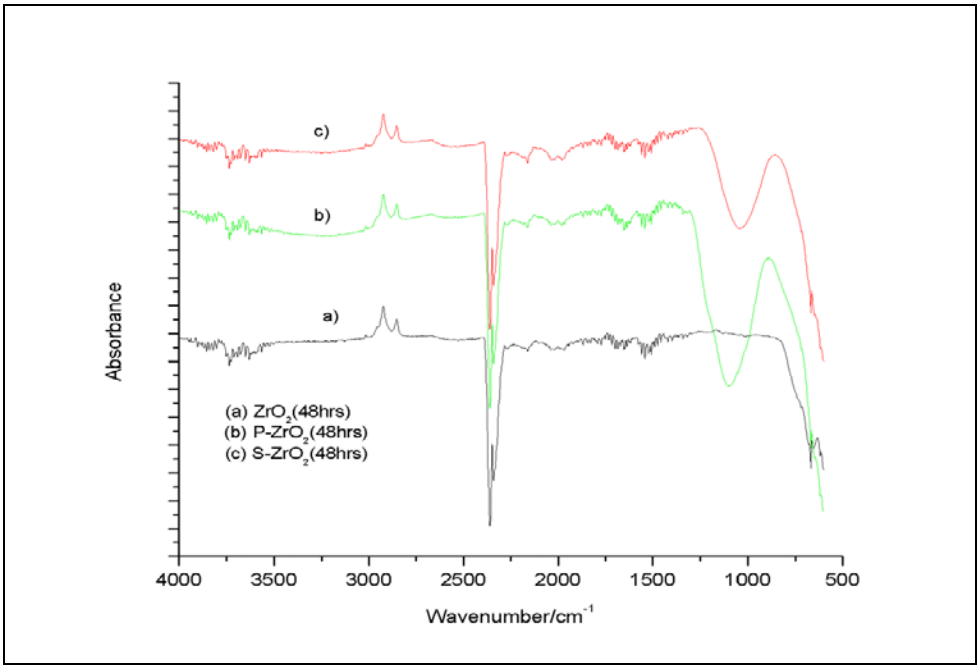

Figure 4. 6: Fourier Transform Infrared analysis of (a) ZrO_2, (c) S-ZrO_2 and (b) P-ZrO_2 nanoparticles aged at 48hrs.

4.3.4. Brunauer-Emmett-Teller (BET)

The BET specific surface areas and the particle sizes of ZrO_2, S-ZrO_2 and P-ZrO_2 nanoparticles materials calcined at 600 ^oC are listed in Table 4.1 and Figure 4.7. The specific surface area of ZrO_2 nanoparticles materials was found to be 32.5 m^2/g which is higher than 23.2 m^2/g [35], with the particle size estimated to be equal to 29.4 nm. The specific surface area of ZrO_2 nanoparticles increase by modifying with sulfuric acid to obtained 39 m^2/g which is greater than that of the pure ZrO_2 this indicate that the presence of sulfate strongly influences the surface area of ZrO_2 as the sulfuric acid impregnation was known to increase the surface area of metal oxide catalysts. Also the

modification with diammonium hydrogen phosphate acid increases the specific surface areas to 37 m^2/g.

Table 4. 1: BET surface area for ZrO_2, S-ZrO_2 and P-ZrO_2 nanoparticles

Samples	calcination Temperature(Oc)	BET surface area (m^2/g)	Particle size (nm)
ZrO2	600	32.5033	29.4413
S-ZrO2	600	39.2426	24.3852
P-ZrO2	600	37.1668	25.7471
ZrO2 (48hrs)	600	71.6178	13.3617
S-ZrO2(48hrs)	600	79.0922	12.0990
P-ZrO2(48hrs)	600	77.0492	12.4198

The aim of aging ZrO_2 nanoparticles was to reduce the particles dimensions down to nanometer domain and also to stabilize the tetragonal phase at low temperature as this phase plays a dominating role in the small particles. Figure 4.7 shows that aging the nanoparticles will enhance the specific surface area as is necessary for application of zirconia as catalyst support. The results show BET surface area measured for ZrO_2, S-ZrO_2 and P-ZrO_2 nanoparticles aged at 48 hours at ambient temperature was equal to 72 m^2/g, 79 m^2/g and 77 m^2/g respectively. The surface area of ZrO_2 nanoparticles aged at 48 hrs at ambient temperature was nearly the same to those nanoparticles that aged at 100 °C for 24 hours which has the surface area of 77 m^2/g [36]. The surface

area of S-ZrO_2 (48 hrs) is double the number of un-aged from (39 to 79 m^2/g) with the particle size ranges from (24.39 nm to 12.10 nm). This indicates that by aging ZrO_2 nanoparticles it increases the surface areas which make them suitable for fuel cell application.

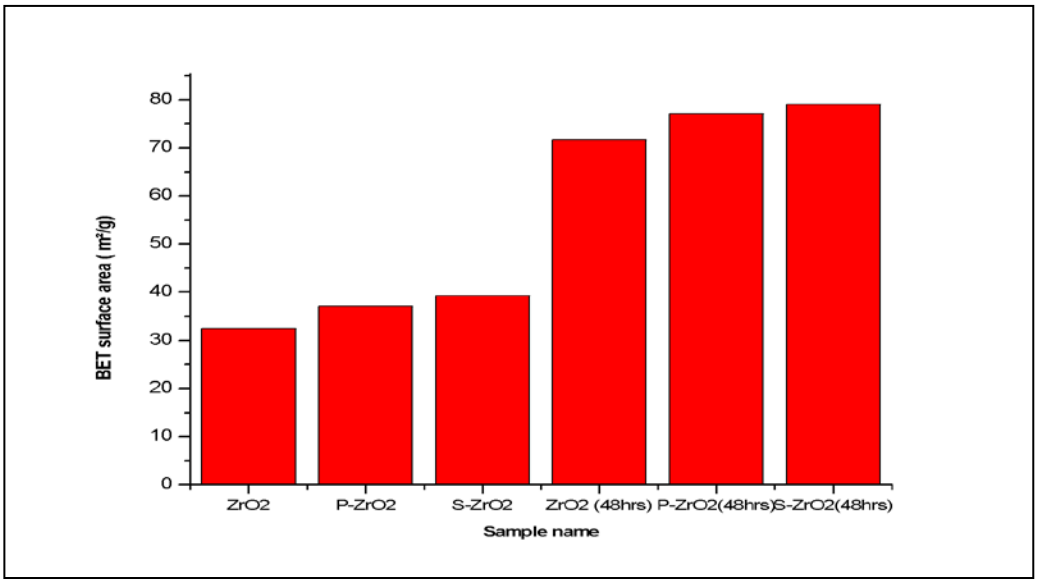

Figure 4. 7: BET surface areas of the nanoparticles calcined at 600^{o}C.

4.3.5. Scanning Electron Microscopy (SEM)

Figure 4.8 shows the SEM images at a high magnification scale bar of 200 nm and 1µm of the ZrO_2 nanoparticles with the average particle size of 13-29 nm. It is observable from Figure 4.8 that a lot of nanoparticles were aggregated into clusters of the ZrO_2. Figure 4.8(a) indicates that the aged nanoparticles consist of primary units of very small dimensions, around 200 nm with the reduced agglomeration when compared to un-aged nanoparticles. Figure 4.8 (b) indicates that the un-aged nanoparticles is in the form of agglomerates, which exhibit a wide size distribution

with dimensions varying to around 1 microns. From Figure 4.8(a) it can be concluded that by aging the nanoparticles can reduces the agglomeration while reducing the particles size also.

(a)

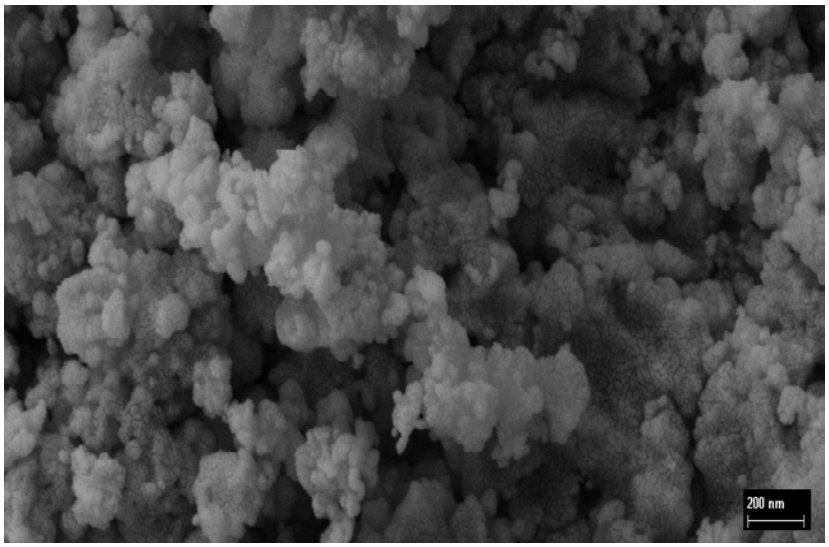

(b)

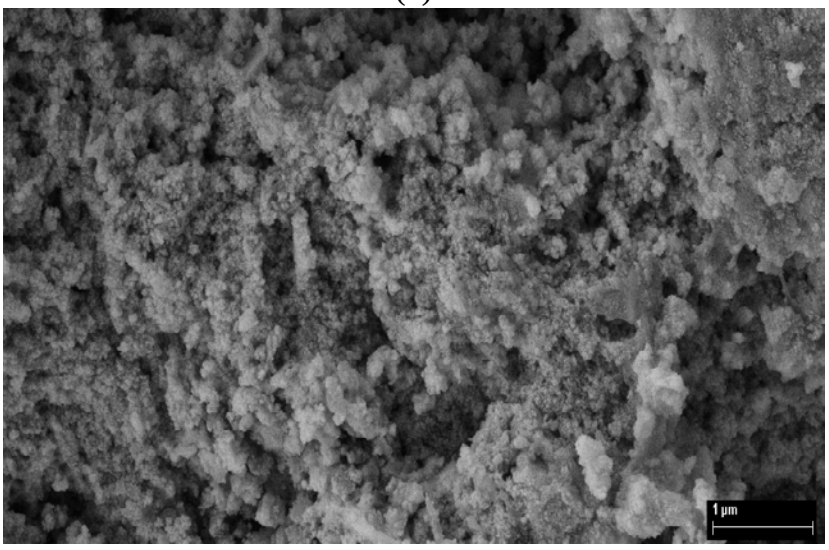

Figure 4. 8: SEM image of the ZrO_2 nanoparticles: (a) aged at 48hrs and (b) un-aged.

Figure 4.9 shows SEM micrographs of S-ZrO_2 nanoparticles un-aged and aged at 48hours. From the SEM image of S-ZrO_2 nanoparticles in Figure 4.9 the particle were less agglomerated, which means that the S-ZrO_2 suspension was well dispersed. It can be observable from the SEM micrographs in Figure 4.9 (a) and (b) that the modification of ZrO_2 nanoparticles with sulfuric acid solution leads to the smaller particles, as the particle sizes ranged from 25 nm to 10 nm respectively. S-ZrO_2 nanoparticles aged nanoparticles present a quite different surface morphology with a slightly aggregated nanoparticle as shown in Figure 4.9 (b). Figure 4.10 shows SEM micrographs of P-ZrO_2 nanoparticles aged at 48 hours, which consists of spherical nanostructures with the length around 100 nm. Figure 4.10 show that the addition of diammonium hydrogen phosphate acid increases the particles size when compared with ZrO_2 nanoparticles. The SEM characterization also supports the assumption based on the dependence of the particle size on the acidic group content as it can observed in Figure 4.10 showing the small particle size around 12nm. Specifically, the higher diammonium hydrogen phosphate acid solution amount incorporated into zirconia nanoparticles the smaller the particle size achieved.

(a)

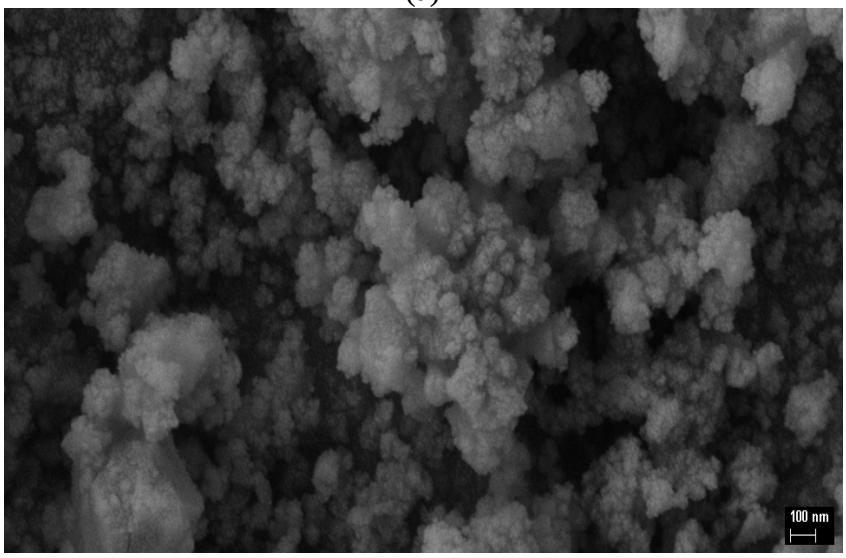

(b)

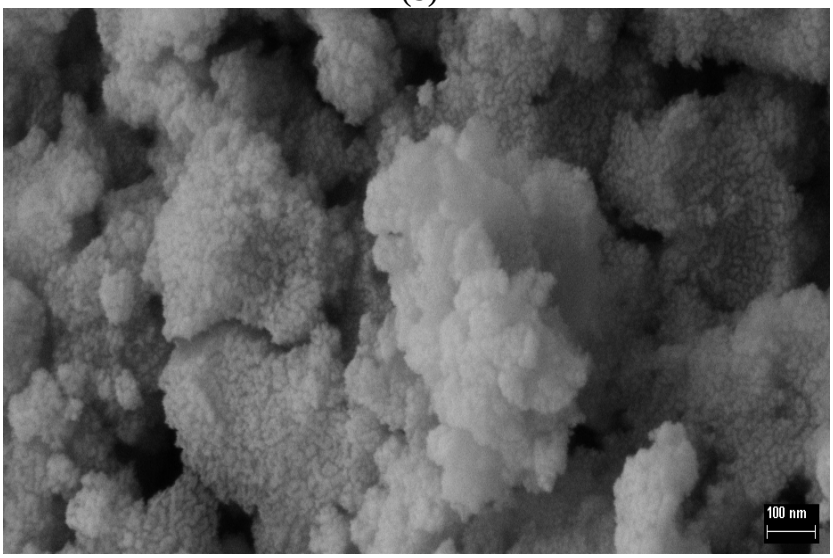

Figure 4. 9: SEM image of the S-ZrO_2 nanoparticles: (a) un-aged and (b) aged at 48hrs.

(a)

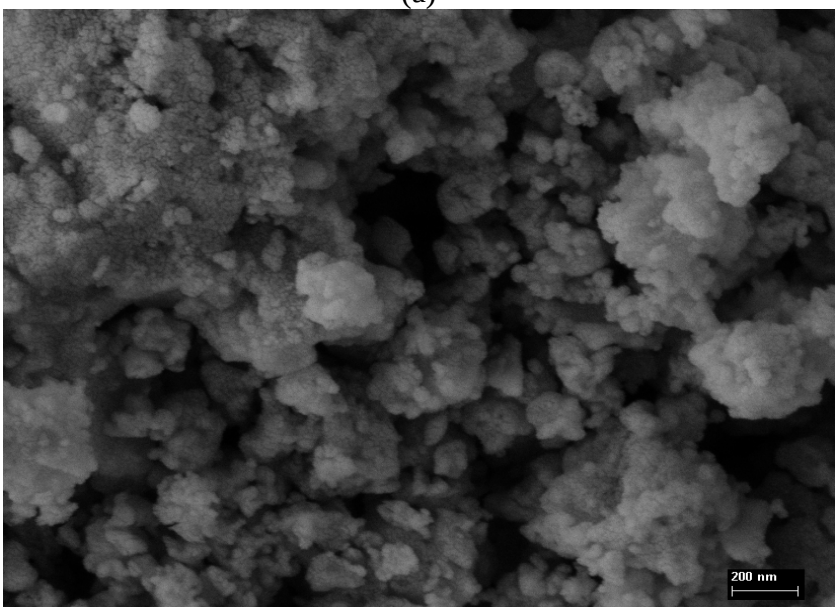

(b)

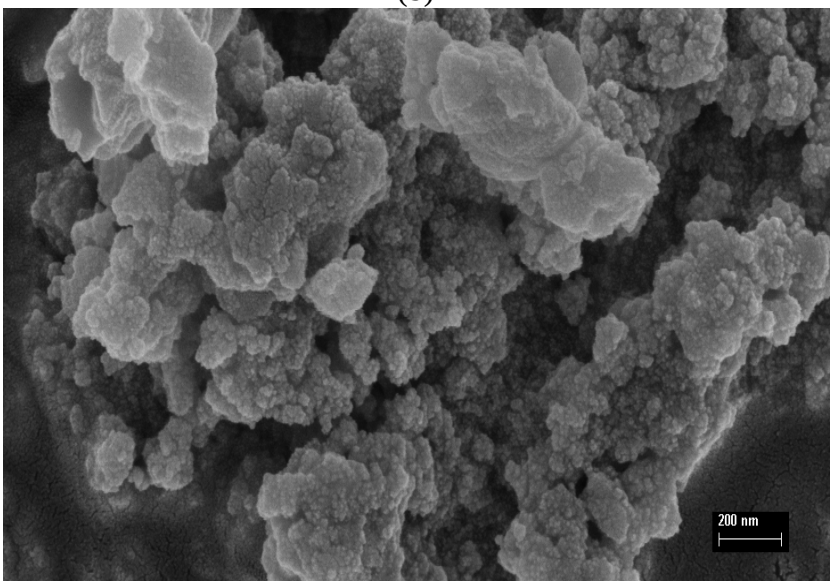

Figure 4. 10: SEM image of the P-ZrO_2 nanoparticles: (a) un-aged and (b) aged at 48hrs.

4.3.6. Transmission electron microscopy (TEM)

Figure 4.11 presents the TEM image of ZrO_2 nanoparticles of aged and un-aged nanoparticles. From Figure 4.11(a) it can be seen that size distribution of particles are

narrowly dispersed with the particle size range from 20-30 nm, having a lesser agglomeration this can be attributed to the calcination temperature [37]. TEM images for the ZrO_2 samples aged nanoparticles shows fine-particle morphologies with the particle size range from 11-25 nm with lesser particle agglomeration. From the results in Figure 4.11(a) indicates that the particles of these nanoparticles were presented in the uniform spherical shape. The TEM images of the aged ZrO_2 nanoparticles shows a lower particle size when compared to those of un-aged ZrO_2 as most of their particles ranges between 10-13 nm as shown in Figure 4.11(b).

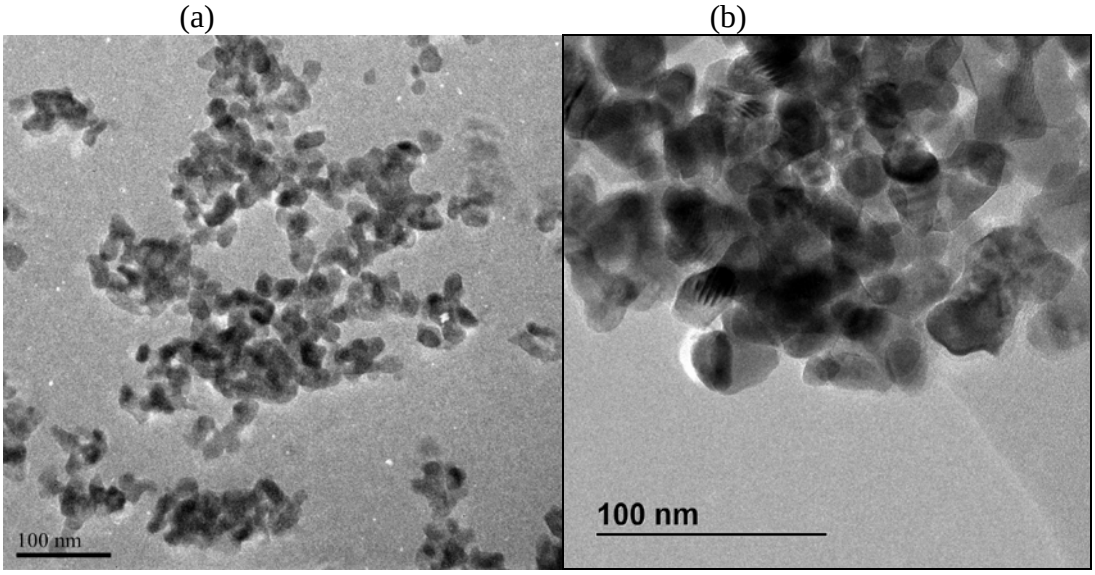

Figure 4. 11: TEM image of the ZrO_2 nanoparticles (a) un-aged and (b) aged at 48hrs.

The average particle size of P-ZrO_2 nanoparticles un-aged is around 25 nm in spherical shapes, as shown in Figure 4.12, whereas, aged nanoparticles has a very small size nanoparticles of around 12 nm. Figure 4.12 (b) and (c) shows the grains

consists of particle size around 20 to 10 nm in width at the edges. Figure 4.12(b) clearly illustrates how nanoparticle sizes of P-ZrO_2 in Figure 4.12 (c) consisted.

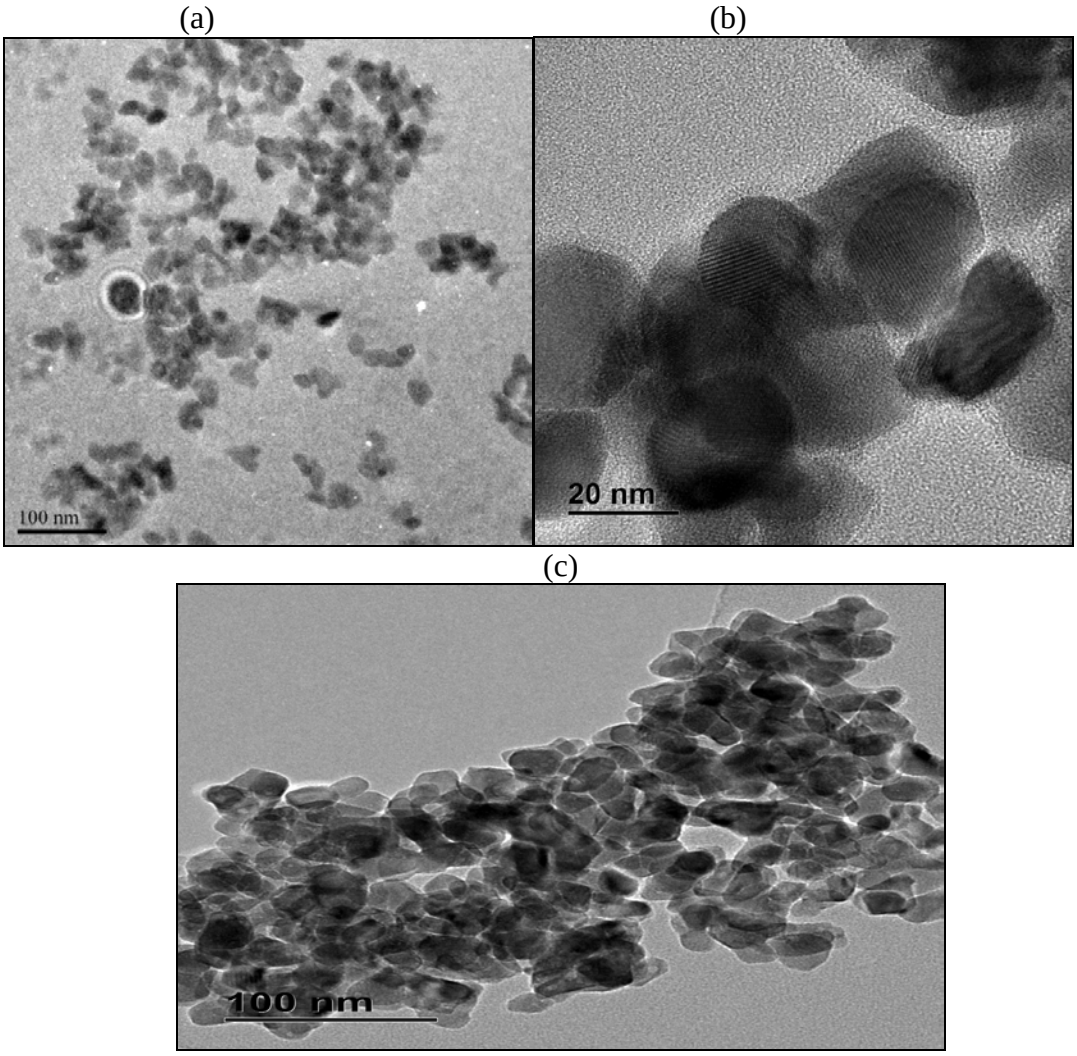

Figure 4. 12: TEM image of the P-ZrO_2 nanoparticles (a) un-aged (b) and (c) aged at 48hrs.

Figure 4.13 shows the TEM images of the S-ZrO_2 nanoparticles aged at 48 hours and un-aged. The TEM image in Figure 4.13 (a), (b), (c) and (d) indicated that the addition of sulphuric acid in zirconium oxide presented the fine nanoparticle morphologies with lesser particle agglomeration. The average particle size of un-aged nanoparticles

is around 20-25 nm in spherical shapes, as shown in Figure 4.13(a), whereas the aged nanoparticles possesses very small and uniform size particles of up to 10-12 nm. The TEM images in Figure 4.13(c) and (d) clearly illustrate how nanoparticle sizes of S-ZrO_2 consisted; it shows the morphology of the smaller particles and also the shape of the particles. The average particle size of S-ZrO_2 aged at 48hrs was about 12 nm, which was smaller than 13 nm of ZrO_2 nanoparticles. Figure 4.13(c) show that the nanoparticles are highly crystalline. Figure 4.13 show that the particles are uniform and spherical with the average particle size estimated of 12-25 nm which is related from that obtained from BET results.

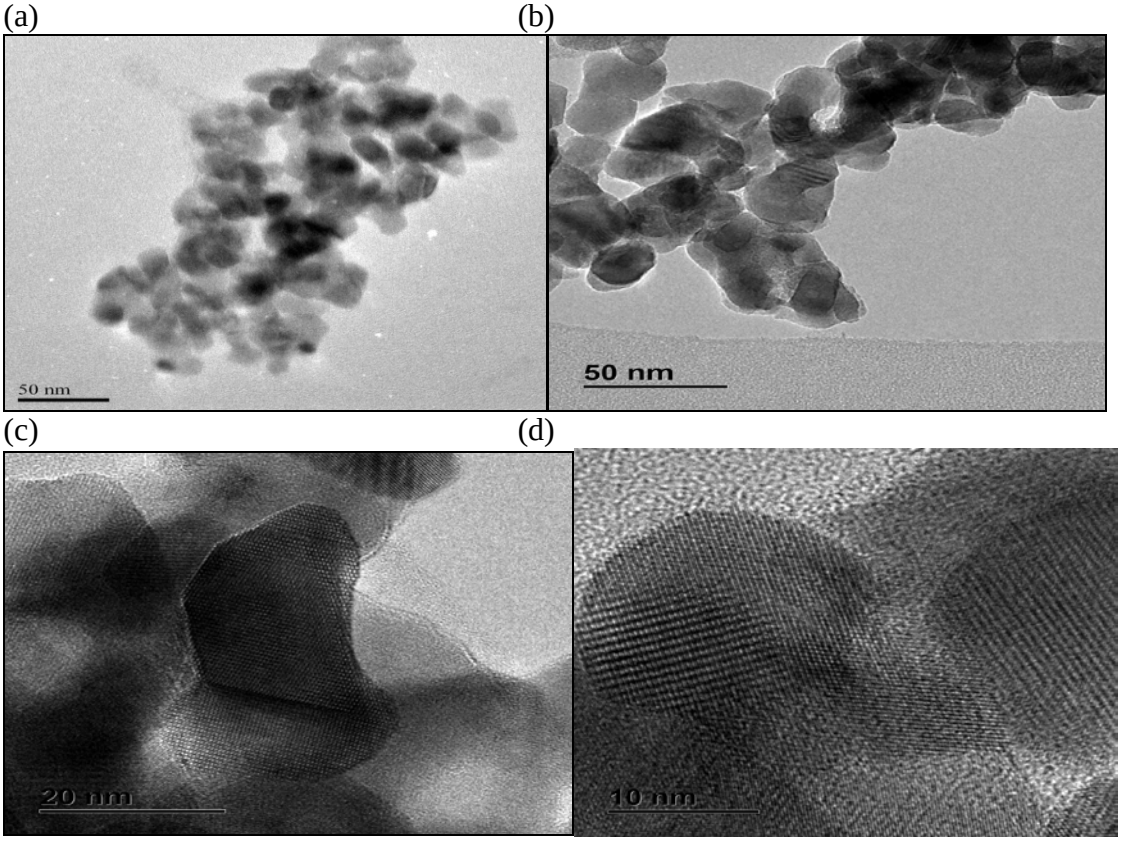

Figure 4. 13: TEM image of the S-ZrO_2 nanoparticles (a) un-aged and (b) aged at 48hrs (c) and (d) shows morphology of the smaller particles.

4.4. Conclusions

It concluded that stabilised tetragonal phase obtained at low temperature by aging the ZrO_2 at 48 hours (ambient temperature), as zirconia bodies containing a tetragonal phase can undergo stress-induced phase transforming as they believed to be tough and strong. The particle sizes ranged from 25 to 30 nm for unmodified ZrO_2 whereas for the modified with sulferic acid or diammonium hydrogen phosphate solution their particles size range from 10-25 nm.

4.5. References

[1] W. Wang, H. T. Guo, J. P Gao, X. H. Dong, Q. X. Qin, *Journal of Material Science* **35** (2000) 1495-1499.

[2] E. Setare, K. Raeissi, M. A. Golozar, M. H. Fathi, *Corrosion Science* **51** (2009) 1802-1808.

[3] I. Valov, D. Stoychev, Ts. Marinova, *Electrochimica Acta* **47** (2002) 4419-4431.

[4] D. Stoychev, J. Ikonomov, K. Robinson, P. Stefanov, M. Stoycheva, Ts. Marinova, *Surface and Interface Analysis* **30** (2000) 69-73.

[5] R. Suyama, T. Ashida, S. Kume, *Journal of American Ceramic Society* **68** (1986) 314-315.

[6] E. P Rajiv, V. E Annamalai, S. K Seshadri, *Journal of Material Science* **11** (1992) 466-468.

[7] M. Skovgaard, K. Almdal, A. van Lelieveld, *Journal of Material Science* **45** (2010) 6271-6274.

[8] A. Zarubica, B. Jovic, A. Nikolic, P. Putanov, G. Boskovic, *Journal of Serbian Chemical Society* **74** (2009) 1429-1442.

[9] K. Föttinger, G. Kinger, H. Vinek, *Applied Catalys A: General* **266** (2004) 195-202.

[10] X. Song, A. Sayari, *Catalysis Reviews-science and Engineering* **38** (1996) 329-412.

[11] N. Katada, J. Endo, K. Notsu, N. Yasunobu, N. Naito, M. Niwa, *Journal of Physical Chemistry B* **104** (2000) 10321-10328.

[12] G. D. Yadav, J. Nair, *Microporous and Mesoporous Materials* **33** (1999) 1-48.

[13] A. D'Epifanio, M. A. Navarra, F. C. Weise, B. Mecheri, J. Farrington, S. Licoccia, S. Greenbaum, *Chemistry of Material* **22** (2010) 813-821.

[14] M. A. Navarra, C. Abbati, B. Scrosati, *Journal of Power Sources* **183** (2008) 109-113.

[15] J. M. Parera, *Catalysis Today* **15** (1992) 481-490.

[16] S. Hara, M. Miyayama, *Solid State Ionics* **168** (2004) 111-116.

[17] C. Li, M. Li, *Journal of Raman Spectroscopy* **33** (2002) 301-308.

[18] V. S. Escribano, E. F. López, M. Penniza, C. Resini, J. M. G. Amores, G. Busca, *Solid State Science* **5** (2003) 1369-1376.

[19] F. Abbattista, A. Delastro, G. Gozzelino, D. Mazza, M. Vallino, G. Busca, V. Lorenzelli, *Journal of the Chemical Society, Faraday Transactions* **86** (1990) 3653-3658.

[20] G. A. H. Mekhemer, H. M. Ismail, *Physicochemical and Engineering Aspects* **164** (2000) 227-235.

[21] Y. F. Zhai, H.M. Zhang, J.W. Hu, B.L. Yi, *Journal of Membrane Science* **280 (**2006) 148-155.

[22] A. Adamski, P. Jakubus, Z. Sojka, *Nukleonika* **51**(2006) 27-33.

[23] X. Jiao, D. Chen, L. Xiao, *Journal of Crystal Growth* **258** (2003) 158-162.

[24] J. C. Ray, R. K. Pati, P. Pramanik, *Journal of the European Ceramic Society* **20** (2000) 1289-1295.

[25] L. Zhou, J. Xu, X. Li, F. Wang, *Materials Chemistry and Physics* **97** (2006) 137-142.

[26] B. Bondars, G. Heidemane, J. Grabis, K. Laschke, H. Boyesen, J. Schneider, F. Frey, *Journal of Material Science* **30** (1995) 1621-1625.

[27] V. G. Deshmane, Y.G. Adewuyi, *Microporous and Mesoporous Materials* **148** (2011) 88-100.

[28] V. Adeeva, J. W. Dehaan, J. Janchen, G. D. Lei, V. Schunemann, L. J. M. Vandeven, W. M. H. Sachtler, R. A. Vansanten, *Journal of Catalysis* **151**(1995) 364-372.

[29] D. Spielbauer, G. A. H. Mekhemer, T. Riemer, M. I. Zaki, H. Knözinger, *Journal of Physical Chemistry B* **101** *(*1997) 4681-4688.

[30] R. L. Frost, S. M. Dutt, *Journal of Colloid and Interface Science* **198** (1997) 330-336.

[31] D. A. Ward, E. I. Ko, *Journal of Catalysis* **150** (1994) 18-33.

[32] D. Sarkar, D. Mohapatra, S. Ray, S. Bhattacharyya, S. Adak, N. Mitra, *Ceramics International* **33** (2007) 1275-1282.

[33] F. Babou, G. Coudurier, J. C. Vedrine, *Journal of Catalysis* **152** (1995) 341-349.

[34] T. Yamaguchi, T. Jin, K. Tanabe, *Journal of Physical Chemistry* **90** (1986) 3148-3152.

[35] G. K. Chuah, S. Jaenike, S. A. Cheong, K. S. Chan, *Applied Catalysis A: General* **145** (1996) 267-284.

[36] P. Jakubus, A. Adamski, M. Kurzawa, Z. Sojka, *Journal of Thermal Analysis and Calorimetry* **72** (2003)299-310.

[37] J. Lai, K. V .P. M. Shafi, A. Ulman, K. Loos, N. -L. Yang, M. -H. Cui,T. Vogt, C. Estournes, D. C. Locke, *Journal of Physical Chemistry B* **108** (2004)14876-14883.

CHAPTER FIVE

5. PREPARATION AND CHARACTERIZATION OF NANOCOMPOSITE MEMBRANES

5.1. Introduction

Due to the increasing concern regarding the storage and transportation of hydrogen and it is necessary to search for an alternate fuel. Methanol is chosen as an alternate fuel, as it possesses a very simple chemical structure that can be oxidized into hydrogen in the presence of a suitable catalyst [1]. Metal oxides have been extensively investigated as inorganic additives in proton conducting membranes used as ionic separators in polymer electrolyte membrane fuel cells (PEMFCs) [2,3]. It was demonstrated that the incorporation of metal oxides, in the form of nanoparticles, improves the water retention and the thermo-mechanical stability of the membranes [4]. But the incorporation of metal acids (e.g S-ZrO_2) in Nafion membrane will have the dual function of improving water retention as well as providing additional acidic sites for proton diffusion [5]. Nafion membranes exhibit reasonable conductivity; thermal and chemical stability, under lower temperature [6-9] but at higher temperatures Nafion will dehydrate and lose proton conductivity [10], and may result in irreversible mechanical damage and poor barrier to methanol crossover. A zirconia based/Nafion nanocomposite membrane should be designed to run at operating temperatures between 120 ^{o}C and 140 ^{o}C because higher temperature operation

reduces the impact of carbon monoxide poisoning, allows attainment of high power density and reduces cathode flooding as water is produced as vapour. This approach of impregnating polymer membrane with phosphated zirconia and sulfated zirconia nanoparticles was adopted in order to improve proton conductivity and reduced the methanol crossover and in the present work consists of synthesizing composite membranes by incorporating inorganic proton conductive material into Nafion polymer [11-21]. Zirconia nanoparticles have the features of increasing conductivity by using high proton mobility on the surface of the particles, and good water retention [7].

5.2. Experimental

5.2.1. Preparation of ZrO_2, P-ZrO_2 and S-ZrO_2 nanoparticles

The procedure is the same as described in Chapter 4, Section 4.2.2 - 4.2.3.

5.2.2. Preparation of composite membranes

5.2.2.1. Recast Method

i) Isopropyl alcohol (IPA) as the casting solvent

Nafion solution (5 wt.%, 1100 EW) and IPA were mixed in an ultrasonic bath for 5 minutes, with a volume ratio of 1:2 (Nafion solution to IPA) [22]. 5% to 15% of the two different ZrO_2, S-ZrO_2 and P-ZrO_2 nanopowders were added to the mixture. The mixture was then mixed ultrasonically for 20 minutes. The mixture was recast in a glass petri dish, dried at 80 °C for 24 hours in an air oven, followed by 160 °C for 30 minutes in the same oven. The recast Nafion was pulled off from the petri dish by adding a small amount of deionised water. The recast Nafion / Zirconia based nanocomposite membrane was treated according to the standard procedure by boiling in 3 vol.% hydrogen peroxide (H_2O_2) for 1 hour to remove the organic impurities, followed by washing with boiling deionised water for 30 minutes. The composite membrane was then boiled in 1 M H_2SO_4 for 1 hour to remove the inorganic impurities and also to complete the protonation and then washed with water for 30 minutes. Washing with water was repeated several times to remove any traces of acidity. Finally the membrane was kept in water prior to measurements.

ii) N, N-dimethylformade (DMF) as casting solvent

The nanocomposite membranes were prepared using 5 % Nafion solution as the standard material for reference. In each case, a membrane precursor solution containing Nafion solution, the two different additives (ZrO_2, S-ZrO_2 and P-ZrO_2 nanoparticles) were prepared. The detail was as follows: 1:5% Nafion solution/DMF

was mixed; the appropriate amount of additive, i.e. ZrO_2, S-ZrO_2 and P-ZrO_2 nanoparticles were added to the Nafion/DMF solution and stirred at room temperature for 2 hours, then ultrasonizing for 30 minutes [23]. The resulting solution was poured onto a piece of flat glass, and placed into an oven at 80 ^oC for 12 hours to remove solvent and finally heated up to 160 ^oC for 30 minutes. The membranes were then removed by peeling off from the glass plate. Before measuring the proton conductivity, all membranes were kept in deionized water for 12 hours.

5.2.2.2. Ion exchange method

The composite membranes were prepared using Nafion 117 films. Nafion films were purified by boiling in 3% hydrogen peroxide for 1 hour, was then rinsed with boiling water, treated in boiling 1 M sulfuric acid for 1 hour and finally rinsed again with boiling water several times.

i) A zirconia/Nafion 117 nanocomposite membrane was prepared by means of ion-exchange of zirconium ions into the Nafion 117. The Nafion 117 membrane was then soaked in $ZrOCl_2$/2-propanol solution at 80 ^oC for 24 hours. The membrane was removed, blotted, and placed in 2-propanol/ H_2O solution for 2 hours at 80 ^oC. After the acid-hydrolysis and condensation reactions, the membrane was removed and dried at 80 ^oC for 24 hours and then at 110 ^oC for 2 hours. Zirconia nanoparticle was incorporated into Nafion 117 membrane via an ion exchange reaction involving ZrO^{2+} ions. For this purpose, the membranes were first swollen in a boiling methanol-water

solution (1:1 vol.) and dipped in a 1 M solution of zirconyl chloride (Aldrich) for 24 hours at 80 °C [7].

ii) A sulfated zirconia/Nafion 117 nanocomposite membrane was prepared by means of ion-exchange of zirconium ions into the Nafion 117 membrane, followed by precipitation of sulfated ZrO_2 by treatment in 5 M H_2SO_4 at 80 ^oC. The Nafion 117 membrane was then soaked in $ZrOCl_2$/2-propanol solution at 80 ^oC for 24 hours. The membrane was removed, blotted, and placed in 2-propanol/ H_2O solution for 2 hours at 80 ^oC. After the acid-hydrolysis and condensation reactions, the membrane was removed and dried at 80 ^oC for 24 hours and then at 110 ^oC for 2 hours. The membrane was then boiled in 5 M H_2SO_4 solution at 60 ^oC for 1 hour to sulfate the ZrO_2 nanoparticles, and finally rinsed in water [7].

iii) Phosphated zirconia nanoparticles was incorporated into Nafion 117 via an ion exchange reaction involving ZrO^{2+} ions followed by precipitation of phosphated zirconia nanoparticles by immersion of the membrane in diammonium hydrogen phosphate acid. For this purpose, the membranes were first swollen in a boiling methanol-water solution (1:1 vol.) and dipped in a 1 M solution of zirconyl chloride for 24 hours at 80 °C. The membranes were then rinsed in cold water to remove excess solution and finally placed in 1 M diammonium hydrogen phosphate acid overnight at 80 °C [24]. The membranes were then repeatedly rinsed in distilled water to remove excess acid. After keeping the samples in an oven at 80 °C for 20 minutes, they were equilibrated to ambient conditions for characterization.

5.2.2.3. Impregnation method

The Nafion-impregnated nanocomposite membranes were prepared by extending the Nafion 117 membranes over a petri-dish, adding a required amount (5 to 15wt %) of ZrO_2, P-ZrO_2 and S-ZrO_2 nanoparticles in methanol solution. The nanocomposites membranes were repeatedly impregnated (up to 5 times) at room temperature [25]. In order to remove any air from the membrane pores, the sol and immersed membranes were heated up to 100 °C, then slowly cooled down to room temperature and kept in the solution for 24 hours. After drying, these membranes were stored in de-ionized water.

5.3. Results and discussion

The techniques used to characterize polymers are The X-ray diffraction (XRD) analysis; Fourier Transform Infrared (FTIR), Scanning Electron Microscopy (SEM) and Transmission electron microscopy (TEM) were used to explore the morphology of the polymers synthesized in this investigation. The water uptake property was determined by measuring the dry weight of the films and the equilibrium wet weight of the polymer. The ion exchange capacity (IEC) was determined by using the titration technique.

5.3.1. The X-ray powder diffraction (XRD) analysis

The X-ray diffraction analysis for the nanocomposite membranes developed by recasting, ion exchange and impregnation method compared to plain recast Nafion membranes shown in Figure 5.1. The XRD results of nanocomposites membrane with that of plain recast Nafion membranes shows a very similar broad diffraction features at Bragg angles (2θ) of the 12-22° [26]. Figure 5.1 shows that initially all the membranes have amorphous phase and then crystalline at (2θ = 17.5°) of polyfluorocarbon chains of Nafion [27]. In Figure 5.1 (b) and (c) these two results shows the broad peak around 40° which is associated with the fluorocarbon chains of Nafion membrane which resemble the poor crystallinity of Nafion matrix [28-30]. The Nafion/10 % S-ZrO_2 (recast) nanocomposite membranes showed some extra peaks as compared to Nafion membrane corresponding to S-ZrO_2 nanoparticles. However, the Nafion/ 10% S-ZrO_2 (ion exchange) nanocomposite membranes showed a pattern essentially identical to Nafion membrane due to the low loading S-ZrO_2 nanoparticles. The Nafion/ 10% S-ZrO_2 (impregnation) nanocomposite membranes show the peaks of the considered S-ZrO_2 powder confirming the presence of the inorganic compound within the Nafion membrane.

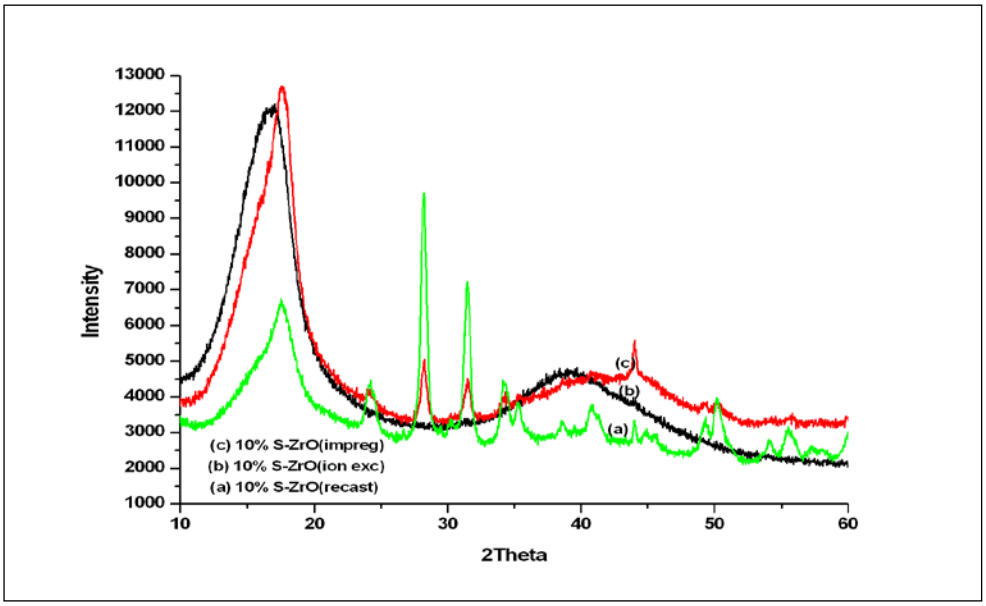

Figure 5. 1: XRD patterns of (a) Nafion/10% S-ZrO_2 (recast), (b) Nafion/10% S-ZrO_2 (ion exc) and (c)Nafion/10% S-ZrO_2 (impregnation) nanocomposite membranes.

Figure 5.2 presents the Nafion/ nanocomposite membranes analyzed by X-ray diffractometry. The results indicate that the Nafion/ 10% ZrO_2, Nafion/ 10% P-ZrO_2 and Nafion/ 10% S-ZrO_2 nanocomposite membranes for un-aged samples have very similar reflections. This shows that there is no crystalline change of mixing these nanoparticles within the membranes. In Figure 5.2 all the nanocomposite membrane presents a sharper peak at 15° 2θ due to the presence of bigger clusters with respect to the Nafion membrane [31]. The results in Figure 5.2 show the peaks of the considered ZrO_2 nanopowder which confirms that the crystalline structure of the ZrO_2 or P-ZrO_2 or S-ZrO_2 did not change even after composited to Nafion membrane. The results present the Bragg angles (2θ) of the monoclinic structure appear at 24.4°, 28.2°, 31.5°,

34.5° and 62.3° whereas the angles for the tetragonal structure are 30.2°, 50.2°, 59.3° and 60.2 which is diffraction feature of ZrO_2, P-ZrO_2 and S-ZrO_2 nanoparticles.

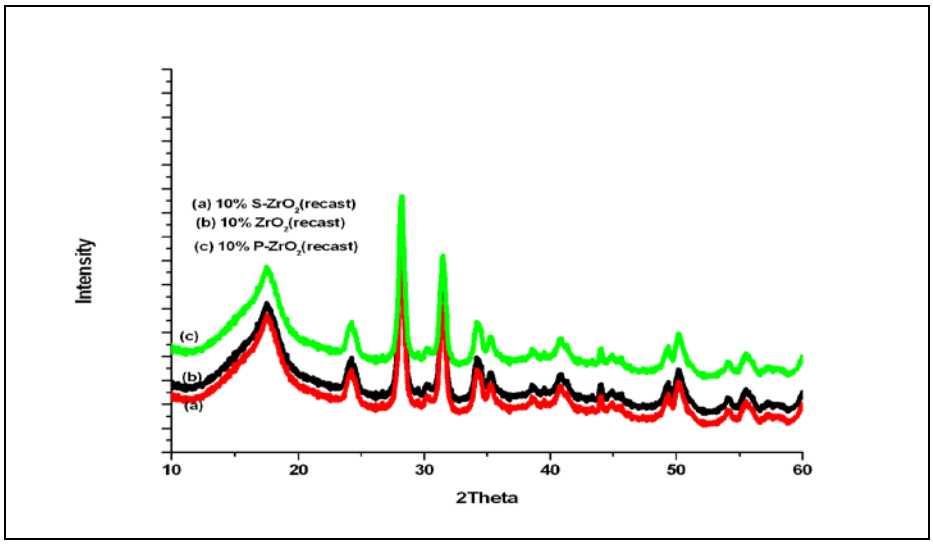

Figure 5. 2: XRD patterns of (a) Nafion/10%S-ZrO_2, (b) Nafion/10% ZrO_2 and (c) Nafion/10% P-ZrO_2 recast nanocomposite membrane (un-aged).

Figure 5.3 shows the X-ray diffraction analysis for the nanocomposite membranes developed by recasting method incorporated with aged nanoparticle at 48 hrs. The results shows a very similar broad diffraction feature of tetragonal (t) phase at Bragg angles (2θ) of 30.2°, 50.2° and 60.2° in all nanocomposite membranes.

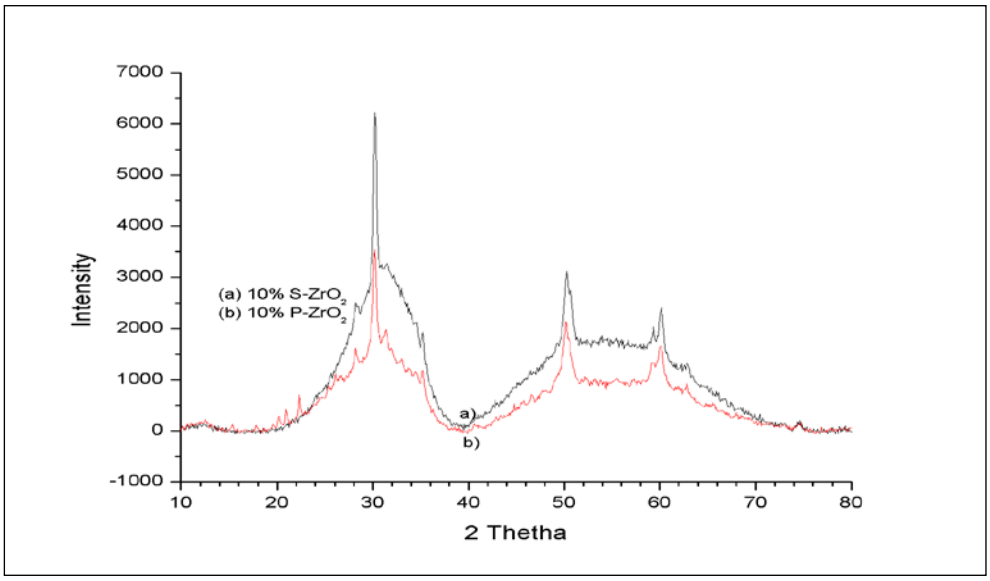

Figure 5. 3: XRD patterns of (a) Nafion /10% S-ZrO_2 and (b) Nafion/ 10% P-ZrO_2 recast nanocomposite membrane (aged).

5.3.2. Fourier Transform Infrared (FTIR) spectroscopy

Figure 5.4 shows the infrared spectra of Nafion/15% ZrO_2, Nafion/15% P-ZrO_2 and Nafion /15% S-ZrO_2 nanocomposite membrane aged at 48hrs. These results indicated that most of the peaks are assigned to the vibration of Nafion membranes. Figure 5.4 (a, b and c) shows that their vibration bands are in the same wave number region of 800 cm^{-1} to 2000 cm^{-1}. Figure 5.4 shows a peak at 1250, 1140 and 1041 cm^{-1} which is attributed to symmetric stretching of sulfonic acid group (SO_3^-) [32,33].

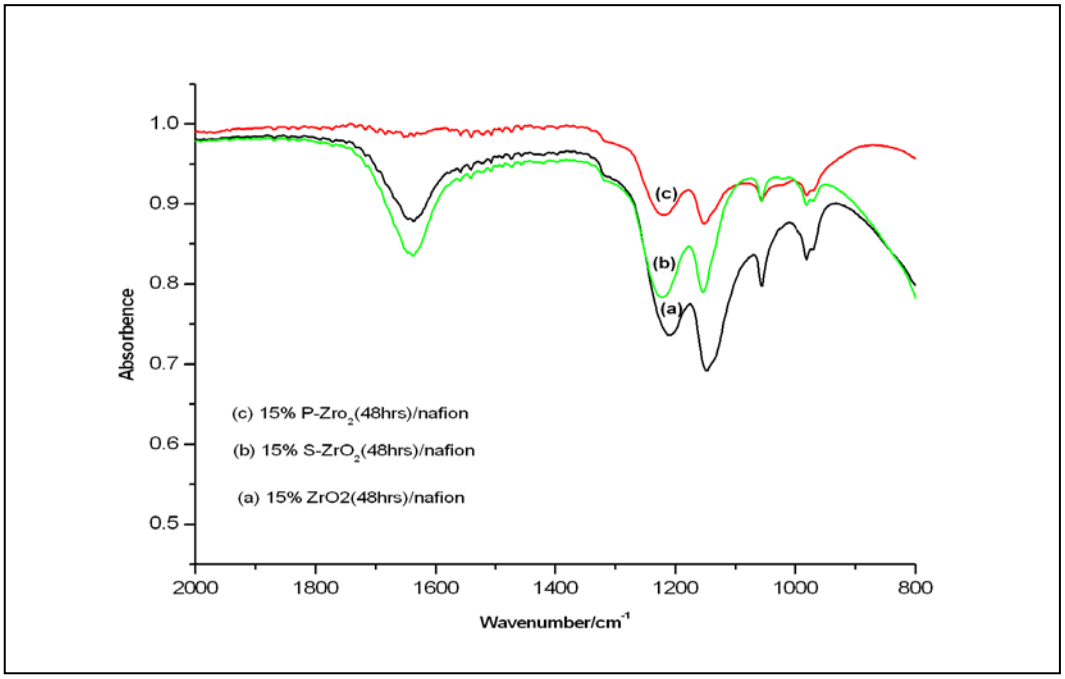

Figure 5. 4: Fourier Transform Infrared analysis of (a) Nafion/ 15% ZrO_2, (b) Nafion/ 15% S-ZrO_2 and (c) Nafion/ 15% P-ZrO_2 nanocomposites membrane.

These results of the FT-IR spectra of the nanocomposite membranes are presented in Figure 5.5. Figure 5.5 shows the vibration structures associated with the Nafion membrane are found in the nanocomposite membrane. Figure 5.5 (a, b and c) shows the peaks at 1058, 1150 and 1202 cm^{-1} which are attributed to the stretching vibrations of $–SO_3^-$ and $–CF_2–CF_2–$ and the peaks at 970 and 980 cm^{-1} to the stretching vibrations of –C–O–C– [34-36]. Figure 5.5 (b) shows that the peak at 1250, 1140 and 1041 cm^{-1} is due to the asymmetric stretching vibrations of sulfate groups [32] and 1630 cm^{-1} is attributed to the vibrations of acidic –OH groups.

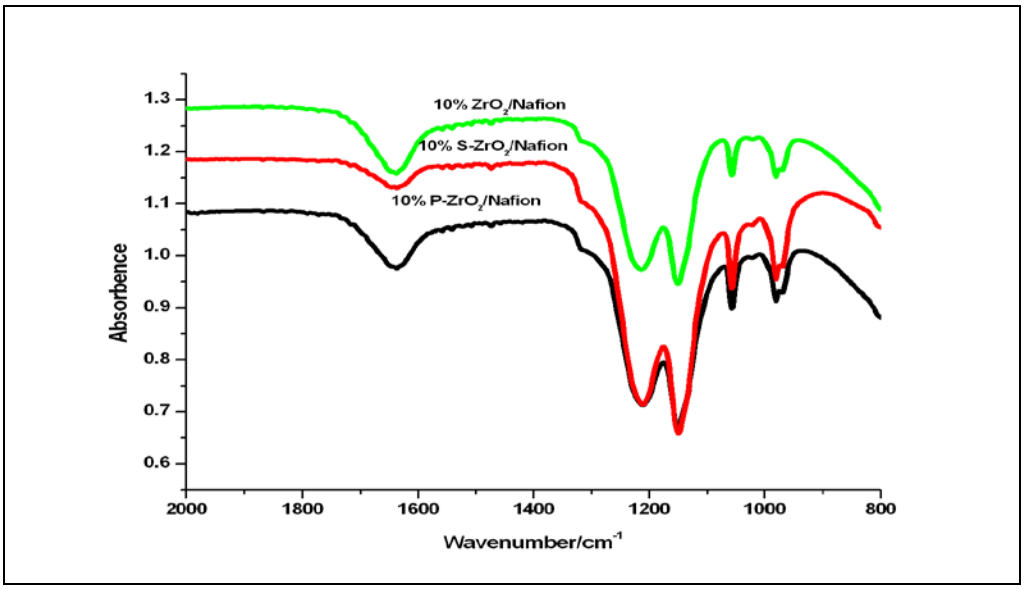

Figure 5. 5: Fourier Transform Infrared analysis of Nafion/ 10% ZrO_2, Nafion/ 10% S-ZrO_2 and Nafion/ 10% P-ZrO_2 nanocomposites membrane.

5.3.3. Scanning Electron Microscopy (SEM)

Figure 5.6 presented the SEM results of Nafion/10% ZrO_2 nanocomposite membrane prepared by recast and ion exchange method. Figure 5.6 (a) shows that SEM was carried out on the cross section of recast Nafion/ ZrO_2 nanocomposite membrane with 10% inorganic. Figure 5.6(a) shows a crack-free nanocomposite membrane with uniform distribution of the inorganic nanoparticles of ZrO_2 in the Nafion matrix with no agglomeration. The result shows the presence of spherical-shaped nanopores in the filler nanoparticles in all the nanocomposite membrane. In Figure 5.6 (b) the results shows that the nanocomposite membrane prepared by ion exchange method was homogenous mixed without any cracks, but with ZrO_2 nanoparticles reflect along the surface of the nanocomposite membrane. SEM results of Nafion/10% ZrO_2

nanocomposite membrane shows that the nanoparticle size was more consistent and ranged from approximately 20 to 100 nm the results are shown in Figure 5.6. An observation from the SEM image in Figure 5.6 revealed that the nanoparticles agglomerates present in the nanocomposite membrane prepared by recast method were generally smaller in size and more evenly distributed within the membrane in comparison with that of nanocomposite membrane prepared by ion exchange method.

(a)

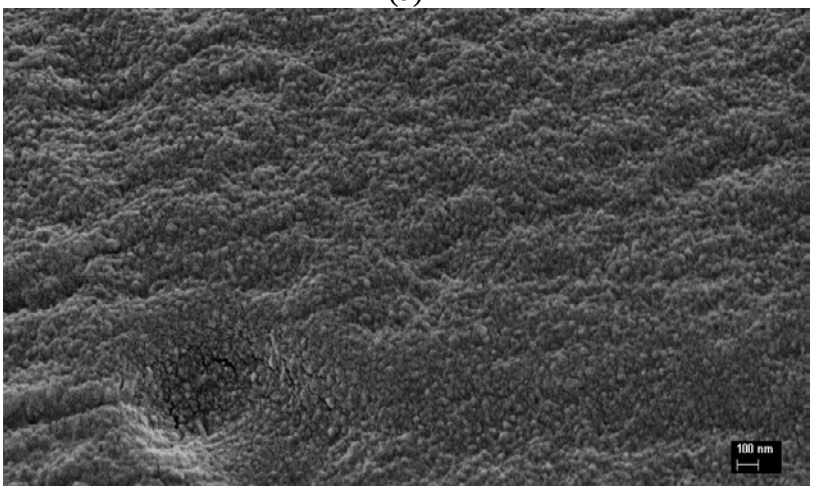

(b)

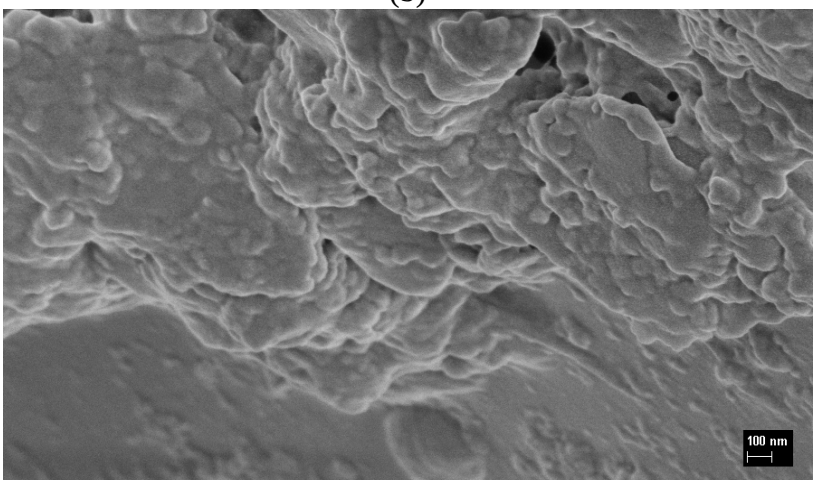

Figure 5. 6: SEM image of the Nafion/ 10% ZrO_2 nanocomposite membrane: (a) recast method and (b) ion exchange method.

Figure 5.7 presents the SEM results of nanocomposite membrane prepared by the impregnation and the recast method. Figure 5.7 shows the nanocomposite membranes with phosphate zirconium oxide nanoparticles. Figures 5.7 (a) shows the membrane having smooth surface as their inorganic nanoparticles were relatively homogenous distributed but it is evident also that there are differences in the particles size of the additive. Figure 5.7 (b) shows that the particle size of Nafion/ P-ZrO_2 nanocomposite membrane was around 25-30 nm which was similar to the size of the P-ZrO_2 nanoparticles measured by XRD was about 27 nm. The inorganic nanoparticles are well dispersed throughout the membrane but in other part of membrane the inorganic particle agglomerates at higher content of the inorganic additive. The morphology of the nanocomposite membranes are presented in Figure 5.8. Figure 5.8 show the surface and cross-section morphology of nanocomposite membranes which were prepared by recast method. As shown in Figure 5.8 (b), the S-ZrO_2 nanoparticles had a very uniform distribution along the cross section of the Nafion/ 10% S-ZrO_2 nanocomposite membrane, which shows a good distribution of S-ZrO_2 nanoparticles in the Nafion membrane. Figure 5.8 (a) shows that the S-ZrO_2 nanoparticle has been more dispersed in the nanocomposite membrane with the less agglomeration of the inorganic nanoparticles in membrane, which resulted in the crake-like membrane. This appearance of crack-like indicated that the membrane has dried up completely. The results indicate that the surface of the nanocomposite membrane was smooth with a homogenous dispersion of S-ZrO_2 particles into the membranes and also showed that the pores of the porous membrane were fully impregnated with S-ZrO_2 as seen in

Figure 5.8(a), although some cracks were detected at the fracture surfaces of the membrane.

(a)

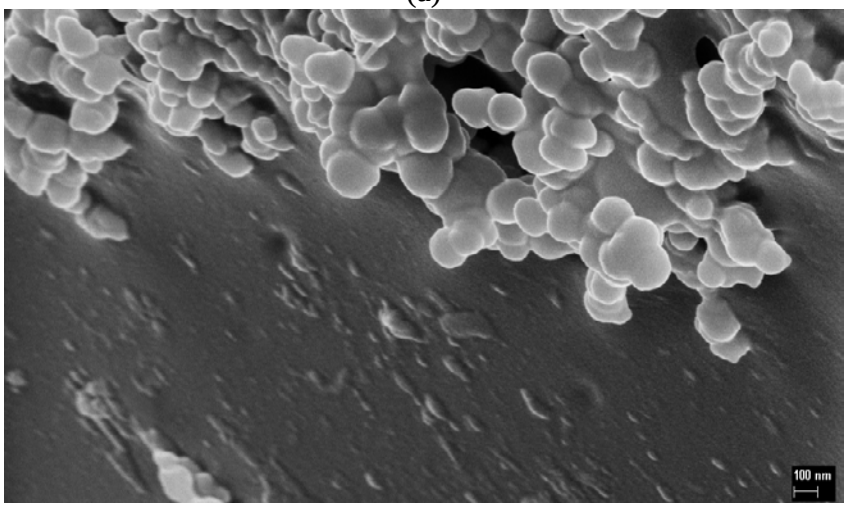

(b)

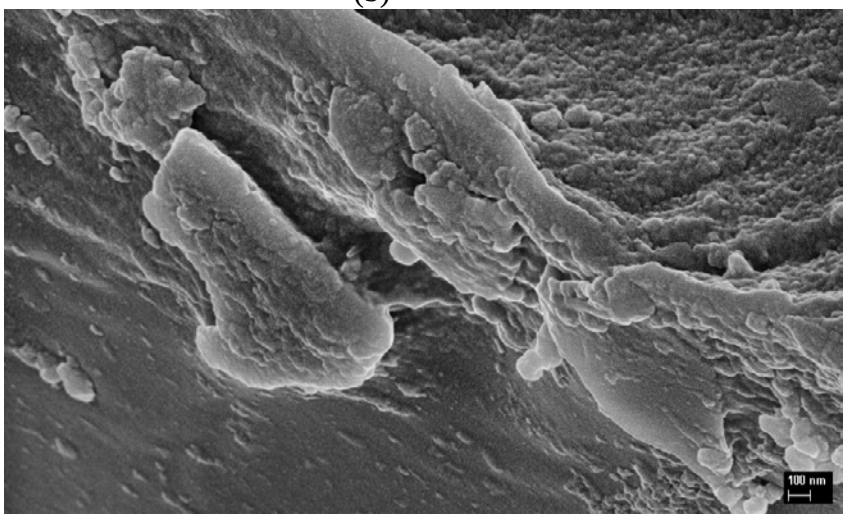

Figure 5. 7: SEM image of the Nafion/ 10% P-ZrO_2 nanocomposite membrane: (a) Impregnation method and (b) recast method.

(a)

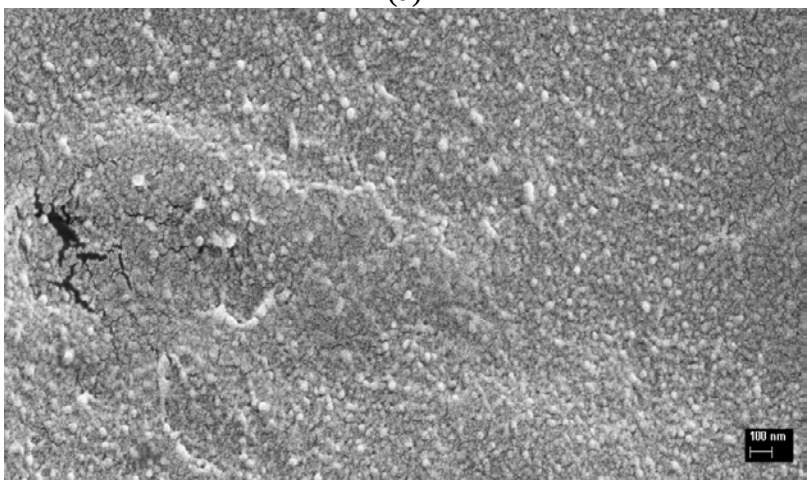

(b)

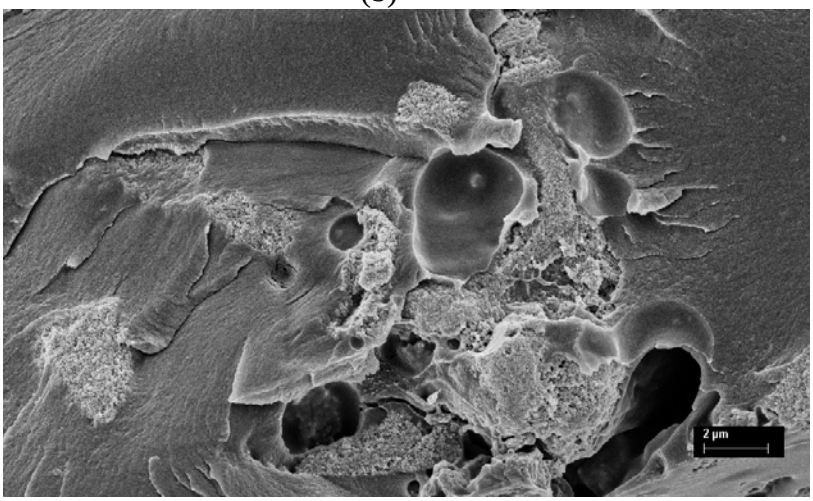

Figure 5. 8: SEM image of the Nafion/ 10% S-ZrO_2 nanocomposite membrane: (a) The surface and (b) cross-section morphology.

5.3.4. Transmission electron microscopy (TEM)

Figure 5.9 (a), (b) and (c) presents the TEM micrographs of Nafion/ 10% S-ZrO_2 nanocomposite membrane prepared by recast method. The TEM image in Figure 5.9(a) shows a well-resolved lattice fringe pattern indicating the single-crystalline-like phase and high crystallinity of the synthesized material. Figure 5.9 (b) shows the

occurrence of agglomerates of inorganic nanofiller extending about 50 nm and the agglomerates may reduce the adhesion of the catalytic layer on the nanocomposite membrane. Figure 5.9(c) indicates that the micrograph consists of S-ZrO_2 nanoparticles with a spherical shape and diameters of 0.5µm. The results shows the uniformly distributed of nanoparticles with the little agglomeration.

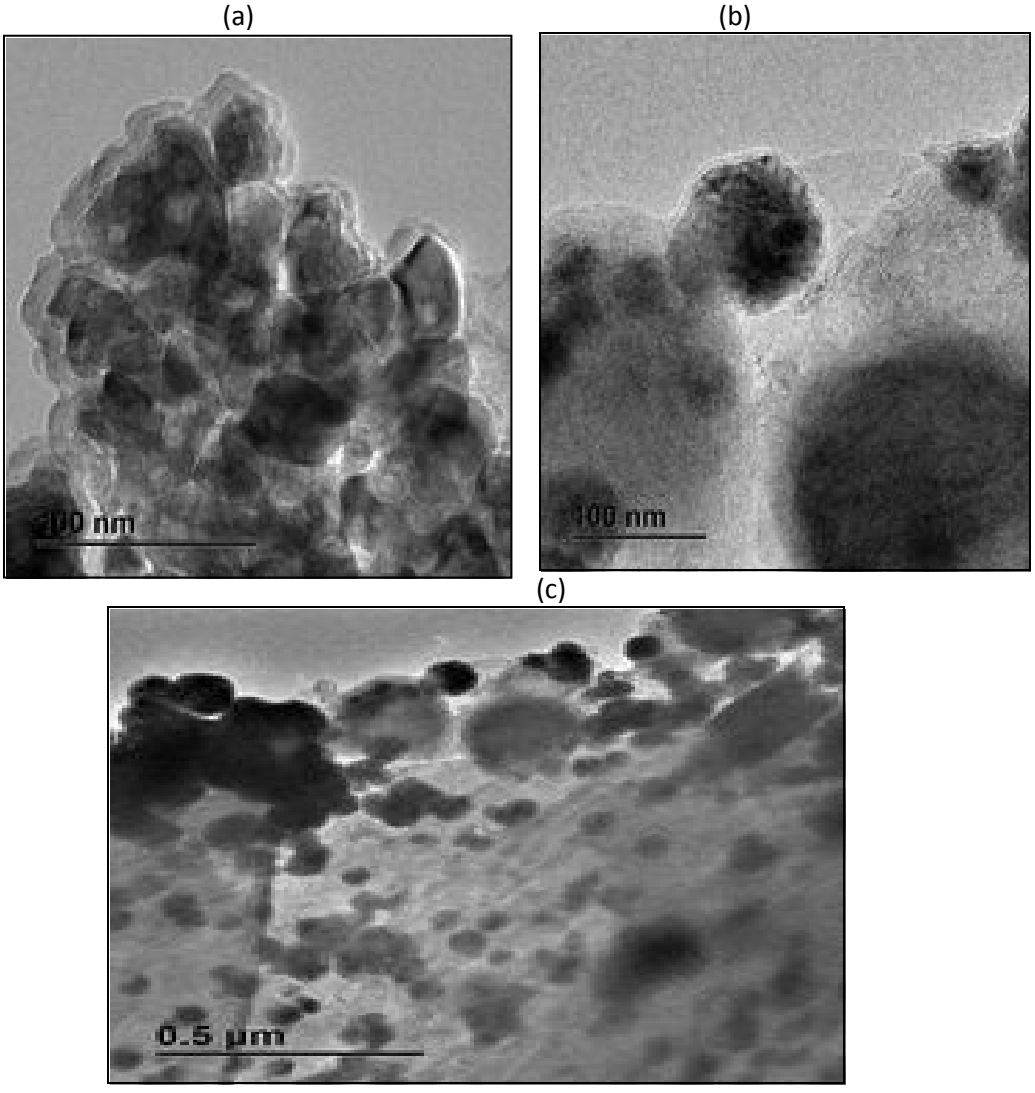

Figure 5. 9: TEM image (a), (b) and (c) of Nafion/10% S-ZrO_2 nanocomposite membrane (recast method).

Figure 5.10 (a), (b) and (c) presents the TEM micrographs of Nafion/ 10% ZrO_2 nanocomposite membrane prepared by Ion exchange method. The micrographs in Figure 5.10 (a), (b) and (c) clearly show that the nanocomposites membrane consists of crystalline ZrO_2 nanoparticles with diameters ranging from 10 to 20 nm, which consists of the small grains of S-ZrO_2 with sizes lower than 2µm. Figure 5.10 (a) and (b) shows that the larger aggregates consist of small nanoparticles which are single crystallites and they are uniformly distributed with their sizes lower than 10 nm. Figure 5.10(c) shows the inset of a locally magnified dark region of ZrO_2 nanoparticles in the nanocomposite membrane.

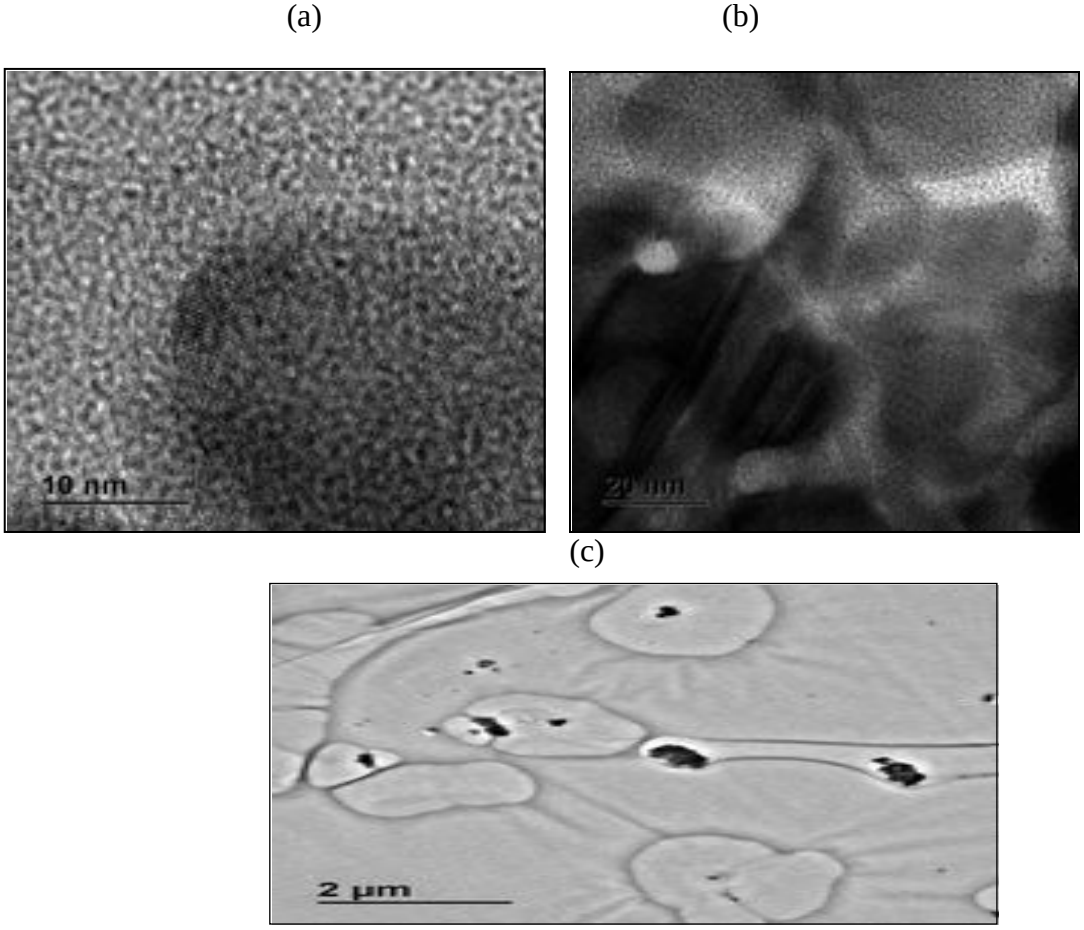

Figure 5. 10: TEM image (a), (b) and (c) of the Nafion/ 10% ZrO_2 nanocomposite membrane (ion exchange method).

Figure 5.11(a) and (b) presents the surface morphology of the Nafion/P-ZrO_2 nanocomposite membrane prepared by recast method. Figure 5.11 (a) shows that the nanofiller are evenly distributed through the membrane within the microscopic scale of 10 nm. The results shows that this method is the best when compared with the other two methods as the nanoparticles cannot be deducted from the membrane. Figure 5.11(b) show that the P-ZrO_2 nanoparticles are highly crystalline.

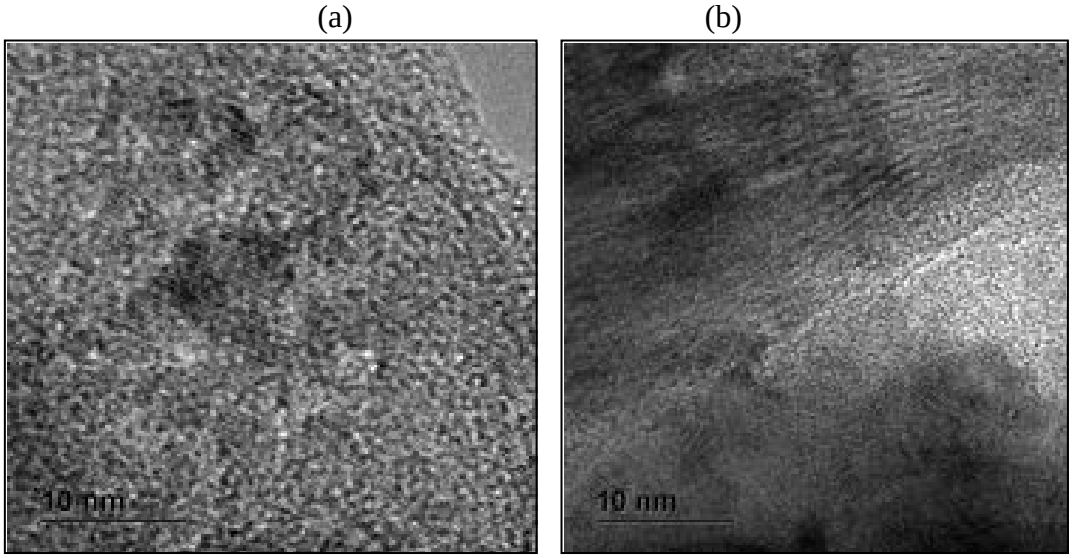

Figure 5. 11: TEM image of the Nafion/P-ZrO_2 nanocomposite membrane prepared by recast method.

5.3.5. Ion exchange capacity (IEC)

Table 5.1 summarized the IEC values of Nafion/ZrO_2, Nafion/S-ZrO_2 and Nafion/P-ZrO_2 nanocomposite membranes synthesis by different method (recast, ion exchange and swelling method) which have been determined via titration. It can be observed from Table 5. 1 and Figure 5.12 that the Nafion/ 15% S-ZrO_2 nanocomposites membrane was the most acid membrane when compared with the other

nanocomposites membrane, having the highest IEC value of 1.42 meg.g^{-1}. These high IEC value may due to the incorporation of superacid S-ZrO_2 nanoparticles which increased the membrane acid property for providing new strong acid site. The results from Table 5.1 show that the IEC of Nafion/ ZrO_2 nanocomposites membrane (ion exchange method) is almost the same with Nafion 117 and Plain recast Nafion membrane with the value of 0.93 meg.g^{-1}; this can be due to loading of zirconia content during preparation. The result show that IEC of the nanocomposite membranes increases with increasing inorganic nanoparticles content. The results show that the IEC of the nanocomposite membrane prepared by the recast method is higher than those of the other nanocomposite membranes prepared by ion exchange or impregnation.

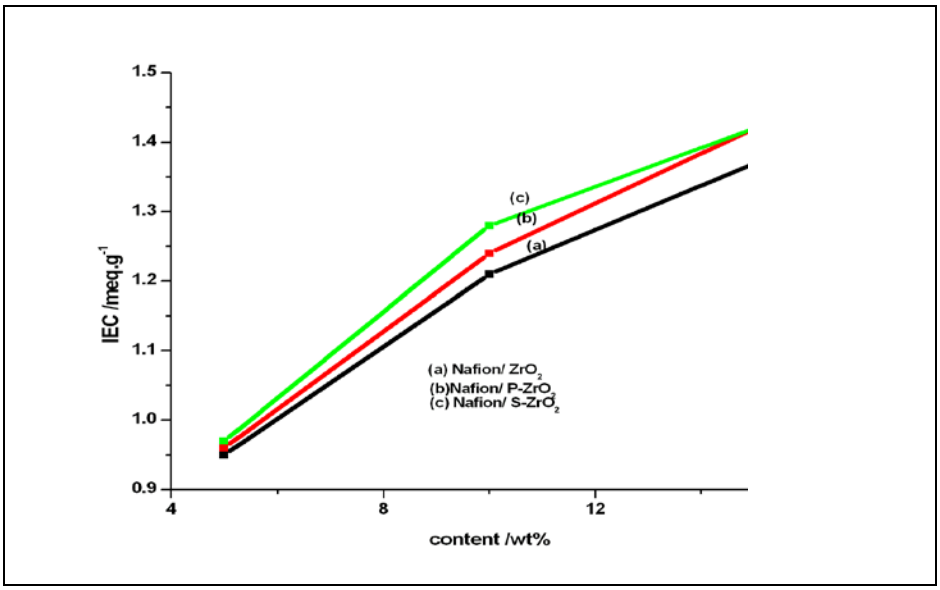

Figure 5. 12: Ion exchange capacity (IEC) of nanocomposites membrane (recast method).

Table 5. 1: The IECs and the water uptake of Nafion/ nanocomposite, Nafion 117 and Nafion plain recast membrane

Samples	Ion Exchange Capacity for Na+ (meq/g)	Water uptake (%)
Nafion 117	0.90	32
Nafion plain recast	0.92	34
Nafion /5% ZrO2 (recast)	0.95	34
Nafion /5% S-ZrO2 (recast)	0.97	36
Nafion /5% P-ZrO2 (recast)	0.96	34
Nafion /5% ZrO2 (impreg)	0.95	34
Nafion /5% S-ZrO2 (impreg)	0.98	35
Nafion /5% P-ZrO2 (impreg)	0.96	34
Nafion / ZrO2 (ion exch)	0.93	36
Nafion / S-ZrO2 (ion exch)	0.96	38
Nafion /P- ZrO2 (ion exch)	0.94	38
Nafion /10% ZrO2 (recast)	1.21	39
Nafion /10% S-ZrO2 (recast)	1.28	42
Nafion / 10% P-ZrO2 (recast)	1.24	40
Nafion /15% ZrO2 (recast)	1.37	39
Nafion /15% S-ZrO2 (recast)	1.42	40
Nafion /15% P-ZrO2 (recast)	1.40	37

5.3.6. Water uptake

Water uptake of the Nafion 117 and the modified nanocomposite membranes was measured by soaking the membranes in water at room temperature for 24 hours and calculated using equation (3.5) from Chapter 3. All the nanocomposite membranes display better water uptake than the Nafion 117 and plain recast Nafion membranes.

The plain recast Nafion shows a slightly higher water uptake than Nafion 117 due to the crystallinity of membrane. Water uptake is also enhanced with increasing ZrO_2 content. The water uptake of Nafion 117 (32 %) is lower than that of Nafion/ 10% S-ZrO_2 nanocomposite membrane which it is 42 %, which it's about 10% higher for modified membranes in comparison to Nafion 117. The incorporation of ZrO_2, S-ZrO_2 and P-ZrO_2 increases the water uptake of the Nafion 117 membranes because inorganic nanoparticles contribute additional hydrogen bonding sites and displace the more volatile bulk water [1, 37,38]. The results from Table 5.1 show that by addition of sulphated and phosphate zirconia nanoparticles increases its water uptake which can be resulted in new acid sites provided for absorption of water. The higher water uptake of nanocomposites membrane can be caused by the incorporated nanoparticles which make cluster in the pore of the physical strength of Nafion. The results from Figure 5.13 show that increasing the amount of inorganic can enhance the water uptake more or less, which might be caused by water being captured inside zirconia nanoparticles or in gaps between zirconia nanoparticles and Nafion membrane.

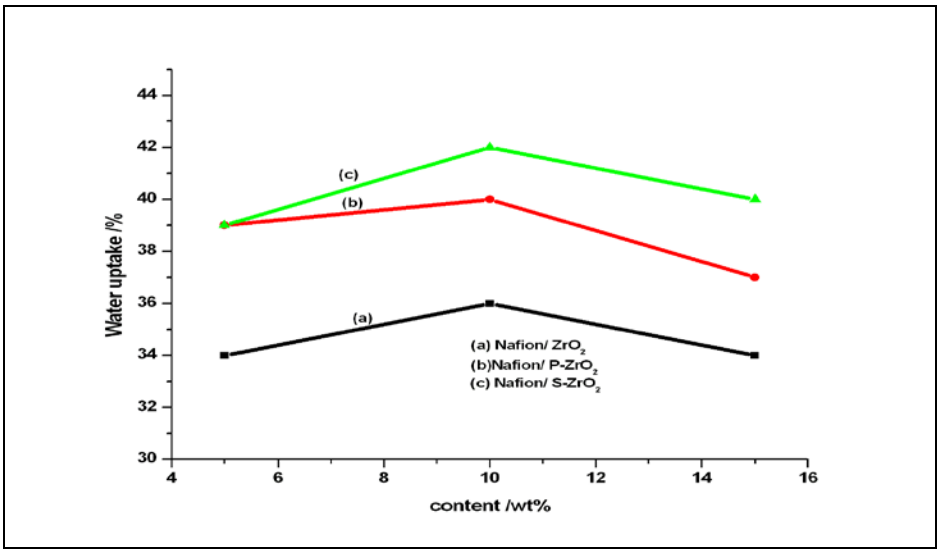

Figure 5. 13: Water uptake of nanocomposites membrane (recast method).

5.3.7. Proton Conductivity.

Table 5.2 presents the proton conductivity of Nafion/ 5% ZrO_2, Nafion/ 5%P-ZrO_2 and Nafion/ 5% S-ZrO_2 nanocomposite membrane compared with Nafion 117 and plain recast Nafion. Table 5.2 shows the proton conductivity of the nanocomposites membranes conducted at 25^{o}C temperature. The results in Table 5.2 indicate that the Nafion/ 5% P-ZrO_2 nanocomposite membrane at 25^{o}C temperature their conductivity is lower than of a plain recast Nafion membrane. The results show that the proton conductivity of plain recast Nafion membrane decreased slightly when compared with that of Nafion 117. The proton conductivity of Nafion 117 membrane is 1.4×10^{-2} S cm^{-1} at 25^{o}C whereas that of the Nafion/ 5% P-ZrO_2 nanocomposite membranes is 4.39×10^{-3} S cm^{-1} which is lower than that of Nafion 117 membrane. These results shows that when increasing phosphated zirconia nanoparticles content in the membrane it will also decreases the proton conductivity of the membrane at lower

temperature. The nanocomposites membrane with 5% S-ZrO_2 nanoparticles has found to have the highest proton conductivity when compared to the unmodified membrane at the lower temperatures of 25^oC. The nanocomposites membranes synthesize by recast method exhibit significantly higher conductivity in comparison to the Nafion 117 and plain recast Nafion membrane. Above 100^oC temperature unmodified membrane has lower proton conductivity due to the insufficient water content in the membrane whereas for the modified Nafion/ 5% S-ZrO_2 nanocomposite membrane has higher conductivity of 2.3 x 10^{-1} [32] as sulfated zirconia nanoparticles provides extra water to the membrane. For the unmodified Nafion membrane the conductivity increases up to 80 ^oC temperature. Figure 5.14 shows typical complex-plane of imaginary impendance (-Z") versus the real impendance (Z') for Nafion/ 5% ZrO_2, Nafion/ 5% S-ZrO_2 and Nafion/ 5% P-ZrO_2 nanocomposite membrane. The plots highlight the part of the impendance spectrum from 1MHz to 10Hz [39]. It can be seen in Figure 5.14 and Table 5.3 that the membrane resistance of Nafion/ 5% P-ZrO_2 nanocomposite membrane is higher than those of Nafion/ 5% ZrO_2 and Nafion/ 5% S-ZrO_2 nanocomposite membrane. It indicate that the addition of 5% P-ZrO_2 nanoparticle in Nafion membrane block the conduction of protons. The resistance of Nafion/ 5% ZrO_2 and Nafion/ 5% S-ZrO_2 nanocomposite membrane prepared by recast method are lower than that of the Nafion/ 5% P-ZrO_2 nanocomposite membrane prepared by impregnation method. It can be concluded that recast method is an effective method on proton conductive.

Table 5. 2: the membrane thickness and resistance of Nafion/nanocomposite

Samples	membrane resistance (Ohm)	membrane thickness (cm)
Nafion/ 5% ZrO_2	565	0.0413
Nafion/ 5% P-ZrO_2	$10.96x10^3$	0.0104
Nafion/ 5% S-ZrO_2	206.1	0.0234

Table 5. 3: The proton conductivity of Nafion/nanocomposite, Nafion 117 and Nafion plain recast membrane at 25°C

Samples	proton conductivity (S/cm) at 25 °C
Nafion/ 5% ZrO_2	0.0413
Nafion/ 5% P-ZrO_2	0.00439
Nafion/ 5% S-ZrO_2	0.1037
Nafion 117	0.015
Plain recast Nafion	0.014

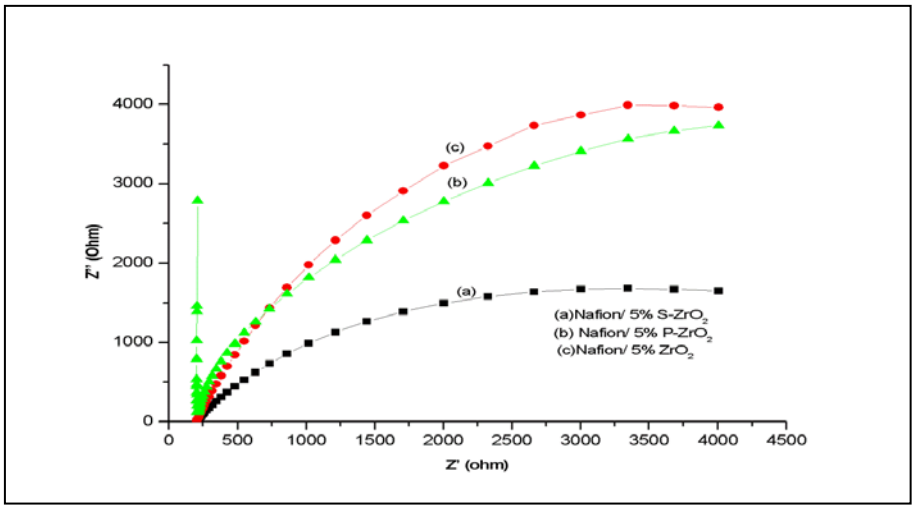

Figure 5. 14: Complex-plane plots obtained by impendance spectroscopy for nanocomposite membranes.

5.4. Conclusion

The nanocomposite membranes incoparated by ZrO_2, S-ZrO_2 and P-ZrO_2 were compared according to their morphology, water uptake, IEC and proton conductivity. The nanocomposite membranes were found to have higher water uptake and higher acidic which makes them suitable candidates for fuel cell applications. The proton conductivity was obtained to be higher with less resistance. It was 0.1037 S/cm at room temperature for Nafion/5% S-ZrO_2 nanocomposite membranes and 0.0413 S/cm for Nafion/5% ZrO_2 nanocomposite membranes which agreed with properties of fuel cell application. It was shown from the results above that the IEC of modified membrane increased with increasing additive content. Zirconium oxide modified by diammonium hydrogen phosphate solution resulted in poor proton conductivity at lower temperature.

The minimum additive of inorganic content in membrane composition was obtained to be 10 wt.%, as increased of additive resulted in decreases of water uptake. Their high proton conductivity and higher water uptake make these modified membranes suitable to be used in fuel cell.

5.5. References

[1] P. P. Kundu, V. Sharma, *Critical Reviews in Solid State & Material Sciences* **32** (2007) 51-66.

[2] M. Watanabe, H. Uchida, Y. Seki, M. Emori, P. Stonehart, *Journal of Electrochemical Society* **143** (1996) 3847-3852.

[3] M. A. Navarra, C. Abbati, B. Scrosati, *Journal of Power Sources* **183** (2008) 109-113.

[4] O. Savadogo, *Journal of Power Sources* **127** (2004) 135-161.

[5] T. M. Thampan, N. H. Jalani, P. Choi, R. Datta, *Journal of Electrochemical Society* **152** (2005) A316-A325.

[6] W. Vielstich, H. Yokokawa, H. A. Gasteiger, *Handbook of Fuel cells Fundamentals Technology and Applications*, John Wiley & Sons, Inc, (2003) ISBN 978-0-72311-1.

[7] S. Ren, G. Sun, C. Li, S. Song, Q. Xin, X. Yang, *Journal of Power Sources* **157** (2006) 724-726.

[8] M. Hogarth, X. Glipa, *High temperature membranes for solid polymer fuel cells***,** Johnson Matthey Technology Centre, DTI Publication, URN 01/893, 1-72.

[9] K. Miyatake, H. Iyotani, K. Yamamoto, E. Tsuchida, *Macromolecules* **29** (1996) 6969-6971.

[10] V. Antonucci, A. Di Blasi, V. Baglio, R. Ornelas, F. Matteucci, J. Ledesma-Garcia, L.G. Arriaga, A.S. Arico`, *Electrochimica Acta* **53** (2008) 7350-7356.

[11] K. T. Adjemian, R. Dominey, L. Krishnan, H. Ota, P . Majsztrik, T. Zhang, J. Mann, B. Kirby, L. Gatto, M. Velo-Simpson, J. Leahy, S. Srinivasant, J . B. Benziger, A. B. Bocarsly, *Chemistry of Materials* **18** (2006) 2238-2248.

[12] K. T. Adjemian, S. J. Lee, S. Srinivasan, J. Benziger, A. B. Bocarsly, *Journal of the Electrochemical Society* **149** (2002) A256-A261.

[13] K. T. Adjemian, S. Srinivasan, J. Benziger, A. B. Bocarsly, *Journal of Power Sources* **109** (2002) 356-364.

[14] G. Alberti, M. Casciola, D. Capitani, A. Donnadio, R. Narducci, M. Pica, M. Sganappa, *Electrochimica Acta* **52** (2007) 8125-8132.

[15] P. Costamagna, C. Yang, A. B. Bocarsly, S. Srinivasan, *Electrochimica Acta* **47** (2002) 1023-1033.

[16] M. Casciola1, D. Capitani, A. Comite, A. Donnadio, V. Frittella, M. Pica, M. Sganappa, A. Varzi, *Fuel Cells* **8** (2008) 217-224.

[17] T. Jian-Hua, G. Peng-Fei, *International Journal of Hydrogen Energy* **33** (2008) 5686-5690.

[18] P. L. Antonucci, A. S. Aroco, P. Creti, R. Ramunni, V. Antonucci, *Solid State Ionics* **25** (1999) 431-437.

[19] P. Dimitrova, K. A. Friedrich, B. Vogt, U. Stimming, *Journal of Electroanalytical Chemistry* **532** (2002) 75-83.

[20] Z. Shao, H. Xu, M. Li, I. Hsing, Solid *State Ionics* **177** (2006) 779-785.

[21] W. Xu, T. Lu, C. Liua, W. Xinga, *Electrochimica Acta* **50** (2005) 3280-3285.

[22] T. Mokrani, "*The development of an inorganic direct methanol fuel cell"* PhD Thesis, University of the Western Cape, November (2004).

[23] Y. Zhai, H. Zhang, J. Hua, B. Yi, *Journal of Membrane Science* **280** (2006) 148-155.

[24] C. Yang, P. Costamagna, S. Srinivasan, J. Benziger, A. B. Bocarsly, *Journal of Power Sources* **103** (2001) 1-9.

[25] G. Vaivars, N.W. Maxakato, T. Mokrani, L. Petrik, J. Klavins, G. Gericke, V. Linkov, *Material Science* **10** (2004)162-165.

[26] R. B. Moore, C. R. Martin, *Macromolecules* **21** (1988) 1334-1339.

[27] K. A. Mauritz, R. B. Moore, *Chemical Reviews* **104** (2004) 4535-4585.

[28] K. A. Mauritz, T. J. Payne, *Journal of Membrane Science **168*** (2000) 39-45.

[29] M. Fujimura, T. Hashimoto, H. Kawai, *Macromolecules* **14** (1981) 1309-1315.

[30] P. Staiti, A. S. Arico, V. Bablio, F. Lufrano, E. Passalacqua, V. Antonucci, *Solid State Ionics* **145** (2001) 101-107.

[31] A. Sacc`a, A. Carbone, R. Pedicini, G. Portale, L. D'Ilario, A. Longo, A. Martorana, E. Passalacqua, *Journal of Membrane Science* **278** (2006) 105-113.

[32] S. Hara, M. Miyayama, *Solid State Ionics* **168** (2004) 111-116.

[33] V. Adeeva, J. W. Dehaan, J. Janchen, G. D. Lei, V. Schunemann, L. J. M. Vandeven, W. M. H. Sachtler, R. A. Vansanten, *Journal of Catalysis* **151** (1995) 364-372.

[34] J. Ostrowska, A. Narębska, *Colloid and Polymer science* **261** (1983) 93-95.

[35] W. S. li, D. S. lu, J. L. luo, K. T. Chuang, *Journal of Power Sources* **145** (2005) 376-438.

[36] J. James, T. Z. McMaster, J. M. Newton, M. J. Miles, *Polymer* **41** (2000) 4223-4234.

[37] N. H. Jalani, K. Dunn, R. Datta, *Electrochimica Acta* **51** (2005) 553-560.

[38] P. Choi, N. H. Jalani, R. Datta, *Journal of the electrochemical society* **152** (2005) E123-E130.

[39] C.L Gardner, A.V. Anantaraman, *Journal of Electroanalytical Chemistry* **395** (1995) 67-73.

CHAPTER SIX

6. CONCLUSIONS AND WORK IN PROGRESS

The synthesis method of precipitation used on preparation of zirconium oxide, sulfated zirconia and phosphated zirconia nanoparticles, were found to play a major role in the particles size. Their calcinations temperature of 600 ^{o}C promoted the crystallites form of the nanoparticles, as well as the concentration of sulfuric acid or diammonium hydrogen phosphate and aging period was strongly increased the particle size of nanoparticles. Both the aging and acid content incorporated into the zirconium oxide nanoparticles has more influenced in the structural properties and the crystal phase, the results can be observed under XRD and TEM in Chapter four. The sulfuric acid additive in the zirconium oxide nanoparticles has more effect in increasing the particles size than diammonium hydrogen phosphate, as the BET results of S-ZrO_2 is 39 m^2/g which is greater than 37 m^2/g of P-ZrO_2 nanoparticles. The effect of the synthesized nanoparticles on Nafion properties was demonstrated in Chapter five where the incorporation of inorganic nanoparticles promoted higher water uptake which leads to the higher proton conductivity of the nanocomposite membranes when compared to the unmodified membrane. The incorporation of the inorganic nanoparticles resulted also in the lower diffusion of methanol solution that makes it suitable for fuel cell application.

The XRD study of ZrO_2, S-ZrO_2, P-ZrO_2 nanoparticles for un-aged samples shows crystalline characteristics with the presence of monoclinic and tetragonal phase when calcinated at 600 ^oC for 6 hours whereas for aged one shows the presence of stabilized tetragonal phase only. It is observed that there are no differences in the FTIR or XRD results for sulfated or phosphated zirconia nanoparticles aged at 48 hours. The SEM image shows that the small nanoparticles are attached to each other to form agglomerated structure. From the SEM image obtained from the results show that the nanoparticles aged at 48 hours (ambient temperature) have high cystallinity and less agglomeration when compared with that of un-aged nanoparticles. The SEM characterization also supports the assumption based on the dependence of the particle size on the acidic group content. Specifically, the higher diammonium hydrogen phosphate acid solution or sulfuric acid amount incorporated into zirconia nanoparticles the smaller the nanoparticle size achieved with less agglomeration. The FTIR results indicate that the sulfonic acid and diammonium hydrogen phosphate acid has been successfully introduced to ZrO_2 nanoparticles. The specific surface area of S-ZrO_2 nanoparticles materials (39 m^2/g) is greater than of the pure ZrO_2 (33 m^2/g) this indicates that the presence of sulfate strongly influences the surface area of ZrO_2 as the sulfuric acid impregnation was known to increase the surface area of metal oxide catalysts. Also the surface area of aged nanoparticles at 48 hours at ambient temperature is higher than that of un-aged nanoparticles with the particle size ranges from (24.39 nm to 12.10 nm). This indicates that increasing of aging hours it increases the surface area of nanoparticles.

The in-corporation of zirconia nanoparticles on Nafion 117 membranes shows the improvement in the proton conductivity and water uptake because of high water affinity and the intrinsic acidity of the zirconia nanoparticles. The water uptake increases with increasing zirconia nanoparticles content in the membrane. This modified Nafion nanocomposite prepared by recast method (Nafion/ 15% S-ZrO_2) have the highest acid in their membrane when compared with the other nanocomposites membrane, having the highest IEC value of 1.42 meg/g. These high IEC value may be due to the incorporation of superacid S-ZrO_2 nanoparticles which increased the membrane acid property. From the results it is deduced that the IEC of ion exchange method is almost the same with Nafion and plain Nafion membrane, this can be due to the lower loading of zirconia content during preparation. From the result it had been observed that the IEC of all the nanocomposite membranes increases with increasing inorganic nanoparticles content in the membrane. The IEC of the all nanocomposite membrane prepared by the recast method was found to be higher than those nanocomposite membranes prepared by ion exchange or impregnation these may due to the uniformly distributed of nanoparticles within the nanocomposite membrane. The results show that the presence of the inorganic nanoparticles in Nafion membrane resulted in higher water uptake even at room temperature for 24 hours. A modified Nafion (Nafion / 10% S-ZrO_2 nanocomposite membrane) shows a higher water uptake of 42% than the recast plain Nafion membrane which is around 34%. The Nafion / 15% S-ZrO_2 nanocomposite membrane show the decrease in water uptake of 40% which is lower than of Nafion / 10% S-ZrO_2 nanocomposite membrane this may be due to the agglomeration that reduced the water sorption within the nanocomposite

membrane. The water uptake of all the nanocomposites membranes prepared by ion exchange increases with respect to Nafion 117 but with a lower %weight when compared to that of impregnation and recast membranes. This work shows that the modified Nafion membranes has higher water uptake these may due to the improvement of water retention throughout the membrane.

The proton conductivity of plain recast Nafion membrane decreased slightly when compared with that of Nafion 117. The proton conductivity of Nafion 117 membrane is 1.4×10^{-2} S cm^{-1} at 25 ^{o}C whereas that of the Nafion/ 5 % P-ZrO_2 nanocomposite membranes is 4.39×10^{-3} S/cm which is lower than that of Nafion 117 membrane. These results shows that when increasing phosphated zirconia nanoparticles content in the membrane it will also decreases the proton conductivity of the membrane at lower temperature. The observation from the all nanocomposites membrane shows that the proton conductivity decreased with the increased of the inorganic content at lower temperature this may due to the inorganic nanoparticle as they agglomerates and that agglomeration can hinder the proton transportation within the nanocomposites membrane by filling up the membrane pores. The nanocomposites membrane with 5% S-ZrO_2 nanocomposites membrane (0.1037 S/cm) has found to have the highest proton conductivity when compared to the unmodified membrane. The results show that the conductivity of the Nafion / 5% S-ZrO_2 increases with the increases of nanoparticles content in comparison to that of Nafion 117 membrane. The Nafion/ 5% ZrO_2 nanocomposite membrane were found to give rise to high proton conductivity

when compared to Nafion membrane proton conductivity. The proton conductivity obtained was around 4.13×10^{-2} S/cm at room temperature and 100% relative humidity.

Work in progress; to measure the methanol permeability by checking whether the incorporated method of inorganic nanoparticles in the Nafion membrane has a higher influence in the methanol permeability. To compare the methanol permeation rate of the nanocomposites membranes incorporated with S-ZrO_2, S-ZrO_2 and P-ZrO_2 nanoparticles. To observed the thermal stability and a better water management of the modified Nafion membranes using TGA.